

EFFECT OF PROCESS PARAMETERS ON METHANOL TO OLEFINS  
REACTIONS OVER SAPO CATALYSTS

Except where reference is made to the work of others, the work described in this thesis is my own or was done in collaboration with my advisory committee. This thesis does not include proprietary or classified information.

---

Luckner Jean

Certificate of Approval:

---

Christopher B. Roberts  
Uthlaut Professor  
Chemical Engineering

---

James A. Guin, Chair  
Professor  
Chemical Engineering

---

Steve R. Duke  
Associate Professor  
Chemical Engineering

---

Stephen L. McFarland  
Dean  
Graduate School

EFFECT OF PROCESS PARAMETERS ON METHANOL TO OLEFINS  
REACTIONS OVER SAPO CATALYSTS

Luckner Jean

A Thesis

Submitted to

the Graduate Faculty of

Auburn University

In Partial Fulfillment of the

Requirement for the

Degree of

Master of Science

Auburn, Alabama

August 8, 2005

EFFECT OF PROCESS PARAMETERS ON METHANOL TO OLEFINS  
REACTIONS OVER SAPO CATALYSTS

Luckner Jean

Permission is granted to Auburn University to make copies of this thesis at its discretion, upon the request of individuals or institutions and at their expense. The author reserves all publication rights.

---

Signature of Author

---

Date

Copy sent to:

Name

Date

## VITA

Luckner Jean, son of Saurel Jean and Anicia Guillaume, was born on May 05, 1970 in Port-au-Prince, Haiti. He left Haiti in 1985 and emigrated to the United States where he is still living ever since. In 1999 he was awarded a degree in Chemical Engineering from the Illinois Institute of Technology (IIT) in Illinois. Upon graduation he continued doing research activities in the Chemistry Department at Chicago State University. In August 2003, he started graduate studies in Chemical Engineering at Auburn University in Alabama.

THESIS ABSTRACT

EFFECT OF PROCESS PARAMETERS ON METHANOL TO OLEFINS  
REACTIONS OVER SAPO CATALYSTS

Luckner Jean

Master of Science, August 8, 2005  
(B.S. Chemical Engineering, Illinois Institute of Technology, 1999)

116 Typed Pages

Directed by Dr. James A. Guin

Acidic catalysts such as silicoaluminophosphate oxides (SAPO) have been known to play an essential role in olefins synthesis reactions. Because of their unique selectivity towards light olefins, these SAPO catalysts offer a promising alternative as reaction media in catalytic reactions based on the abundant supply of natural gas. In this thesis several studies were undertaken in order to examine the effects of process parameters on the methanol to olefins reactions (MTO) with particular emphasis on catalytic activity, lifetime, and product selectivity. All of the MTO reactions were performed under atmospheric pressure with catalyst bed temperature maintained at 400 °C in a continuous

fixed bed reactor by employing small pore SAPO catalysts: SAPO-34, SAPO-44, SAPO-47, and SAPO-56 (0.3 ~0.9 Si).

In order to judiciously make good use of the limited catalyst stocks, a scale-down analysis was performed by reducing all reaction parameters by 40%, i.e. catalyst load, methanol feed, and nitrogen flow. Product distribution profiles between before and after parameter reductions indicated almost identical catalytic activities with minor variations. A significant portion of this thesis was devoted to the particle size effects on the reaction behavior. The results from the ground particles demonstrated all catalysts maintained their stability. With the exception of SAPO-56 which showed no apparent activity difference for reduced particles, all SAPO's tested showed enhanced catalytic activity and lifetime. Improvements in C<sub>2</sub> to C<sub>4</sub> olefins selectivity and methanol conversion were observed as well. These same effects were also apparent upon temperature variation (300 °C to 500 °C). Effect of silicon content over SAPO-56 prepared with three different silicon amounts (0.3, 0.6, and 0.9 Si) indicated optimum olefins selectivity at 0.6 Si. Also, a spent catalyst was ground and tested for activity. From that reaction, only dimethyl ether (DME) and methanol (MeOH) were present in the product stream, indicating that all of the particle active sites have been covered with coke deposits. A thorough examination of all reactions over ground particles pointed to increased DME yields after catalyst deactivation began, as compared to before grinding. Reactions over catalysts modified with Ru only showed slight improvements when compared with the unmodified catalysts. Modification with metals such as palladium (Pd) and platinum (Pt) would be interesting.

## ACKNOWLEDGEMENTS

The author would like to express his sincere appreciation and gratitude to various people. Mr. Joe Aderholdt for helping repair equipment malfunction and breakdown; Dr. Prakash M. Adekkanattu for preparing all the original SAPO samples and Dr. Richard Ernst group at the University of Utah for the SAPO modification; Dr. Xiwen Huang for assisting him in the lab in various capacities; Dr. Dave Kanis for all his encouragements; and Dr. Nimir Elbashir for providing him with valuable advice. Also, the author would like to extend a warm thanks to the Chemical Engineering Department staff for their assistance: Mses. Sue Abner, Nancy Borland, Jennifer Harris, and Kellie Wilson.

In addition the author is very grateful both to Dr. Steve Duke and Dr. Christopher Roberts for serving in his oral committee and for offering him valuable advice in the toughest of times. Most of all, he owes much of the success of this study to his advisor Dr. James Guin for guiding him throughout the course of the project.

The author is very thankful to his friends back in Chicago for their continued friendly advice and moral support in the challenging days: Marie, Yvrose, Dieudonne, Enold, Sandra, and Franklin just to name a few. Also, he would like to acknowledge those friends he had come to know since being here in Alabama. To his family, he would like to thank his brothers and sisters for always being there in believing in him. To his mom and dad, he can't thank them enough for the wisdom and humility they instilled in him which guided him to this point, he loves them very much.

Style manual or journal used Guide to Preparation and Submission of Theses and Dissertations, Applied Catalysis A: General

Computer software used Microsoft Word, Microsoft Excel, Microsoft Paint, Microsoft Photo Editor, EndNote for Students



## TABLE OF CONTENTS

LIST OF TABLES	xii
LIST OF FIGURES	xiii
I. INTRODUCTION	1
II. LITERATURE REVIEW	3
Background	3
Methanol to Olefins (MTO)	8
Methanol to hydrocarbons Mechanism	9
SAPO Impregnation	12
Effect of Acid	13
Template (Structure Directing Agent)	14
Coke Formation (Catalyst Deactivation)	16
Role of water	18
Catalyst Regeneration	19
SilicoAluminoPhosphate (SAPO)	20
Particle Size and Shape	21
III. EXPERIMENTAL	24
Sample Preparation	24
Modified Catalysts	24
Particle Characterization	25
SAPO-47 Fractionation	25
Grinding of Particles	26
Standard Analysis (Olefins, Paraffins, DME and MeOH)	27
Product Analysis (Actual Runs)	29
Reaction Procedures	31
Temperature Method	34
IV. RESULTS AND DISCUSSIONS	35
SEM Analysis	35
Scale-Down Analysis	36
Temperature Studies	38
Temperature Study (SAPO-34), (P-5)	39

Temperature Study (SAPO-44), (P-6)	41
Temperature Study (SAPO-56), (P-18), (0.6 Si)	43
Catalytic Reaction Study	45
SAPO-44, (P-6)	46
SAPO-34, (P-5)	53
SAPO-47, (P-31)	57
SAPO-56	61
SAPO-56 (P-18), (0.6 Si)	61
SAPO-56 (P-28), (0.3 Si)	65
SAPO-56 (P-29), (0.9 Si)	68
Effect of Silicon Content	71
SAPO-56 (P-18), (0.6 Si) Spent Catalyst	72
SAPO Incorporated with Ruthenium	73
Ru-SAPO-34 (Ru-P-5)	73
Ru-SAPO-44 (Ru-P-6)	74
Ru-SAPO-56 (Ru-P18)	75
V. CONCLUSION	78
VI. REFERENCES	80
VII. APPENDICES	84
Appendix A	85
A-1. Table of Zeolite structures.	86
A-2. Wig-L-Bug.	87
Appendix B (SEM Micrographs)	88
B-1. SAPO-34	89
B-2. SAPO-44	89
B-3. SAPO-44 (After 5 min Grinding)	90
B-4. SAPO-44 (After 10 min Grinding)	90
B-5. SAPO-44 (After 15 min Grinding)	91
B-6. SAPO-47	91
B-7. SAPO-47	92
B-8. SAPO-47 (Sonicated in Acetone)	92
B-9. SAPO-47 (Sonicated in Acetone)	93
B-10. SAPO-56 (0.3 Si)	93
B-11. SAPO-56 (0.6 Si)	94
B-12. SAPO-56 (0.9 Si)	94
B-13. RuSAPO-56	95
B-14. RuSAPO-44	95
B-15. RuSAPO-44	96

B-16. RuSAPO-56	96
B-17. RuSAPO-56	97
Appendix C (Calculation Procedure)	98
C.1 – C.12 (List of Equation)	99

## LIST OF TABLES

Table 2.1. Acronyms for Framework Composition	5
Table 2.2. Typical SAPO and MeAPO Framework Composition	5
Table 2.3. Typical Structures in AlPO <sub>4</sub> -based Molecular Sieves	7
Table 3.1. Retention Time for Olefins Standard Components	28
Table 3.2. Retention Time for Paraffins Standard Components	28
Table 3.3. Retention Time for Methanol Standard.	29
Table 3.4. Retention Time for Dimethyl Ether Standard.	29
Table 3.5. MTO Product Distribution over SAPO-47(Finer Particles)	34
Table 4.1. Product Distribution over SAPO-44 (P-6), After 10 min. Grinding.	49
Table 4.2. Product Distribution over SAPO-44 (P-6), After 15 min. Grinding.	51
Table 4.3. Product Distribution over SAPO-56 (P-28), No Grinding.	65
Table 4.4. Product Distribution over SAPO-56 (P-28), After 15 min. Grinding.	67
Table 4.5. Product Distribution over SAPO-56 (P-29), No Grinding.	68
Table 4.6. Product Distribution over SAPO-56 (P-29), After 15 min. Grinding.	70
Table 4.7. Product Distribution over Ru-SAPO-56 (Ru-P-18).	76

## LIST OF FIGURES

Figure 2.1. Illustration of the molecular sieve effect.	4
Figure 2.2. Shape Selectivity	8
a) Reactant	8
b) Product	8
c) Transition-state	8
Figure 2.3. View of two adjoining cages formed at channel intersections in the all-silica zeolite SSZ-23 (STT) showing the position of the structure directing agent TMAda <sup>+</sup> around which the frameworks forms.	15
Figure 3.1. Illustration for packed bed reactor.	27
Figure 3.2. GC Profile of Olefins Standard.	27
Figure 3.3. GC Profile of Paraffins Standard.	28
Figure 3.4. GC Profile of Methanol Standard MeOH.	29
Figure 3.5. GC Profile of Dimethyl Ether (DME).	29
Figure 3.6. Spreadsheet for MTO Analysis.	31
Figure 3.7. Close-Up View of the Quartz Tube Reactor.	32
Figure 3.8. MTO Reactor Diagram.	33
Figure 3.9. GC Product Distribution Profile over SAPO-47 (P-31) (Finer Particles), Temp= 400°C.	34
Figure 4.1. Distribution of C <sub>2</sub> – C <sub>4</sub> Olefins, DME, and MeOH over SAPO-56 (P-18), (0.6 Si), (Load = 0.504 g, MeOH flow = 0.005 ml/min, WHSV = 0.5 hr <sup>-1</sup> ).	37
Figure 4.2. Distribution of C <sub>2</sub> – C <sub>4</sub> Olefins, DME, and MeOH, SAPO-56 (P-18), (0.6 Si), (Load = 0.307 g, MeOH flow = 0.003 ml/min, WHSV = 0.5 hr <sup>-1</sup> ).	38

Figure 4.3. Temperature Effect on Product Distribution over SAPO-34 (P-5), (No Grinding).	40
Figure 4.4. Temperature Effect on Product Distribution over SAPO-34 (P-5), (After 15 min. Grinding).	40
Figure 4.5. Temperature Effect on Product Distribution over SAPO-44 (P-6), (No Grinding).	42
Figure 4.6. Temperature Effect on Product Distribution over SAPO-44 (P-6), (After 15 min. Grinding).	42
Figure 4.7. Temperature Effect on Product Distribution over SAPO-56 (P18), (0.6 Si), (No Grinding).	43
Figure 4.8. Temperature Effect on Product Distribution over SAPO-56 (P-18), (0.6 Si), (After 15 min. Grinding).	44
Figure 4.9. Distribution of Ethylene, Propylene, C <sub>2</sub> – C <sub>4</sub> Olefins, MeOH, and DME over SAPO-44 (P-6), 400°C, (No Grinding).	47
Figure 4.10. Distribution of Ethylene, Propylene, C <sub>2</sub> – C <sub>4</sub> Olefins, MeOH, and DME over SAPO-44 (P-6), 400°C, (After 5 min. Grinding).	47
Figure 4.11. Distribution of Ethylene, Propylene, C <sub>2</sub> – C <sub>4</sub> Olefins, MeOH, and DME over SAPO-44 (P-6), 400°C, (After 10 min. Grinding).	49
Figure 4.12. Distribution of Ethylene, Propylene, C <sub>2</sub> – C <sub>4</sub> Olefins, MeOH, and DME over SAPO-44 (P-6), 400°C, (After 15 min. Grinding).	51
Figure 4.13. Effect of Grinding Time over SAPO-44 (P-6).	52
Figure 4.14. Distribution of Ethylene, Propylene, C <sub>2</sub> – C <sub>4</sub> Olefins, MeOH, and DME over SAPO-34 (P-5), 400°C, (No Grinding).	53
Figure 4.15. Distribution of Ethylene, Propylene, C <sub>2</sub> – C <sub>4</sub> Olefins, MeOH, and DME over SAPO-34 (P-5), 400°C, (After 5 min. Grinding).	54
Figure 4.16. Distribution of Ethylene, Propylene, C <sub>2</sub> – C <sub>4</sub> Olefins, MeOH, and DME over SAPO-34 (P-5), 400°C, (After 10 min. Grinding).	55
Figure 4.17. Distribution of Ethylene, Propylene, C <sub>2</sub> – C <sub>4</sub> Olefins, MeOH, and DME over SAPO-34 (P-5), 400°C, (After 15 min. Grinding).	56

Figure 4.18. Effect of Grinding Time On Product Distribution. (GT = Grinding Time)	57
Figure 4.19. Distribution of Ethylene, Propylene, C <sub>2</sub> – C <sub>4</sub> Olefins, MeOH, and DME over SAPO-47 (P-31), 400°C, Coarse Particles.	58
Figure 4.20. Distribution of Ethylene, Propylene, C <sub>2</sub> – C <sub>4</sub> Olefins, MeOH, and DME over SAPO-47 (P-31), 400°C, Coarse Particles. (No Grinding).	58
Figure 4.21. Distribution of Ethylene, Propylene, C <sub>2</sub> – C <sub>4</sub> Olefins, MeOH, and DME over SAPO-47 (P-31), 400 °C, Finer Portions. (No Grinding).	59
Figure 4.22. Distribution of Ethylene, Propylene, C <sub>2</sub> – C <sub>4</sub> Olefins, MeOH, and DME over SAPO-47 (P-31), 400 °C, (Finer Particles) (After 15 min Grinding)	60
Figure 4.23. Methanol Conversion Profile over SAPO-47 (P-31), 400 °C, (Finer Particles).	61
Figure 4.24. Distribution of Ethylene, Propylene, C <sub>2</sub> – C <sub>4</sub> Olefins, MeOH, and DME over SAPO-56 (P-18), 400 °C, (0.6 Si), (No Grinding).	62
Figure 4.25. Distribution of Ethylene, Propylene, C <sub>2</sub> – C <sub>4</sub> Olefins, MeOH, and DME over SAPO-56 (P-18), 400 °C, (0.6 Si), (No Grinding).	63
Figure 4.26. Distribution of Ethylene, Propylene, C <sub>2</sub> – C <sub>4</sub> Olefins, MeOH, and DME over SAPO-56 (P-18), (0.6 Si), 400 °C, (After 15 min. Grinding).	64
Figure 4.27. Distribution of Ethylene, Propylene, C <sub>2</sub> – C <sub>4</sub> Olefins, MeOH, and DME over SAPO-56 (P-18), (0.6 Si), 400 °C. (After 15 min. Grinding)	64
Figure 4.28. Distribution of Ethylene, Propylene, C <sub>2</sub> – C <sub>4</sub> Olefins, MeOH, and DME over SAPO-56 (P-18), (0.3 Si), 400 °C, (No Grinding).	66
Figure 4.29. Distribution of Ethylene, Propylene, C <sub>2</sub> – C <sub>4</sub> Olefins, MeOH, and DME over SAPO-56 (P-18), (0.3 Si), 400 °C, (After 15 min. Grinding).	67
Figure 4.30. Distribution of Ethylene, Propylene, C <sub>2</sub> – C <sub>4</sub> Olefins, MeOH, and DME over SAPO-56 (P-29), (0.9 Si), 400°C, (No Grinding).	69

Figure 4.31. Distribution of Ethylene, Propylene, C <sub>2</sub> – C <sub>4</sub> Olefins, MeOH, and DME over SAPO-56 (P-29), (0.9 Si), 400°C . (After 15 min. Grinding).	70
Figure 4.32. Effect of Silicon Content on Olefins Selectivity over SAPO-56, (No Grinding).	71
Figure 4.33. Effect of Silicon Content on Olefins Selectivity over SAPO-56, (No Grinding).	72
Figure 4.34. Distribution of Ethylene, Propylene, C <sub>2</sub> – C <sub>4</sub> Olefins, MeOH, and DME over Spent SAPO-56 (P-18), (0.6 Si) catalyst. (After 15 min. Grinding)	73
Figure 4.35. Distribution of Ethylene, Propylene, C <sub>2</sub> – C <sub>4</sub> Olefins, MeOH, and DME over Ru impregnated SAPO-34 (Ru-P-5), 400°C.	74
Figure 4.36. Distribution of Ethylene, Propylene, C <sub>2</sub> – C <sub>4</sub> Olefins, MeOH, and DME over Ru impregnated SAPO-44 (Ru-P-6), 400°C.	75
Figure 4.37. Distribution of Ethylene, Propylene, C <sub>2</sub> – C <sub>4</sub> Olefins, MeOH, and DME over Ru impregnated SAPO-56 (Ru-P-18), 400°C.	77



## I. INTRODUCTION

With the world economy becoming more interconnected and dependent, finding new sources of energy and industrial valuable products has become very critical to remain competitive in meeting market demand. With energy demand far outstripping energy supply this focus seems more relevant than ever. In recent years the methanol to olefins (MTO) process has received wide attention as it provides an indirect route in reaching that goal. Since their discovery at Union Carbide laboratory small pore molecular sieves have been in the center of the MTO phenomenon. In catalytic reactions these microporous materials particularly silicoaluminophosphate oxides (SAPO) give a narrow range of product distribution with a high selectivity towards C<sub>2</sub>-C<sub>4</sub> olefins, however, diffusion of larger molecules through their narrow pores is very restricted. Their unique selectivity ability has spurred considerable interest in the research community in finding better ways to making them more efficient in performance and overcoming rapid coke formation brought about by larger molecules formed inside the pores. Variations in parameters such as silicon content, acid site density, acid strength, crystallite size, nature of template, silicon and aluminum source and hydrothermal conditions have been known to influence catalytic activity and selectivity towards light olefins.

In the present work, testing of various microporous SAPO catalysts has been undertaken with particular emphasis on several process parameters such as: particle

size, temperature, silicon content and metal incorporation. How these parameters are varied would indicate the extent of their influence towards light olefins selectivity, catalyst activity, and methanol conversion. To complement the SAPO testing analyses, a few other studies were pursued as well. With the available catalyst stock running low, a scale-down study was undertaken to assess the impact of process variables reduction on reaction behavior. Methanol feed, nitrogen flow and catalyst load were all reduced by a 40% margin. A study on a spent catalyst was performed in order to see if some of the catalyst activities could be regenerated in which the catalyst was ground for 15 minutes and tested for activity.

## II. LITERATURE REVIEW

### Background

The history of zeolites didn't begin until 1756 when a Swedish mineralogist by the name of Cronstedt first discovered the mineral zeolite: stilbite. This mineral which appeared like crystals would swell or enlarge when heated in a blow tube flame. And from that point on Cronstedt would characterize the mineral a '*zeolite*', the combination of two Greek words: *zeo* and *litho* meaning to boil and a stone, respectively. In 1840, Damour observed that crystals of zeolites could be reversibly dehydrated with no observable change in their transparency or morphology. Way and Thompson, who in 1850 studied the nature of ion exchange in soil, had their work expanded upon by Eichhon who showed in 1858 the reversibility of ion-exchange on zeolite minerals. Friedel, who noticed that various liquids such as alcohol, benzene, and chloroform, were occluded by dehydrated zeolites, developed the porous nature of zeolites in 1896. The behavior of zeolites as molecular sieves, a term developed by McBain 1932 was reported in 1925 by Weigel and Steinhoff. This feature which is unique to zeolites structures selectively allows passage of certain molecules within their pores while limit passage of other molecules due to their sizes and shapes (**Figure 2.1**).

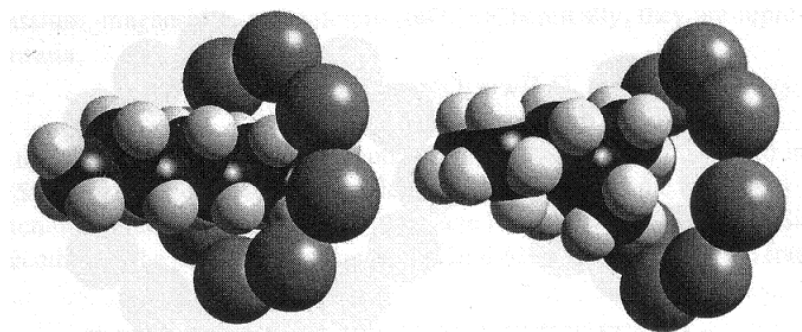


**Figure. 2.1. Illustration of the molecular sieve effect.**

The straight chain molecular normal octane (left) passes through the eight-ring aperture 5A zeolite. The branched molecule iso-octane (right) cannot. (Flanigen et al., 2001)

Many zeolites occur naturally as minerals, they are mined extensively in many parts of the world. Others, however, are synthetic – they are made for commercial uses – or produced by research scientists trying to understand more about their chemistry (See **Figure A-1**, in Appendix A). Early discovery of some twenty synthetic aluminosilicate zeolites in the late 1940's and early 1950's by researchers at the Union Carbide Laboratories and the potential applications for many of these materials formed the basis for the molecular sieve industry. To date there are more than 40 known natural zeolites and almost 200 synthetic ones, and new ones are being discovered continuously. Zeolites are microporous crystalline solids with well-defined structures. They generally contain silicon, aluminum and oxygen in their framework, with a normalized formula,  $TO_2$ , representing the concentration of elements in the composition (**Tables 2.1** and **2.2**).

Because of their unique porous properties, they are used in a variety of applications. In the western world, they are used in petrochemical cracking, ion-exchange (water softening and purification), and in the separation and removal of gases and solvents. Properties such as ion-exchange, sorption capacity, shape selectivity, catalytic activity among others are characteristics of zeolites determined essentially by their structures.

**Table 2.1. Acronyms for Framework Compositions (Flanigen et al., 1986)**

TO <sub>2</sub> , T=	Acronym	TO <sub>2</sub> , T=	Acronym
Si, Al, P	SAPO	Me, AL, P, Si	MeAPSO
Me, AL, P	MeAPO	Fe, Al, P, Si	FAFSO
Fe, Al, P	FAPO	Mg, Al, P, Si	MAPSO
Mg, Al, P	MAPO	Mn, Al, P, Si	MnAPSO
Mn, Al, P	MnAPO	Co, Al, P, Si	CoAPSO
Co, Al, P	CoAPO	Zn, Al, P, Si	ZAPSO
Zn, Al, P	ZAPO		
Other Elements:			
El, Al, P	EIAPSO	El, Al, P, Si	EIAPSO

**Table 2.2. Typical SAPO and MeAPO Framework Composition. (Flanigen et al., 1986)**  
x, y, z: mole fractions of the respective elements.

SAPO Species	$(\text{Si}_x \text{AL}_y \text{P}_z)\text{O}_2$			Net Framework Charge/TO <sub>2</sub>
	x	y	z	
5	0.14	0.45	0.41	-0.04
11	0.14	0.44	0.42	-0.02
34	0.13	0.50	0.37	-0.13
37	0.16	0.50	0.34	-0.16
MAPO Species	$(\text{Me}_x \text{AL}_y \text{P}_z)\text{O}_2$			Net Framework Charge/TO <sub>2</sub>
	x	y	z	
5	0.08	0.42	0.50	-0.08
36	0.09	0.42	0.49	-0.11
11	0.08	0.42	0.50	-0.08
44	0.14	0.36	0.50	-0.14
20	0.16	0.33	0.51	-0.14

These zeolite frameworks are made up of 4-connected networks of atoms. These networks of atoms form tetrahedrals with a silicon atom in the middle and oxygen atoms at the corners. These tetrahedrals link together by their corners to form a variety of beautiful structures. The framework structure may contain linked cages, cavities, or channels, which are of the right size to allow small molecules to enter. The limiting pore sizes are roughly between 3 and 10 Å in diameter depending on the number of rings (McCusker and Baerlocher, 2001).

There are about 130 different framework structures that are now known. Aside from having a silicon or aluminum as the tetrahedral atom, other compositions have also been synthesized, with the growing category of microporous aluminophosphates, known as ALPOs (**Table 2.3**).

Zeolites have the ability to act as catalysts for chemical reactions which take place within the internal cavities. Many organic reactions including crude oil cracking, isomerization and fuel synthesis involve the catalyzed reaction by hydrogen-exchange zeolites whose framework bound protons give rise to very high acidity. Also, zeolites can serve as oxidation or reduction catalysts, especially after metals have been introduced into the framework. Examples include titanium ZSM-5 in the production of caprolactam and copper zeolites in NO<sub>x</sub> decomposition.

A key feature in the nature of microporous zeolites is their shape-selective attribute. Three types of shape selectivity have been identified (Weisz, 1980): a) reactant shape selectivity; b) product shape selectivity; and c) transition-state shape selectivity (**Figure 2.2**). Different types of molecules enter the zeolite, but some diffuse through the channels more quickly, leaving others stuck behind, as in the purification of paraxylene by silicalite (Attfield, 2002). This feature has been given enormous attention in order to synthesize high-value chemicals for the pharmaceuticals and cosmetics industries.

**Table 2.3: Typical Structures in AlPO<sub>4</sub>-based Molecular Sieves (Flanigen et al., 1986)**

Species	Structural Type	Pore Size(nm)
<b>Very Large Pore</b>		
VPI-5	Novel	1.25
8	Novel	0.9
<b>Large Pore</b>		
5	Novel	0.8
36	Novel	0.8
37	FAU	0.8
40	Novel	0.7
46	Novel	0.7
<b>Intermediate</b>		
11	Novel	0.6
31	Novel	0.65
41	Novel	0.6
<b>Small Pore</b>		
14	Novel	0.4
17	ERI	0.43
18	Novel	0.43
26	Novel	0.43
33	Novel	0.4
34,44,47	CHA	0.43
35	LEV	0.43
39	Novel	0.4
42	LTA	0.43
43	GIS	0.43
52	Novel	0.43
56	Novel	0.43
<b>Very Small Pore</b>		
16	Novel	0.3
20	SOD	0.3
25	Novel	0.3
28	Novel	0.3

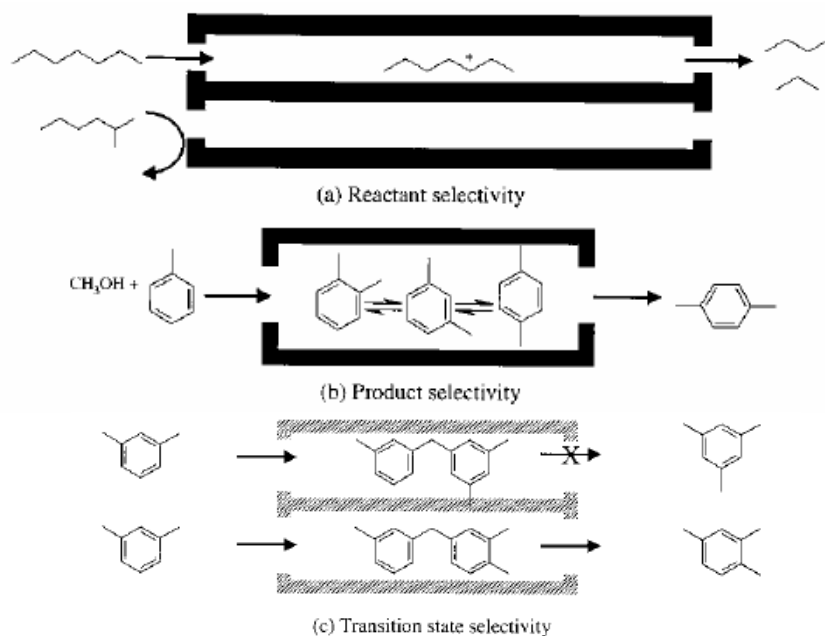


**Figure 2.2. (a) Reactant Selectivity; (b) Product Selectivity; (c) Transition-state Selectivity. (Attfield, 2002)**

### **Methanol To Olefins (MTO)**

New zeolite derived catalysts began to appear on the scene in the early 80's with the discovery of crystalline microporous aluminophosphates ( $\text{AlPO}_4$ ). Further improvement of these structures eventually led to the discovery SAPO-n framework where n denotes structure type. Since then these SAPO structures have received considerable attention due to their role in the methanol to olefins process (MTO). This process provides an indirect way of converting fossil resources to industrially valuable olefins and other value-added products.

Because of their narrow pore openings ( $\sim 0.43$  nm) microporous SAPO catalysts like SAPO-17, SAPO-18, SAPO-35 and SAPO-44 are good candidates for the MTO process as their small pore openings can only sorb straight chain molecules such as primary alcohols, linear paraffins, and olefins, but not branched isomers and aromatics.

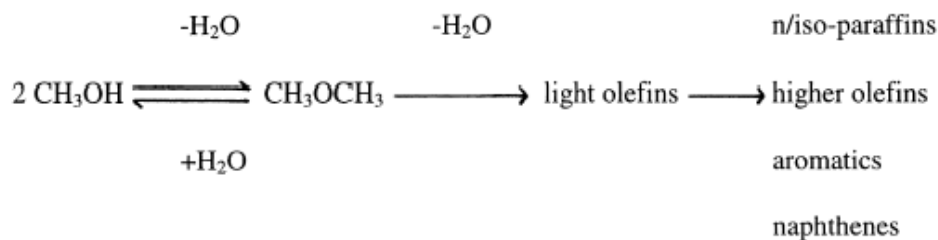


These small pore molecular sieves have been reported to be very selective towards ethylene and propylene (Wilson and Barger, 1999; Chen et al., 1994; Djieugoue et al, 1994).

Of all SAPO catalysts known to date SAPO-34 is by far the most widely studied and desirable catalyst for the MTO process. Other catalysts such as SAPO-44, SAPO-47 and SAPO-56 have received much less attention. The technology for methanol production from natural gas is widely used and well-established, however, the mechanism for converting the methanol to hydrocarbons is still not understood. The effects of adsorption, diffusion, secondary reactions including coke formation are aspects of the MTO reaction that are still not resolved.

### **Methanol to Hydrocarbons Mechanism**

The selective dehydration of methanol to olefins is a potential route for the production of C<sub>2</sub> -- C<sub>4</sub> lower olefins. Understanding the reaction mechanism is important for the development of a high efficiency catalyst. The mechanism involves C-C bond formation from C<sub>1</sub> fragments generated in the presence of certain acidic catalysts. The mechanism, though not well understood, is believed to go through a dimethyl ether (DME) intermediate:



The main reaction steps of methanol conversion to hydrocarbons can be summarized as follows: Methanol is first dehydrated to dimethyl ether. The equilibrium

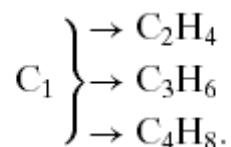
mixture formed, consisting of methanol, dimethyl ether and water, is then converted to light olefins. In the last step of this scheme, the light olefins react to form paraffins, aromatics, naphthenes, and higher olefins by hydrogen transfer, alkylation and polycondensation (Stocker, 1999).

There has been a general consensus that the intermediate in the dehydration of methanol to dimethyl ether over solid acid catalysts is a protonated surface methoxyl, which is subject to a nucleophilic attack by methanol (Chang et al., 1988). The subsequent conversion of light olefins to paraffins, aromatics, naphthenes and higher olefins, which proceeds via classical carbenium ion mechanisms with concurrent hydrogen transfer, is well known from hydrocarbon chemistry in acid media (Froment et al., 1992). However, the second step which represents the initial C—C bond formation from the C<sub>1</sub> reactants, has been the topic of extensive discussion throughout the years. For the last 25 years over 20 possible mechanistic proposals for the formation of C -- C bond have been offered and the most discussed and relevant of these mechanisms can be classified as follows:

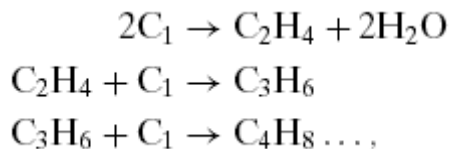
- a) The **oxonium ylide mechanism**
- b) The **carbine mechanism**
- c) The **carbocationic mechanism**
- d) The **free radical mechanim**

However, those proposed mechanisms may be broadly classified and lumped into two groups:

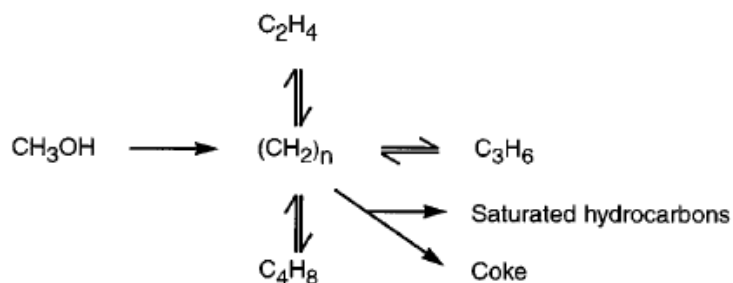
- 1) The **consecutive type mechanism:**



2) The **parallel type mechanism**:



Dahl and Kolboe (1993, 1994) showed the consecutive mechanism was not appropriate, and therefore proposed what they called a “carbon pool mechanism” which is a kind of modified parallel mechanism:



This model (**Hydrocarbon Pool Mechanism**) implies a dynamic situation in which large carbonaceous species build up inside the cages of the structure. These carbonaceous compounds are continuously adding reactants and splitting off products (Dahl et al., 1999).

### SAPO Impregnation

Because of the rapid deactivation that often occurs in methanol to olefin conversion reaction, researchers continuously look for ways to improve catalyst performance and simultaneously minimize or control the rate of coke formation. Some of the commonly used methods in modifying the SAPO framework include: impregnation, ion-exchange, and isomorphous substitution. SAPOs incorporated with transitional metal ions have been shown to have much improved activity and physical properties, with the

attribute of inhibiting unwanted side reactions such as paraffins and aromatics formations.

Fougret and Holderich (2001) in the hydration of ethylene over metal phosphates impregnated with phosphoric acid, found that impregnated aluminum, zirconium and cerium phosphate catalysts showed higher conversions than phosphoric acid on silica gel. In the case of impregnated aluminum phosphate, it was shown that the acidity of  $\text{AlPO}_4$  carrier determined by TPD of ammonia decreased dramatically during the impregnation process. They concluded the acidity was more dependent upon the existence of liquid phosphoric acid on the surface of the carriers.

Inui and Kang (1997) observed that the incorporation of nickel into the tetrahedral framework positions of SAPO-34 leads to a higher selectivity towards ethylene. They attributed the higher selectivity to framework distortion and acidity modification after the nickel incorporation.

Coke formation inside catalyst pore often plays a major factor in the deactivation of SAPO catalyst. Dubois et al (2003) studied SAPO-34 modified with Ni, Mn, Co, and Ni-SAPO-34. While these catalysts exhibited activities and selectivities towards ethylene through butene, they concluded SAPO-34 modified with Mn (MnSAPO-34) to be better based on the catalyst's lifetime (TOS = 54 hr). And as for the two Ni containing catalysts, they noticed a major difference in the methane present in the product. They thought the difference could be due to the Ni location inside the catalyst and suggested this might be an interesting and convenient way to improve catalyst lifetime for MTO reaction.

## Effect of Acid

The aluminophosphate (AIPO) framework is neutral, therefore AIPOs exhibit no acidity, which restricts their use as acid catalysts. However, introduction of silicon atoms into the framework results in Brønsted acidity and these silicoaluminophosphates (SAPOs) can be used as acid catalysts. For instance, substituting either the P or Al for a metal - Si, for instance - the framework becomes electrically negative and therefore possesses acidic properties (Derouane et al, 1988; Flanigan et al, 1986). Also, increasing the silicon amount can lead to a high acidity, therefore control of the SAPO synthesis is of extreme importance in order to obtain a high silicon content catalyst.

Chen et al (1994) prepared and studied samples of SAPO-5, SAPO-17, SAPO-18, and SAPO-34 to understand their Brønsted acidity. Using DRIFT spectroscopy for analysis, it turned out that the acidic strength present in the samples was in the following order SAPO-5 < SAPO-17 < SAPO-18 < SAPO-34. They found that smaller cages SAPO-18 and SAPO-34 yielded higher activity and selectivity towards olefins for the MTO reaction than samples SAPO-5 and SAPO-17. However, among the samples - SAPO-5 exhibited the longest life time because the accumulation of coke is less favorable for its one-dimensional 12 ring channels.

Inui and Kang (1997) incorporated crystal ingredients P, Si, and Ni into the framework of SAPO-34, and they concluded that the crystallites with the solid acid density distributed within their framework exhibited the highest ethylene selectivity (88%). These crystals also exhibited a minor deactivation due to the lower amounts of coke formation primarily to no space-restrictions on the external surface that would facilitate the growth of bulky aromatic coke.

Hocevar et al., 1993, incorporated MeAPSO-44 with: Co, Mn, Cr, Zn, and Mg. These metal incorporated catalysts were investigated for their acidity and catalytic activity along with SAPO-44,  $\text{AlPO}_4\text{-5}$  and  $\text{AlPO}_4\text{-14}$  molecular sieves and compared with SAPO-34 and NiAPSO-34. And the order of acidic strength was determined as follows:  $\text{MnAPSO-44} > \text{CoAPSO-44} \simeq \text{ZnAPSO-44} > \text{MgAPSO-44} > \text{CrAPSO-44} > \text{SAPO-44} \gg \text{AlPO}_4\text{-5} \simeq \text{AlPO}_4\text{-14}$ . As for catalytic activity, the order was as follows:  $\text{AlPO}_4\text{-14} > \text{AlPO}_4\text{-5} \simeq \text{SAPO-44} > \text{CoAPSO-44} > \text{MnAPSO-44}$ .  $\text{AlPO}_4\text{-14}$  which showed the least acidic strength displayed the highest catalytic activity, where MnAPSO-44 followed the opposite trend. However, among the samples investigated, CoAPSO-44 exhibited the highest selectivity towards ethylene production. The authors concluded that metal type could play a role in degree of selectivity. However, when samples MeAPSO-44 and MeAPSO-34 were compared side by side, the -44 structures were 3 times more selective to olefins than the -34 structures.

### **Template (Structure Directing Agent)**

One particular useful strategy in the formation and design of new microporous materials has been the inclusion of quaternary ammonium ions (as a hydroxide or halide salt) or organic amines in the synthesis mixture. These organic guest molecules act as structure directing agents and are incorporated into the final product where they replace the usual charge compensating metal cations and other extra-framework molecules. Shape and size (**Figure 2.3**) of the organic guest molecules play important roles that can lead to the formation of new and novel microporous structures that often cannot be produced by any other methods. In other words, these organic guests provide the basis

upon which host structures could be crystallized and retained the shape consistent with the respective template. They fill the void space around which the framework of the microporous material forms but for which a particular structure can be formed by more than one particular type of guest molecule and guest molecules that are specific to the formation of a certain framework structure only. For instance, SAPO-17 and SAPO-44 – ERI and CHA, respectively – can be synthesized with morpholine as the template; the same type of zeolite (CHA) may be crystallized using various templates i.e.: SAPO-34, SAPO-44, and SAPO-47.

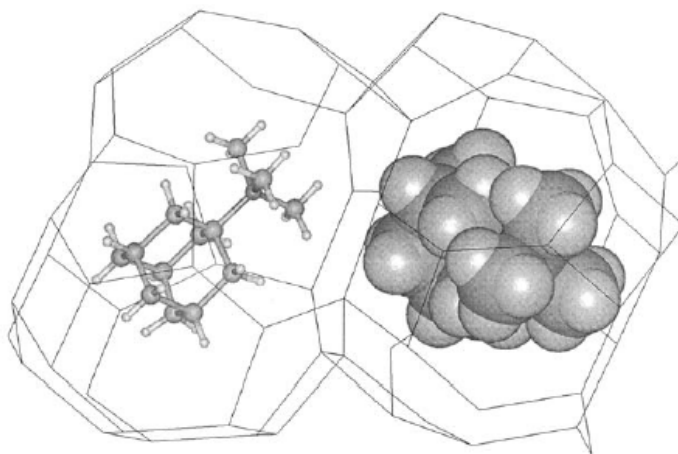


**Figure 2.3.** View of two adjoining cages formed at channel intersections in the all-silica zeolite SSZ-23 (STT) showing the position of the structure directing agent TMAda<sup>+</sup> around which the framework forms. (Attfield, 2002)

Tetrapropylammonium and tetraethylammonium hydroxides are good templates for obtaining CHA structures. Diethylethanolamine and cyclohexylamine may also act as templates giving rise to more or less pure phases. Morpholine and methylbutylamine exhibit appreciable selectivities towards the formation of pure SAPO-34 and SAPO-47, respectively (Dumitriu et al., 1977).

But obtaining pure phases of a particular SAPO can be tricky as factors such as chemical concentration, pH value of the synthesis gel, and sequence of chemical mixing

impact significantly the final product. For instance the order of chemical mixing can determine whether a pure phase or combination of phases is realized. Although SAPO-34 could be synthesized with piperidine as a template, Dumitriu et al (1977) had found that SAPO-34 and SAPO-20 were competing phases at high piperidine concentrations, whereas SAPO-3, SAPO-17 and SAPO-35 are the phases present at low template concentrations.

The SAPO-5 structure can transform into the SAPO-34 structure with increase of crystallization time. Jung et al.(2003) found this to be due probably to the relative stability of the two phases at the reaction conditions. But SAPO-5 can be selectively formed by fast crystallization of alkaline or acidic reactants gels.

Prior to testing, catalysts must undergo calcinations to remove the organic guest molecules (template) present in the framework. This is often accomplished by heating the material under flowing oxygen or air at temperatures greater than 400 °C, or in some instances the guest molecule can be washed out under acidic or basic conditions. During the template removal, some host molecules undergo structural collapse. Collapse occurs when the constituent bonds of the framework are too weak to maintain the structural integrity of the framework without the aid of the favorable electrostatic, hydrogen bonding or van der Waals interactions between the components of the framework and the structure directing agent (Attfield, 2002).

### **Coke Formation (Catalyst Deactivation)**

Loss of catalytic activity presents a major problem in regard to catalysis. There are three main categories into which the loss of activity can be divided: sintering or



aging, fouling or coking, and poisoning. Of those three types, the deactivation by coking or fouling is common to reactions involving hydrocarbons. Basically, coke material is being deposited on the surface of the catalyst as the reaction proceeds.

Little attention was paid to this phenomenon in the early days of zeolite catalysis except for a few notable studies by Eberly et al. (1966). But beginning in the late seventies, many papers dealing with coke formation continued to emerge due in no small part to industrial applications and fundamental research on zeolite catalysis.

Voorhies, in 1945, had developed a model to quantify the amount of coke deposited on the surface after some time  $t$ :

$$C_c = At^n$$

where  $C_c$  is the concentration of carbon on the surface and  $n$  and  $A$  are fouling parameters dependent of the feed rate. This model has been found to hold for a wide variety of catalysts.

The deactivation of all zeolites has been considered to occur in three ways depending on the coke content (Chen et al., 1994):

- (a) Limited access for the reactant molecules on the active sites (site coverage);
- (b) blockage of the access to the active sites in the cavities (or in the channel intersections) where coke molecules are located;
- (c) blockage of the access to the active sites in the cavities (or in the channel intersections) where there are no coke molecules.

Coke by its nature appears to be mainly paraffinic, but polycyclic aromatics have been found to be present as well (Aguayo et al., 1999). Eisenbach and Gallei (1974) visualized this process as the build-up of very bulky, polyaromatic systems with even graphite-like structure. Other aspects of their presence offered new insight into their nature. According to Froment et al. (1992), the deactivation by coke and its effect on the

product selectivities depend on the way the coke is deposited on the catalyst. Bos et al. (1995) developed a kinetic model for the MTO process based on small pore molecular sieve catalyst of the class SAPO-34. They have found the coke content of the catalyst to be the main factor governing selectivity and activity of the catalyst.

One other way in understanding catalyst deactivation has to account for one important factor: pore structure. Because these small-pore zeolites adsorb linear hydrocarbons but exclude the larger branched or aromatic hydrocarbons, these bulkier species, when formed internally, cannot diffuse out. Since Sahini and Tsotsis (1985) recognized that catalyst deactivation is a percolation phenomenon, a number of approaches have used the percolation concepts for modeling catalyst deactivation (Mann et al., 1986; Beyne et al., 1990, 1993).

Chen et al. (1994) have recently studied the role of coke deposition in the conversion of MeOH to olefins over SAPO-34. They found that the coke formed from oxygenates, referred to as active coke, promoted olefin formation, while the coke formed from olefins, referred to as inactive coke, only had a deactivating effect. In addition coke was found to reduce the DME diffusivity, which enhances the formation of olefins, particularly ethylene (Wilson and Barger, 1999).

### **Role of Water**

To control product distribution and diminish coke effect over time in the course of catalytic reactions, methanol is often coupled with water in the feed stream. It has been proposed that the presence of water in the feed lessens coke formation, either by

converting Lewis to Brønsted sites or by competing for surface sites with coke precursors (Aguayo et al., 1999).

When the reaction is carried out with SAPO-34, Liang et al. (1990) and Marchi and Froment (1991) have proven that the presence of water in the feed gives way to a considerable increase in the selectivity to olefins C<sub>2</sub> - C<sub>4</sub>, which is not observed when nitrogen is used as the diluent. Froment et al. (1992) attribute this result to the competition of water against olefins for adsorption on the strong acid sites.

Also water present in the zeolite nanocage significantly increases ethylene selectivity at the expense of propene, and that has been attributed to enhanced state shape selectivity. According to Song et al. (2001) co-feeding of water with methanol significantly increased the average number of methyl groups per ring at steady state relative to identical conditions without additional water, and also increased ethylene selectivity, apparently through transition state shape selectivity (**Figure 2.2(c)**).

Zhao and Wojciechowski (1996) carried out a rigorous study which has proven that an alteration in the mechanism of 2-methylpentane cracking over USHY zeolite occurs because of the presence of water in the reaction medium. In the MTO process on HZSM-5 zeolite, the presence of water gives way to an increase in the selectivity to light olefins (by decreasing the formation of aromatics) and also changes their distribution by increasing the ethene selectivity.

### **Catalyst Regeneration**

Many studies have shown thermal treatment to be effective in reversing coking effects and prolonging reaction operation. This technique is sometimes used in

conjunction with a fluidized bed scheme where spent catalyst can be re-circulated along the reactor to be treated at elevated temperature. For example, it has been found that spent catalyst completely recovers its activity by burning the deposited coke with air at a temperature of 823 K when operating in reaction generation cycles (Gayubo et al., 2000).

Temperature choice is significant in catalyst regeneration. Cai et al. (1995) had found that catalysts regenerated at temperature higher than 550 °C took much shorter to decoke (10 min) compared to those treated at lower than 550 °C (30 min). The activity and selectivity of the catalyst are almost the same as those of the fresh catalysts after long time treatment in steam or in air flow at 800 °C. X-ray diffraction results show only little decrease of the crystallinity of the treated samples, as compared with that of the fresh catalysts.

This strategy is considered as the most suitable by Mobil for the MTO process on ZSM-5 zeolites. However, results for on-stream testing in a fixed bed reactor shows that activity of SAPO-34 had decreased within about 2 hr under the reaction conditions 450 °C, WHSV (MeOH) = 0.6hr<sup>-1</sup>. Thermal treating of the catalyst in a stream of air at 500 °C – 650 °C completely restores its activity (Cai et al., 1995).

### **SilicoAluminoPhosphate (SAPO)**

Small pore molecular sieves such as SAPO-34 have been the subjects of extensive studies primarily due to their inclination for lower olefins selectivity and high activity (Wilson and Barger, 1999). Depending on the reaction conditions, lower olefins selectivity up to 90% could be easily achieved at 100% methanol conversion. Such selectivity performance is attributed to their narrow pore structures. However, their high

activity is primarily due to the high Brønsted acidity arising from isolated silicon substitution for framework phosphorus. Other small pore molecular sieves include SAPO-44 and SAPO-47 with an 8 oxygen ring and a pore aperture of 0.35 – 0.45 nm.

SAPO-34, SAPO-44 and SAPO-47 are analogs of the Chabazite Structure (CHA) with stacking sequence of AABBC; cell dimensions of  $a = 13.675 \text{ \AA}$  and  $c = 14.767 \text{ \AA}$ ; space group R3m; and the number of atoms per unit cell ( $Z$ ) = 36. SAPO-56 on the other hand, is a novel type catalyst. Although it is classified as a small molecular sieve, it belongs to the (AFX) structure type with a stacking sequence of AABBCBB formation with cell dimensions of  $a = 13.674 \text{ \AA}$ ,  $c = 19.695 \text{ \AA}$  and space group of  $P6_3/mmc$  with  $Z$  (atoms per unit cell) = 48. But its pore size is equivalent to that of SAPO-34 at 0.43 nm with 8-oxygen ring size (Wilson et al., 1999).

### **Particle Size and Shape**

Particle size and shape are of primary importance because they determine a wide range of physical and chemical properties. Both the particle size distribution and the particular shape have a strong effect on particle product quality. For example, in the area of drug delivery, the degree and rate at which a substance is absorbed into a living system or is made available at the site of physiological activity often depends on both the particle size and shape. In paint opacity is a function of size, whereas coating layer properties are a function of the shape distribution (Lohmander, 2000). In catalysis, shape is important because it affects catalyst effectiveness (Buffham, 2000).

Crystal size and, more importantly, the crystal pore size, have major influences in the catalysis deactivation rate and life (Wilson and Barger, 1999). The strict pore

restriction imposed by small aperture crystals enable the buildup of branched compounds inside the compounds triggering secondary reactions which facilitates coke deposits inside the pores and ultimately the rapid deactivation of the catalysts (Guisnet, 2002). In the process, olefins production which is highly desirable is often suppressed.

Another important factor in particle analysis is particle breakage. It is of interest because it occurs both naturally and in many manufacturing processes. These processes span a range of industries including pharmaceuticals, pigments, agricultural chemicals, and foods. It is of particular interest in chemical processing plants because it can have a strong impact on unit operations. Breakage may be beneficial and intentional as in the case of crushing; or it may be detrimental and unintentional as in the case of fragmentation and attrition in fluidized bed reactors and combustors (Shamlou et al., 1990).

According to Miller (1994) and Campello and Lafont (1995) the geometry and the size of the SAPO channels were found to be a prerequisite for the preferential formation of monobranched alkane isomers. They noted further that medium-pore silicoaluminophosphate molecular sieves were found to be most suitable for the selective hydroisomerization of linear alkanes. From a comparative study of large and small crystals of Pt/SAPO-11 it was concluded that small crystals were more active in the hydroisomerization of n-octane owing to the higher number of pore entrances present as the crystal size decreases (Miller, 1992). It was hence suggested that parameters such as the acidity, the pore structure and the grain size of SAPO catalysts could affect their hydro-isomerization behavior.

While catalyst grain size can be influenced greatly during the synthesis phase of preparation, mechanical treatment (ball milling) of fresh catalyst particles also lends itself as a viable route for obtaining much smaller particle size. In addition to the lowering of particle size, other advantages offered by this method include: increase of specific surface area and change in particle morphology. Kosanovic et al. (1992) studied the effect of mechanical treatment on physicochemical properties of several zeolites. XRD analysis of the treated particles revealed loss of crystallinity indicated by the decrease of the peak intensities as a function of milling time. SEM analysis of one of the samples showed formation of polydispersed powder with irregular particle shape. IR spectra during the ball mill showed decrease of cation-exchange capacity and an increase of solubility caused by breaking of Si-O-Si and Si-O-Al bonds in the zeolite structure.

### III. EXPERIMENTAL

#### Samples Preparation

All original SAPO catalysts utilized for this research were prepared by Dr. Prakash M. Adekkanattu based on information provided on the literature with the following chemicals: orthophosphoric acid (85 wt %), aluminum isopropoxide (98+ %), pseudoboehmite (Catapal-B, 70 wt %  $\text{Al}_2\text{O}_3$ ), fumed silica (99.8 wt %, 380  $\text{m}^2/\text{g}$ ), colloidal silica (Ludox LS, 30 wt %), nickel acetate tetra hydrate (99.98 wt %), cyclohexylamine (99+ wt%), NN-diisopropylethylamine (99 wt%), morpholine (99+ wt %), tetraethylammonium hydroxide (30 wt % in water), methylbutylamine (96 wt %), N,N,N',N' -tetramethylhexane 1,6-diamine (99 wt %). All the chemicals except pseudoboehmite were from Aldrich. Pseudoboehmite was from Vista. Detailed information including temperature, crystallization time, pH, and gel composition for all samples in addition to XRD analysis can be found in a report submitted by Adekkanattu, (2003).

#### Modified Catalysts

Three samples (SAPO-34, SAPO-44, and SAPO-56) were sent to Dr. Richard Ernst at the University of Utah to be impregnated with ruthenium using a vapor phase vacuum technique (Wilson et al., 1986). Appropriate amounts of bis (2,4-dimethylpentadienyl) ruthenium were added to each sample to give a 1% Ru load. The



SAPO-56 sample incorporated the Ru compound relatively quickly - within 16 hrs. The SAPO-44 incorporated the Ru compound over 72 hrs and the SAPO-34 never fully incorporated the Ru compound, even at 40 °C for 168 hours. All the samples took on a yellow color after incorporation. After the incorporation each sample underwent an oxidation step where colors changed to either black or charcoal gray.

### **Particle Characterization**

For characterization purposes SEM analysis was performed at the Auburn University Research Instrumentation Facility. Samples were studied by scanning with a Zeiss DSM940 microscope. Prior to introducing samples inside the machine chamber, particles were treated with a gold coating.

Because of the large amount of agglomerates formed when particles undergo mechanical treatment (grinding operation), samples were often mixed with acetone then sonicated prior to SEM analysis in order to spread particles for proper size characterization.

### **SAPO-47 Fractionation**

Particle sizes revealed by SEM observation for SAPO-47 were not as uniform as other SAPOs analyzed. With that in mind, it was decided that particles should be separated into their respective sizes and tested in catalytic reactions. Results from those various size particles would be analyzed and compared with ground particles. Particles were separated by water settling and divided into two sets: coarse and finer fractions.

## Grinding of Particles

In order to achieve smaller sized particles, use of planetary ball mills is often required to reduce the particle size. Ball milling is recognized as an efficient way to optimize powder properties (Kano, J. et al., 1998). For our study we employed a grinder (Wig-L-Bug, Model 30, #3110-3A) from Dentsply/Rinn (**Figure A-2**) to enable us to process small amounts of samples available for experiments. This machine operates at 3200 RPM with 110V, 0.65 Amp and 60 Hz. Sample preparation can be reproduced from sample to sample by replicating the cycle time. Grinding operation is controlled by a 30-min timer or manual button.

The grinder comes with a small agate vial (1 5/16" h x 9/16" dia.) and a capacity of approximately 2 ml. Once the sample is placed inside the vial, a small ball (about 1/4" dia.) is added to the sample and the vial is tightly capped with the cover. Finally, it is mounted and securely seated on the grinder. When the system is operating the sample material is hit alternately from various sides by the grinding ball while the grinder performs radial vibrations in a horizontal setting.

SEM analysis revealed extensive particle size reduction after grinding operations. For SAPO-34 and SAPO-44, effect of grinding time on product distribution and catalyst activity was studied. Grinding times (GT) were chosen as: 5, 10, and 15 minutes.

Because of the finer sized particle resulting from the grinding process and the void constraints imposed by the particle contacts, reactions over ground particles often experienced great pressure drop and brief flow fluctuation as a consequence (**Figure 3.1**).

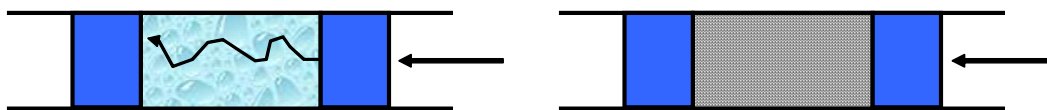


Figure 3.1. Left-hand legend, reacting fluid channels out freely without difficulty around catalyst particles. Right-hand legend, fluid moves along particles with great difficulty.

### Standard Analysis (Olefins, Paraffins, DME and MeOH)

Knowing that products resulting from the MTO catalytic reactions consist primarily of olefins and paraffins and oxygenates, a set of calibrations was devised so that accurate recognition of the resulting peaks could be obtained. Using a syringe (SGE, P/N 005250, 100 $\mu$ l) a 100  $\mu$ l sample was extracted from a mixture of C<sub>2</sub> – C<sub>6</sub> olefins (Matheson Tri-Gas, GMT10358TC) then injected into the GC for calibration. The same procedure was repeated for the C<sub>1</sub> – C<sub>6</sub> paraffins (Matheson Tri-Gas, GMT10411TC). From this operation, retention time values for each compound were obtained and recorded for olefins and paraffins. The area under each peak represents large quantities of ions proportional to the number of organic molecules for each organic compound present (**Table 3.1, Figure 3.2**).

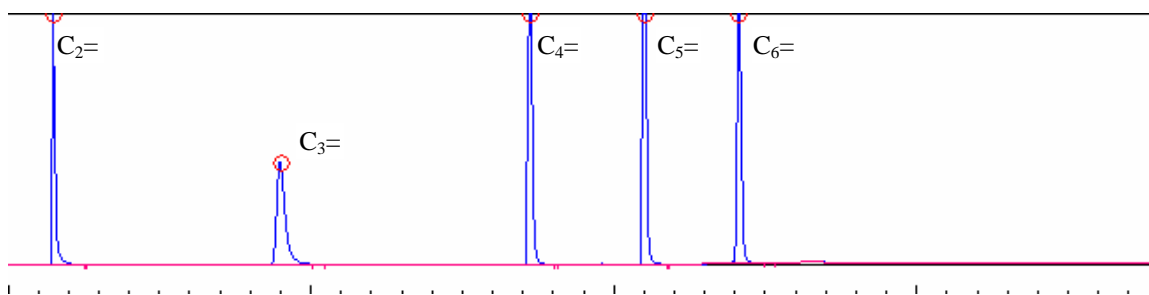
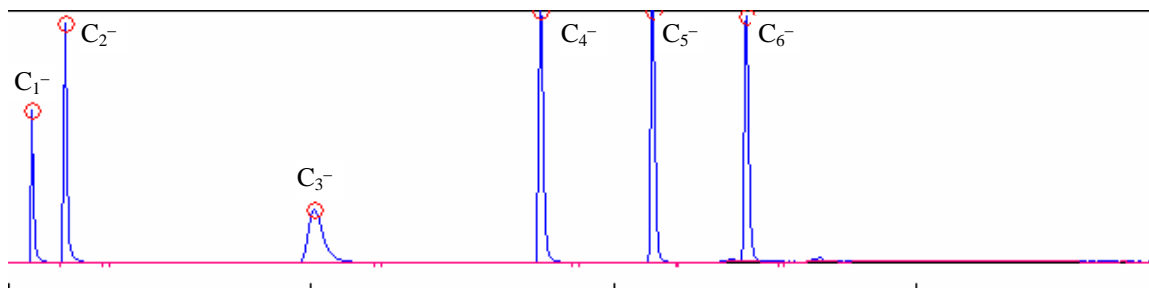


Figure 3.2. GC Profile of Olefins Standard.

**Table 3.1. Retention Times for Olefins Components.**

Component	Symbol	Retention Time (min)	Area	Area %
Ethylene	C <sub>2</sub> =	1.433	89.003	12.422
Propylene	C <sub>3</sub> =	8.933	125.471	17.512
1-Butene	C <sub>4</sub> =	17.166	161.497	22.541
1-Pentene	C <sub>5</sub> =	20.933	174.431	24.346
1-Hexene	C <sub>6</sub> =	24.066	166.067	23.179

**Figure 3.3. GC Profile of Paraffins Standard.****Table 3.2. Retention Times for Paraffins Components.**

Component	Symbol	Retention Time (min)	Area	Area %
Methane	C <sub>1</sub> -	0.75	50.888	7.237
Ethane	C <sub>2</sub> -	1.85	88.531	12.591
Propane	C <sub>3</sub> -	10.133	134.783	19.169
Butane	C <sub>4</sub> -	17.55	149.33	21.238
Pentane	C <sub>5</sub> -	21.233	152.396	21.674
Hexane	C <sub>6</sub> -	24.316	127.193	18.09

Retention times determination for methanol (MeOH) and dimethyl ether (DME) followed differently. In the case of methanol, with no catalyst inside the reactor tube, both N<sub>2</sub> and MeOH ( set at 36.0 sccm and 0.003 ml/min - respectively ) were allowed to flow at 400°C and atmospheric pressure. One hour later a sample (exactly 100 µl) was extracted from the collection point of the reactor and injected into the GC FID port to obtain the MeOH retention time. For dimethyl ether, 1.0 ml. of pure DME was injected into a nitrogen filled glass collecting bulb (V = 29.7 ml.) and allowed to mix (N<sub>2</sub> + DME)

for about 60 minutes. From that mixture 100  $\mu$ l was extracted, and then injected into the FID port of the GC to obtain the DME retention time.

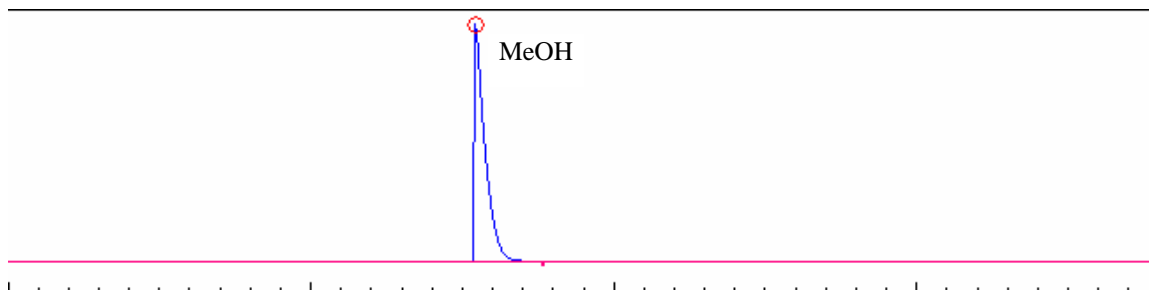


**Figure 3.4. GC Profile of Methanol (MeOH) Standard.**

**Table 3.3. Retention Times for Methanol (MeOH).**

Component	Symbol	Retention Time (min)	Area	Area %
Methanol	MeOH	15.433	1252.2	100

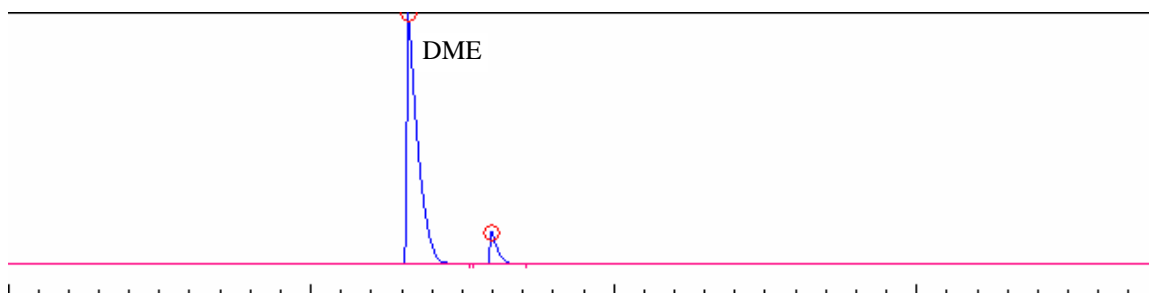


**Figure 3.5. GC Profile of Dimethyl Ether (DME) Standard.**

**Table 3.4. Retention Times for Dimethyl Ether (DME) Component.**

Component	Symbol	Retention Time (min)	Area	Area %
Dimethyl Ether	DME	13.183	1457.09	92.4737
Other		15.933	118.59	7.5263

### 3.7 Product Analysis (Actual Runs)

Product composition was analyzed by a GC (Varian 3000) equipped with a Flame Ionization Detector (FID) using a Plot-Q capillary column (Agilent, P/N: 19095P-Q04,

S/N: 60231117) with column length being 30 m, inside diameter being 0.543 mm, and film thickness about 40.0  $\mu\text{m}$ . This is a polystyrene-divinylbenzene bonded based column made specifically for hydrocarbon (Olefins, Paraffins, and Oxygenates) separation.

As reactions proceeded, manual injections were made hourly into the GC. Data handling was performed by PeakSimple Chromatography Data Systems (Model 203, 220 V) mounted in the GC via a 20-bit high resolution A/D board. Data can be acquired at the rate of 50 Hz in one channel. Each separated component is identifiable from their characteristic retention time. PeakSimple software enables quick and easy data analysis which otherwise would have required enormous amount of time such as when an HP3396A integrator was employed for this task. After the reaction stopped, data were translated into an Excel spreadsheet for product analysis (**Figure 3.6**). Detailed information about the calculations can be found in Appendix C.

16-Nov		1	TOS hr	StopWatch Time	16.3	s	WHSV	0.5	hr <sup>-1</sup>
MeOH flow	0.003	mL/min		Outlet Gas Flowrate	36.81	ml/min			
Catalyst weight	0.306	g		Outlet molar flowrate	0.00150	mol/min			
peaks	name	Retention Time	standard ppm	Standard Area for 100 $\mu$ L	Sample peak area 100 $\mu$ L	ppm of sample product	% of compound	mol/min of compound	mol C / min
C1	methane	0.75	1000	50.888	40.716	800	4.00	1.20E-06	1.20E-06
C2	ethane	1.85	1000	88.531	26.309	297	1.48	4.47E-07	8.94E-07
C2=	ethylene	1.433	1000	89.003	724.24	8137	40.64	1.22E-05	2.45E-05
C3	propane	10.133	1000	134.783	198.033	1469	7.34	2.21E-06	6.63E-06
C3=	propene	8.933	1000	125.471	816.379	6507	32.50	9.79E-06	2.94E-05
C4	C4	17.55	1000	149.33	207.026	1386	6.92	2.09E-06	8.34E-06
C4=	1-butene	17.166	1000	161.497	79.006	489	2.44	7.36E-07	2.94E-06
C4=			1000	161.497	32.742	203	1.01	3.05E-07	1.22E-06
C5	C5	21.233	1000	152.396	63.165	414	2.07	6.24E-07	3.12E-06
C5=		20.933	1000	174.431	17.209	99	0.49	1.48E-07	7.42E-07
C6	C6	24.316	1000	127.193	20.715	163	0.81	2.45E-07	1.47E-06
C6=		24.066	1000	166.067	9.33	56	0.28	8.45E-08	5.07E-07
DME		13.183	33670	1457.09	0	0	0.00	0.00E+00	0.00E+00
MeOH		15.433	40075	1252.2	0	0	0.00	0.00E+00	0.00E+00
Total					2234.87	20021		3.01E-05	8.09E-05
							total products, moles	3.01E-05	
Methanol IN (moles/min)		7.416E-05					methane sel	4.00	
Carbon IN (mol/min)		7.416E-05		SUM of C2= to C4=			ethylene sel	40.64	
Carbon OUT (mol/min)		8.094E-05		76.60			Propylene sel	32.50	
Carbon OUT - Carbon IN		6.781E-06					others sel	22.09	
% Gain		9.1					C2-C4 sel	76.598847	
							Methanol conv	100.00	

Figure 3.6. Spreadsheet for MTO Analysis.

## Reaction Procedures

MTO reactions were performed in a quartz tube, fixed-bed reactor (**Figures 3.7** and **3.8**). The process was continuous and pressure was maintained at 1 atm. Temperature was kept fixed at specific designated setpoint, 400 °C. Prior to catalytic testing, 0.307 (+/- 0.003) g was loaded inside the quartz tube reactor firmly held between two pieces of quartz wool to secure it in place. If wool was too tightly pressed, a large pressure drop resulted. This is often the case when ground particles are in the bed even when the wool plugs are not too tight. The reactor tube is then placed inside the furnace (Lindberg/Blue, TP55035A - 1) equipped with a UP 150 Controller. Nitrogen (carrier gas) flow is turned on to precondition the catalyst for about 1 hr. During this time, soap

bubble (Snoop) solution is used to check for possible gas leak(s) along the reactor lines. In the second hour the furnace is turned on. It takes about 1 hour for the furnace to reach the setpoint (reaction temperature). Temperature was monitored by a thermocouple placed in a quartz probe well inside the catalyst bed. The temperature observed in the catalyst bed (400 °C) was always greater than the furnace temperature setpoint (384 °C). When the catalyst bed temperature (400 °C) was reached liquid methanol was pumped (KD Scientific, SN. 12953, Model 101) to the system at a rate of 3  $\mu\text{l}/\text{min}$  (0.003 ml/min). Up to this point 3.0 hours have already elapsed plus an additional 1 hour before the first data point is taken for analysis. For every data point, a check is made for leaks as mentioned before and effluent gas flow was measured via the bubble flow meter and recorded.

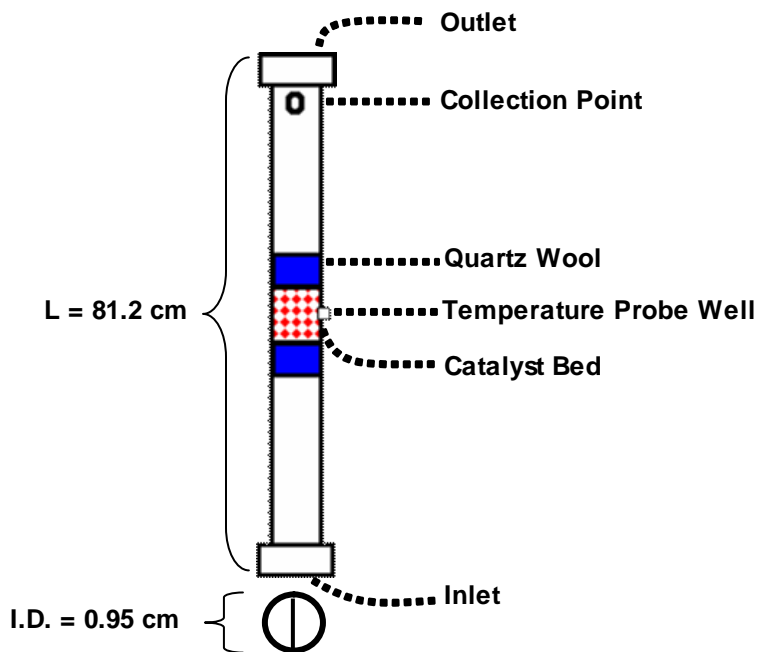


Figure 3.7. Close-Up View of the Quartz Tube Reactor



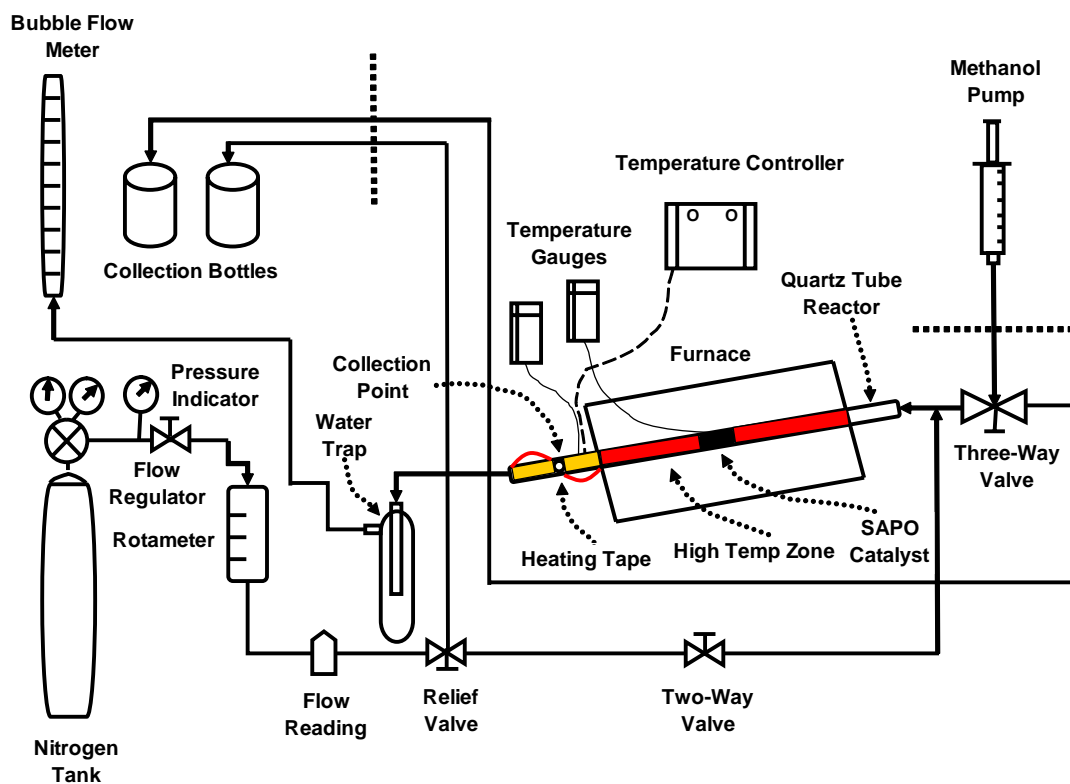


Figure 3.8. MTO Reactor Diagram.

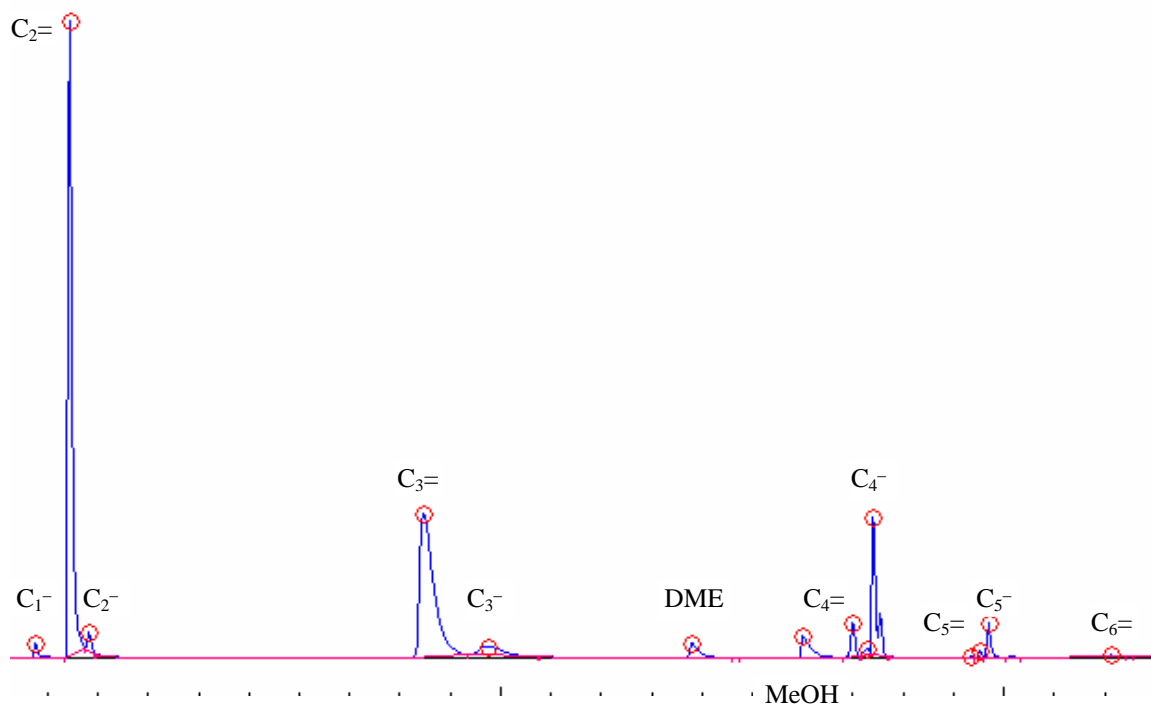


Figure 3.9. GC Product Distribution Profile Over SAPO-47 (P-31), (Finer Particles), Temp=400°C.

**Table 3.5. MTO Product Distribution over SAPO-47 (P-31), (Finer Particles).**

<b>Component</b>	<b>Symbol</b>	<b>Retention Time (min)</b>	<b>Area</b>	<b>Area %</b>
Methane	C <sub>1</sub> <sup>-</sup>	0.716	14.798	0.9361
Ethylene	C <sub>2</sub> <sup>=</sup>	1.4	587.254	37.1495
Ethane	C <sub>2</sub> <sup>-</sup>	1.783	15.688	0.9924
Propylene	C <sub>3</sub> <sup>=</sup>	8.433	584.44	36.9715
Propane	C <sub>3</sub> <sup>-</sup>	9.7	63.769	4.034
Dimethyl Ether	DME	13.75	36.624	2.3168
Methanol	MeOH	15.966	55.158	3.4893
Butene	C <sub>4</sub> <sup>=</sup>	16.95	36.79	2.3273
		17.25	8.154	0.5158
Butane	C <sub>4</sub> <sup>-</sup>	17.366	139.684	8.8364
Pentene	C <sub>5</sub> <sup>=</sup>	19.3	1.003	0.0634
		19.483	4.206	0.2661
Pentane	C <sub>5</sub> <sup>-</sup>	19.65	28.501	1.803
Hexene	C <sub>6</sub> <sup>=</sup>	22.083	4.718	0.2985

### Temperature Method

This study was conducted primarily to assess temperature effects on product distribution, and catalyst deactivation. Dubois (2002), in her thesis, undertook such a study over SAPO-34. Here, however, we extend that study to SAPO-44 and SAPO-56. Basically, the idea is same as we had done in other experiments with WHSV being the same (about 0.5 hr<sup>-1</sup>), except temperature is varied from 300 °C to 500 °C at 50 °C increments. At each temperature, reaction was allowed to run for one hour before sample extraction. After sample extraction, the temperature was raised to the next temperature setpoint and reaction was again allowed to proceed for another hour before the next extraction. This process was repeated until temperature had reached 500 °C.

## IV. RESULTS AND DISCUSSIONS

In this section details of the MTO experiments will be analyzed and the results will be compared with related works by Dubois (2002) and Adekkanattu (2003). Catalyst particles were analyzed using SEM. In addition three of the original SAPO samples were incorporated with ruthenium (SAPO-34, -44, and -56(0.6 Si)) in Dr. Richard Ernst's lab at the University of Utah. These incorporated samples were investigated to confirm if the ruthenium did indeed confer any improvement in the catalysts' performance.

All reactions reported here were operated under atmospheric pressure, with methanol delivery at a rate of 0.003 ml/min, and a catalyst loading of 0.307 (+ / - 0.003) g. Catalyst bed temperature was maintained at 400 °C. To ensure that a good separation of olefins and paraffins components derived from the product mixture takes place, the GC was set with the following temperature program: initial temp set at 40 °C, hold for 10 min, then ramp at a rate of 10 °C/min to 100 °C, hold for 15 min, again ramp at a rate of 10 °C/min to finally 170 °C.

### **SEM Analysis**

All SEM micrographs can be found in Appendix B. Examination of the micrographs shows distinct shape variations among all the present SAPO materials. SAPO-34 shows very well defined cubic morphology with particle size varying between 12 to 14  $\mu\text{m}$ . SAPO-44 shows intergrowth of cubic crystals to form circular or oval discs

with sizes ranging between 45 and 55  $\mu\text{m}$ . SAPO-47 crystallized in widely varying crystallite sizes between 35 to 220  $\mu\text{m}$  with very irregular cubic morphology. SAPO-56 had been synthesized with varying silicon amounts (0.6 – 0.9). The effect of these silicon concentrations can be observed in the relative morphologies. For instance, at low concentrations of (0.3 Si) the crystal takes on a hexagonal shape with sizes varying between 60 to 70  $\mu\text{m}$ . However, when the silicon amount was increased to (0.6 Si) the crystal appears more like a disk with sizes varying between 50 to 60  $\mu\text{m}$ . At (0.9 Si) the crystal shape approaches more of a doughnut shape with sizes varying between 80 to 90  $\mu\text{m}$ . Morphologies for the ruthenium modified samples are very close to the corresponding unmodified types.

### **Scale-Down Analysis**

In earlier studies it was common practice to use 500 mg of SAPO as a standard loading capacity for each run while the nitrogen and methanol were maintained at 60 sccm and 0.005 ml/min, respectively, with weight hourly space velocity (WHSV) maintained at 0.5  $\text{hr}^{-1}$ . However, anticipating continued use of such a quantity would rapidly deplete our catalyst stockpile, we decided as a first task to conduct a scale-down analysis to ascertain as to whether any significant difference would occur both in terms of catalyst activity and product distribution profile. For this analysis, 40% less catalyst (300 mg) was charged in the reactor. Similarly, nitrogen and methanol flows were scaled back by the same factor (40%) thereby ensuring same WHSV of 0.5  $\text{hr}^{-1}$  in both operations. This study can appropriately be summarized as follows:

- Standard method (Load = 500 g, N<sub>2</sub> flow = 60 ml/min, MeOH feed = 0.005 ml/min)
- Scale-down method (Load = 300 g, N<sub>2</sub> flow = 36 ml/min, MeOH feed = 0.003 ml/min)

The catalyst of choice for this study was SAPO-56 (0.6 Si). While a similar study was conducted on CoSAPO-34, our discussion in this section refers exclusively to results from the SAPO-56 (0.6 Si) experiments.

**Figures 4.1** and **4.2** depict results for activity over SAPO-56 (0.6 Si). From these figures it seems obvious that both catalysts exhibited similar profiles. From hour 6 and beyond both DME and MeOH reached their plateau (**Figure 4.1**) where they maintained the same levels for the remainder of the experiment. Judging from that result it became logical that a similar trend or pattern would follow in **Figure 4.2** so this experiment was immediately stopped at the 7<sup>th</sup> hr.

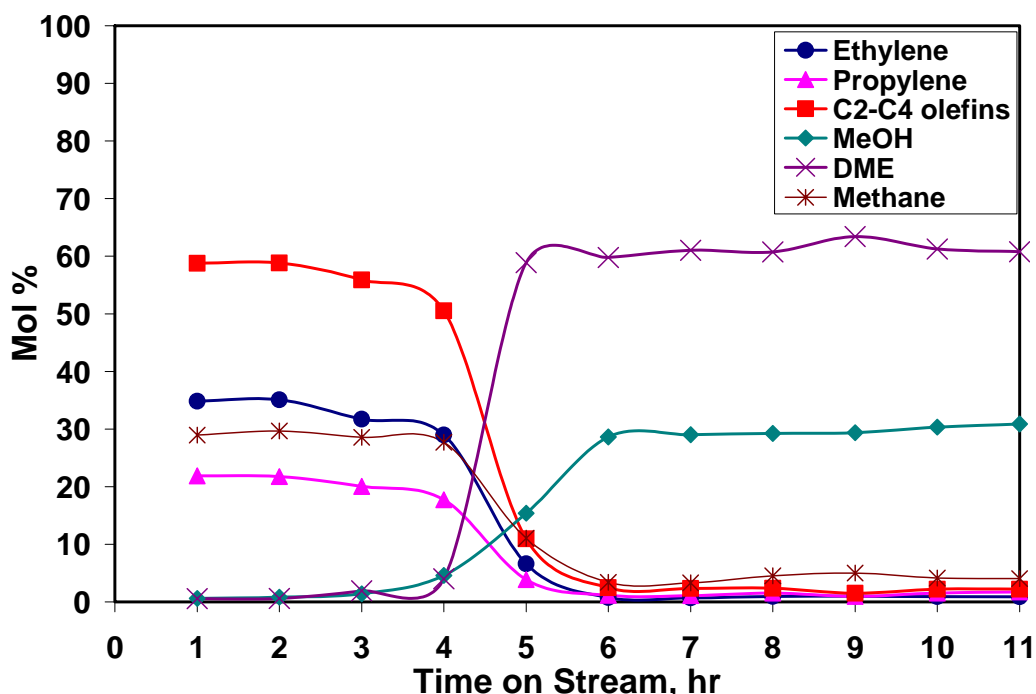


**Figure 4.1.** Distribution of Ethylene, Propylene, C<sub>2</sub> --C<sub>4</sub> Olefins, DME, and MeOH, (SAPO-56) (P-18), (0.6 Si), Temp = 450 °C, MeOH Flow = 0.005ml/min, Load = 0.504 g, WHSV = 0.5 hr<sup>-1</sup>)

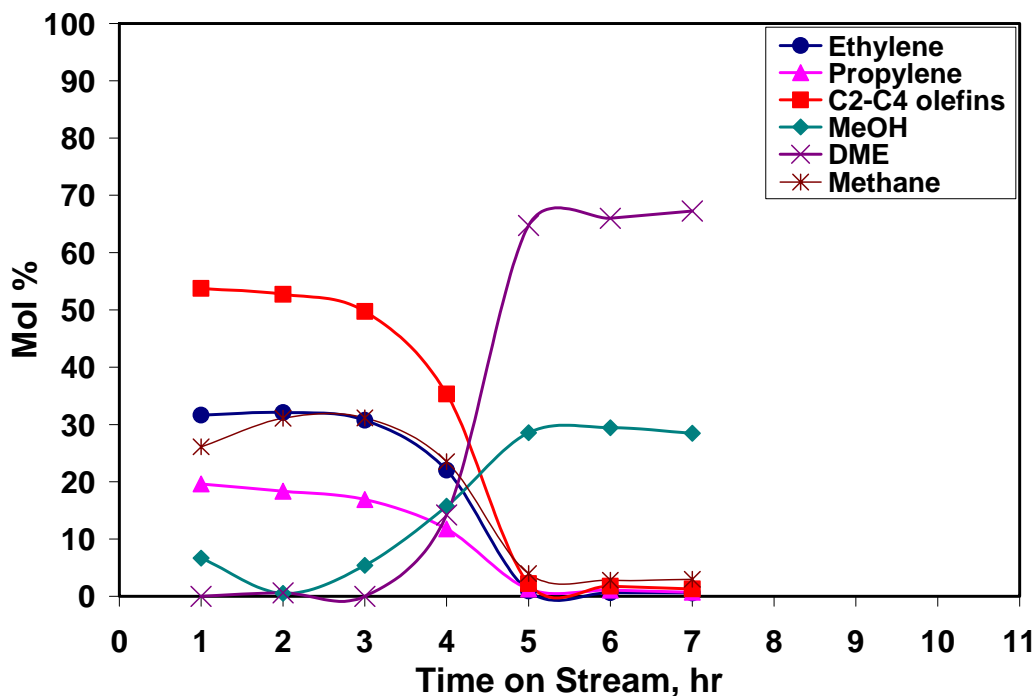


Figure 4.2. Distribution of Ethylene, Propylene, C<sub>2</sub> -- C<sub>4</sub> Olefins, DME, and MeOH (SAPO-56), (P-18), (0.6 Si), Temp = 450 °C, MeOH Flow = 0.003m./min, Load = 0.307 g, WHSV = 0.5 hr<sup>-1</sup>)

In both experiments, the catalyst remained active for the first 4 hrs and profiles for both experiments looked almost identical. A closer look reveals some slight differences. C<sub>2</sub> to C<sub>4</sub> yields in **Figure 4.2** appear a little bit higher than in **Figure 4.1** signaling slightly more olefins is produced during that time. Also, **Figure 4.2** shows complete deactivation starts in hour 6 compared to hour 5 in **Figure 4.1**. Both DME and MeOH appeared early on in the 1<sup>st</sup> hr in **Figure 4.2**, then dropped in the 2<sup>nd</sup> hr and then increased thereafter.

### Temperature Studies

In this study both the effects of coke formation brought about by temperature increase and product distribution due to rapid oligomers quenching were studied over a wide range of temperature from an initial 300 °C with an increment of 50 °C to a

maximum of 500 °C. The reactions were performed over SAPO-34, SAPO-44, and SAPO-56 (0.6 Si).

### **Temperature Study (SAPO-34), (P-5)**

**Figures 4.3** and **4.4** show product distribution at each temperature point for SAPO-34. Over the temperature range chosen, 300 °C seems to be the best operating condition where significant amounts of olefins C<sub>2</sub> to C<sub>4</sub> were produced. However, increasing the temperature to 350 °C and higher (**Figure 4.3**) resulted in significantly lower methanol conversion. Since higher temperatures favor faster catalyst deactivation due to coke formation and lower selectivity to olefins, in the present study we did not expect olefins formation to precipitously drop that rapidly with temperature rise. Dubois (2002) in conducting a similar study found olefins amounts at each temperature tested which is counter to what is experienced here.

In **Figure 4.4**, however, where particles undergo grinding treatment we found improvements both in catalyst activity and product distribution. Unlike the previous case where no olefins were detected beyond the initial temperature of (300 °C), here olefins products were still present up to temperature of 400 °C. As temperature rose to 450 °C and higher, both DME and MeOH became the dominant components in the product stream. However, DME was present at a far higher level than MeOH, 70% to 27% at 450 °C and 65% to 34% at 500 °C, respectively.

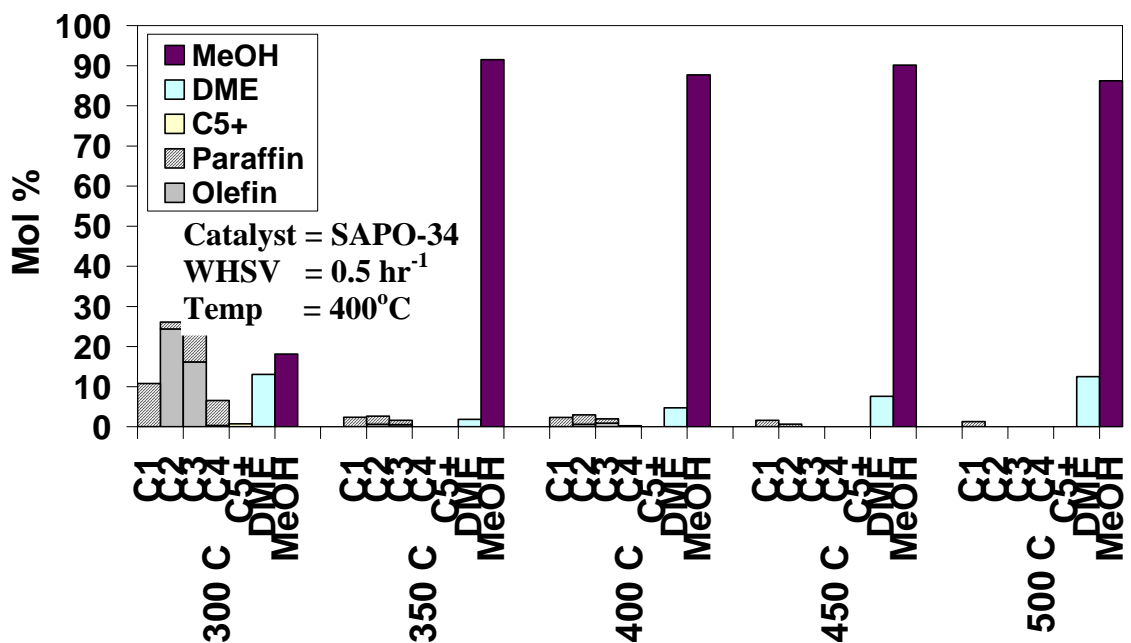


Figure 4.3 Temperature Effect on Product Distribution. SAPO-34 (P-5), No Grinding.

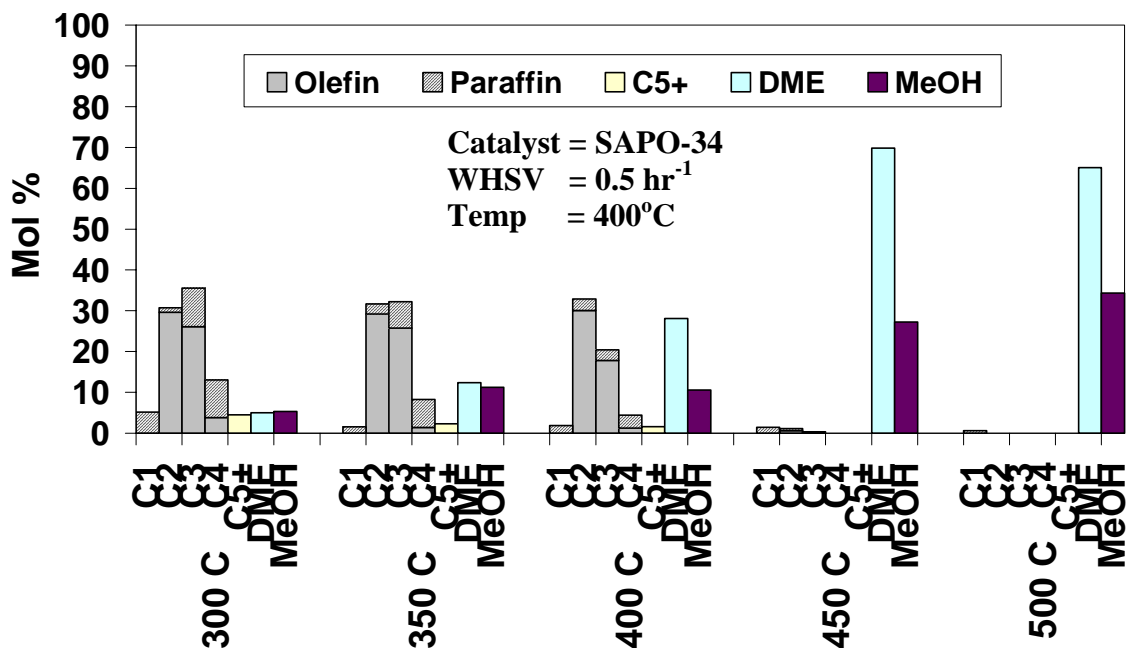


Figure 4.4. Temperature Effect on Product Distribution. SAPO-34 (P-5), After 15 min Grinding.



### **Temperature Study (SAPO-44), (P-6)**

In addition to SAPO-34, a temperature study was also conducted over SAPO-44. Like SAPO-34, all operating conditions were the same: nitrogen flow, methanol flow, and temperature range.

In the case of SAPO-44, both olefins and paraffins components were continually present in the product stream over the temperature spectrum for the original size particles. But as the temperature increased (**Figure 4.5**), these amounts decreased along with an increase of methanol suggesting incomplete methanol conversion. DME amounts fluctuated over the same temperature range, from a high 27% at 350 °C then gently decreased to a low 14% at 400 °C and came right back up to a high of 28% at 500 °C. This behavior is reasonable because DME is an intermediate in the MTO reaction. Low olefins conversion occurred at 350 °C and deactivation was observed at 500 °C accompanied by high DME amounts.

Both the yield and catalytic activity over SAPO-44 particles greatly increased (**Figure 4.6**) after grinding. Olefins distribution remained significant throughout except at 500 °C where both DME and MeOH became dominant components in the product stream. This catalyst showed great resistance to DME and MeOH runaways. Of the five temperature points, 450 °C seemed to be the best operating point where ethylene to propylene ratio was highest. Overall both DME and MeOH were present early on, but at relatively low levels compared to olefin levels.

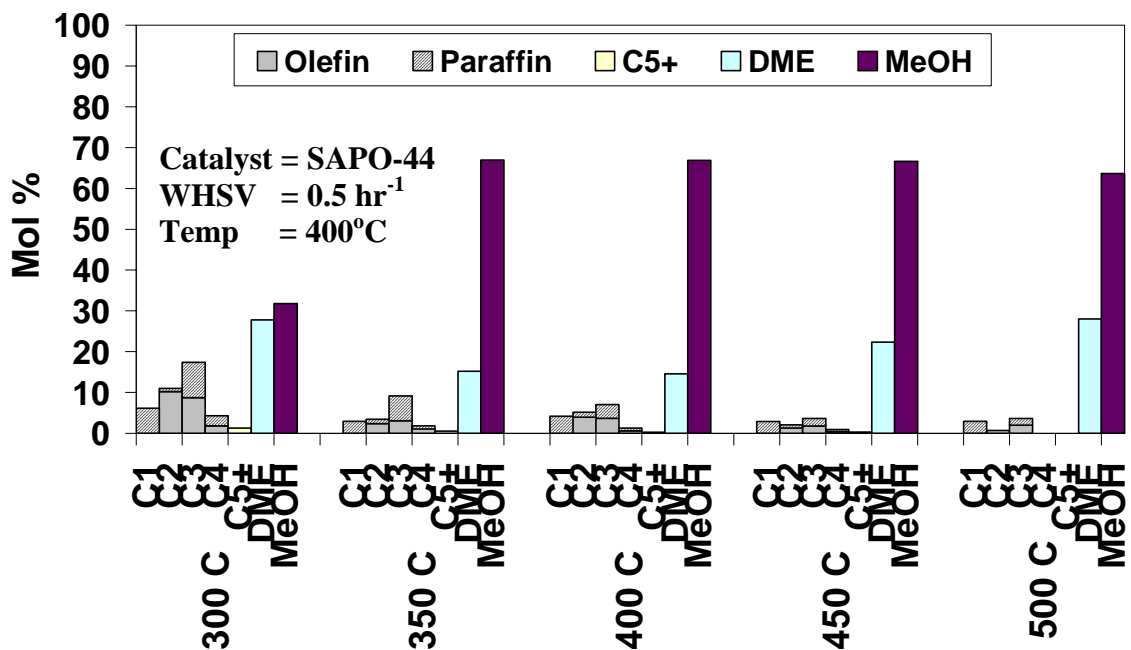


Figure 4.5. Temperature Effect on Product Distribution. SAPO-44 (P-6), No Grinding.

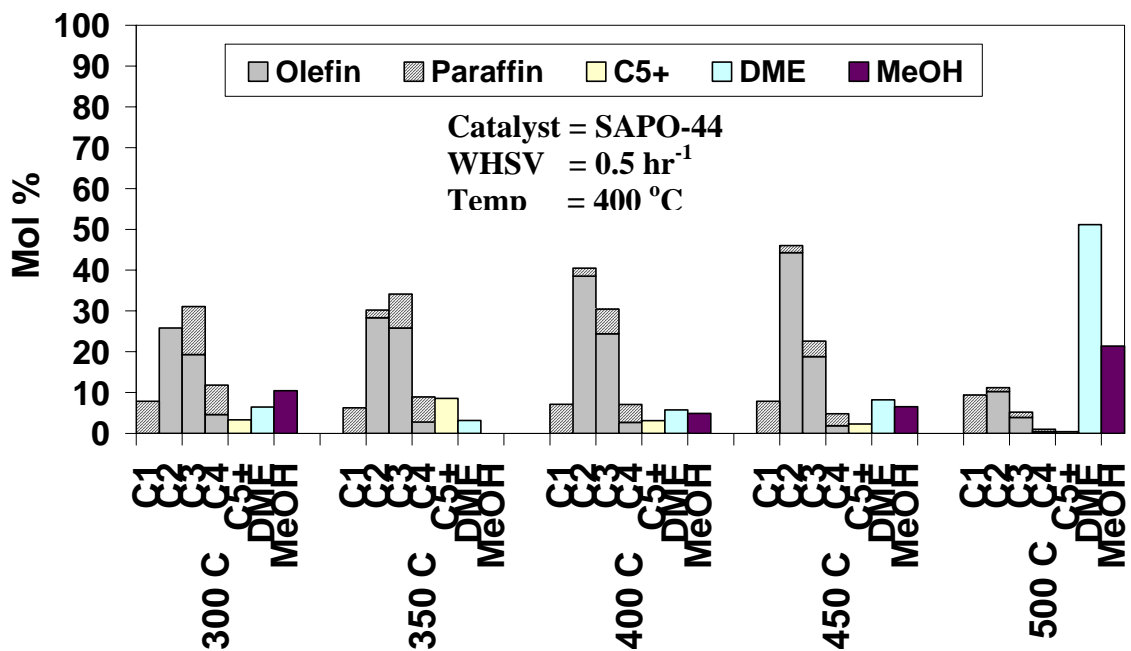


Figure 4.6. Temperature Effect on Product Distribution. SAPO-44 (P-6), After 15 min Grinding.

### Temperature Study (SAPO-56), (P-18), (0.6 Si)

A temperature study was also conducted over SAPO-56 both before and after grinding. **Figures 4.7** and **4.8** show these results. Product distribution profiles in both cases appear quite similar. Throughout the temperature spectrum, except at 500 °C, both C<sub>2</sub> and C<sub>4</sub> were present in significant amounts. The high olefins yield could be the result of oligomer cracking reactions taking place inside the catalyst pores thereby favoring continued olefins production. At 500 °C however, these olefins decreased rapidly coupled with the DME and MeOH rise.

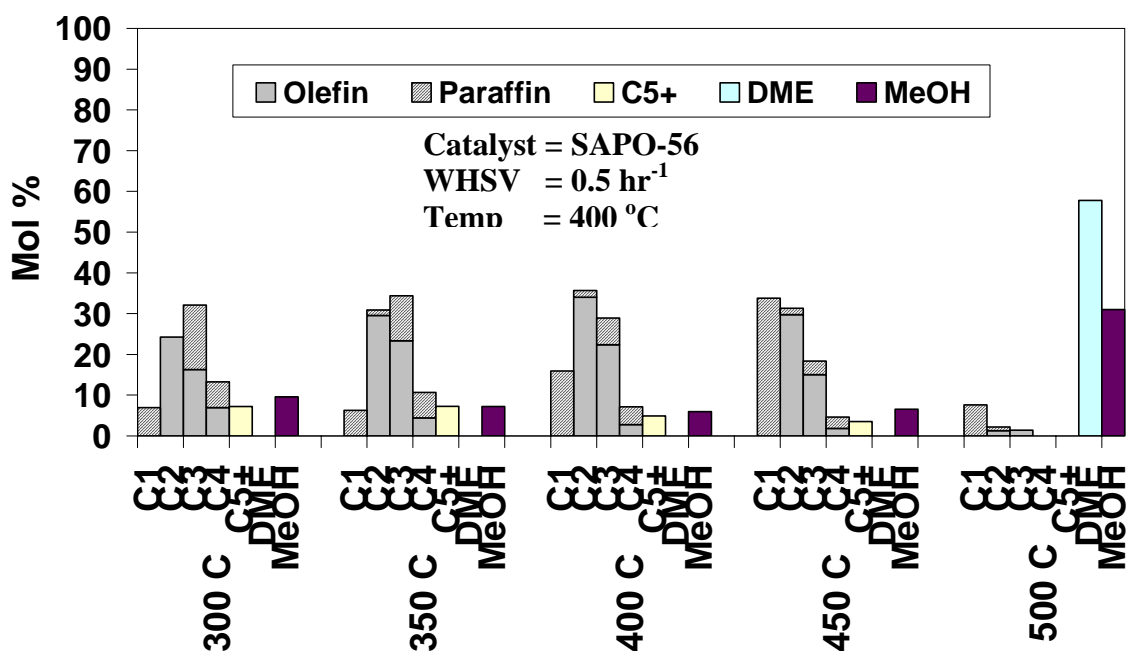


Figure 4.7. Temperature Effect on Product Distribution. SAPO-56 (P-18), (0.6Si), (No Grinding).

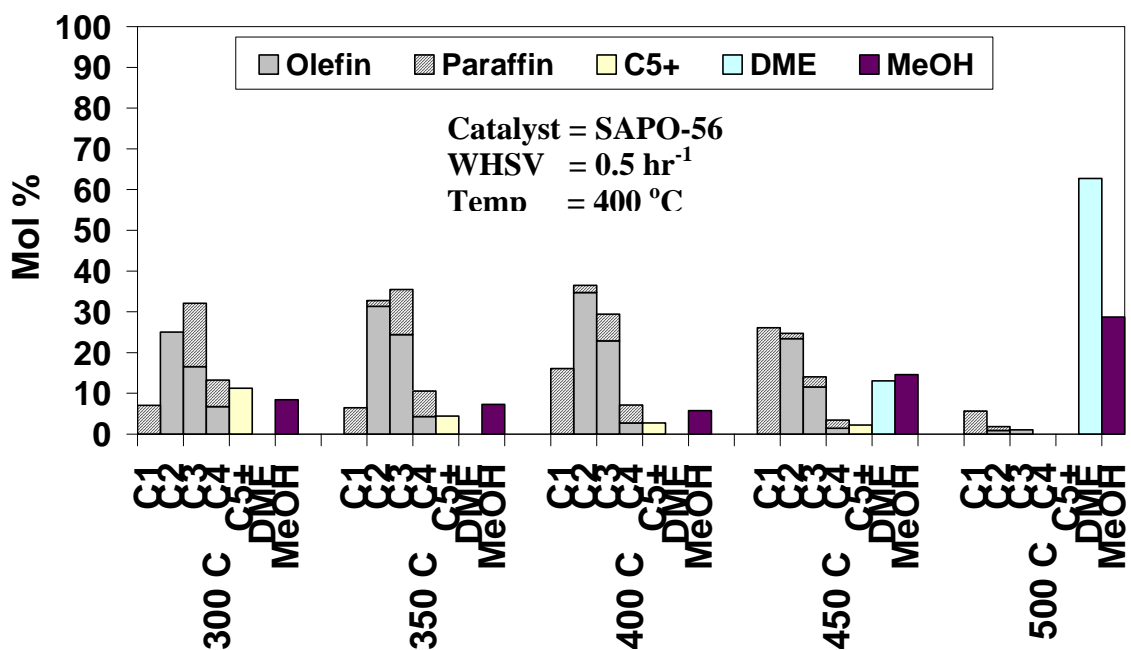


Figure 4.8. Temperature Effect on Product Distribution. SAPO-56 (P-18), (After 15 min Grinding).

Temperature studies over SAPO-34, SAPO-44, and SAPO-56 (0.6 Si) were carried out over a broad temperature range (300 °C – 500 °C). Except for SAPO-56, catalysts in their original size were prone to rapid deactivation very early on, even after the first hour of time on stream (TOS). MeOH breakthrough appeared at the first hour suggesting incomplete conversion at the lowest temperature. Particle size reduced by mechanical grinding significantly increased catalyst yield, activity and olefin distribution, however, both DME and MeOH still maintained their presence in the product stream to a small extent. It could be argued that better diffusion in ground particles enabled greater access to active sites inside the pores thereby facilitating reactions at higher rates. It was found that the best operating condition was generally somewhere between 400 °C to 450 °C. For the catalysts tested, SAPO-44 turned out to be the best in terms of olefins

distribution before and after grinding, followed by SAPO-34 and finally SAPO-56. SAPO-56, however, showed no significant improvement with the product distribution remaining almost the same. The effective initial particle size could perhaps be one reason this result is obtained.

### **Catalytic Reaction Study**

Given the interest in SAPO catalysts, it is fitting to extend our studies to other areas where our understanding of these catalysts can be further enhanced. This process provides us with a greater appreciation for the complexity and intricacy of SAPO's catalytic reactions. Like SAPO-34, SAPO-44 and SAPO-47 are analogues of the Chabazite structure and are potential candidates for the MTO process. Of the MTO SAPO catalysts known to date, only SAPO-34 has shown promise of reaching the commercialization stage. There still remains a lot to learn about the other SAPOs and research is under way in various quarters of the scientific community to learn as much as possible about them.

In addition to SAPO-34, here we will report results on SAPO-44, SAPO-47, and SAPO-56 (0.3 Si), SAPO-56 (0.6 Si) and SAPO-56 (0.9 Si). For each catalyst, two catalytic tests were undertaken, and the effect of particle size variation on activity, lifetime, and selectivity is reported.

To study particle size effects, samples were ground for 5, 10, and 15 mins. Approximately 0.307 (+ / - 0.003) g of sample with a supply of 0.003 ml/min of MeOH were used for each reaction, which is equivalent to a WHSV of 0.5 hr<sup>-1</sup>. Temperature was set at 400 °C and pressure at 1atm.

## SAPO-44, (P-6)

**Figures 4.9 – 4.12** illustrate profiles of product selectivity over SAPO-44 for different grinding conditions. In **Figure 4.9** with no grinding treatment the catalyst remained active for nearly 6 hours. For the first three hours, olefins production  $C_2$  to  $C_4$  was significant and accounts for more than 60% of the overall product. Ethylene to propylene ratio was a little above unity indicating selectivity towards these two components was about the same. During the initial period (3hrs) both DME and MeOH did not appear as major constituents in the product stream. But after the third hour there was a precipitous decline in MeOH conversion, and by the fourth hour almost all the product constituents remained flat (nearly zero) with the exception of DME which remained at about 13% the total product. At the same time MeOH level in the output increased from a mere 15% to a high of 80% and stayed at this level until the reaction was stopped.

**Figure 4.10** shows the profile of product selectivity after 5 minutes of grinding. SEM analysis shows a great size reduction when compared with the original size (Appendix B, **Figure B-3**). Grinding effects are clearly evident when compared to (**Figure 4.9**). First and foremost is the catalyst activity as the reaction remained ongoing for a relatively long time of 11 hours. For the first six hours  $C_2$  to  $C_4$  olefins selectivity was significant, and the highest selectivity occurred during hours 3 and 4 where  $C_2$  to  $C_3$  ratio was highest. Then afterwards olefins production declined after the fourth hour to the ninth hour where it remained steady at around 5% selectivity.

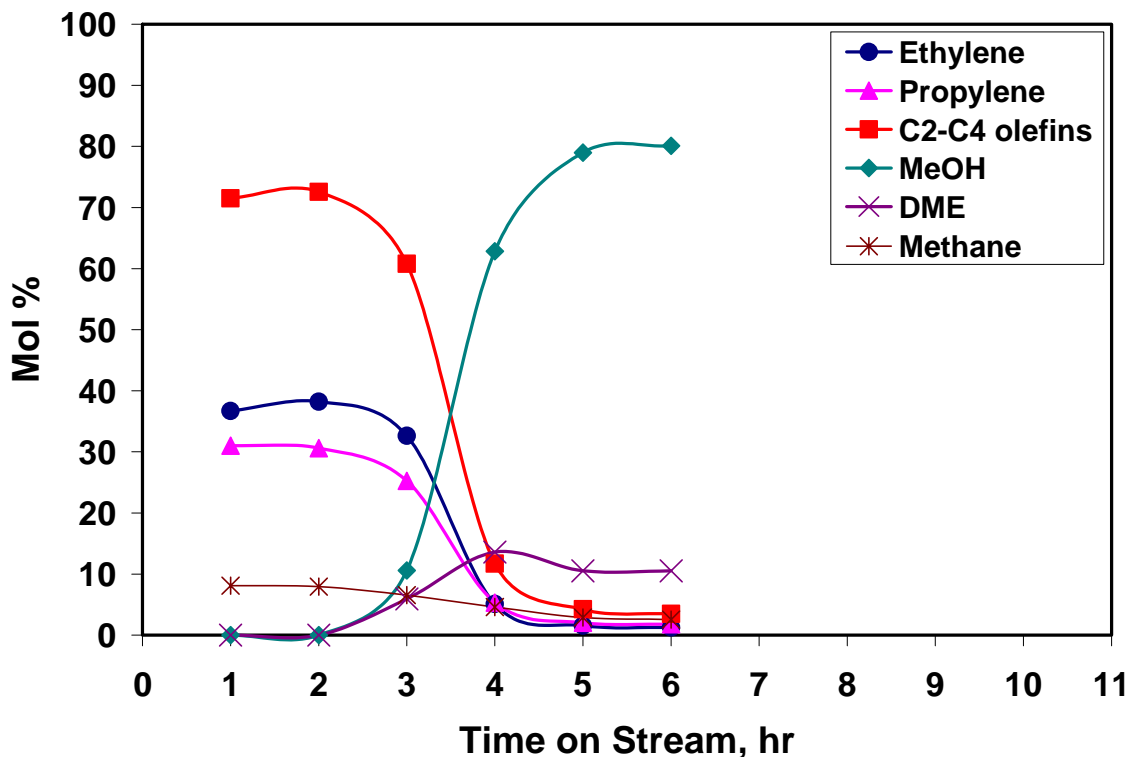


Figure 4.9. Distribution of Ethylene, Propylene, C<sub>2</sub> – C<sub>4</sub> Olefins, MeOH, and DME, over SAPO-44 (P-6), 400 °C, (No Grinding).

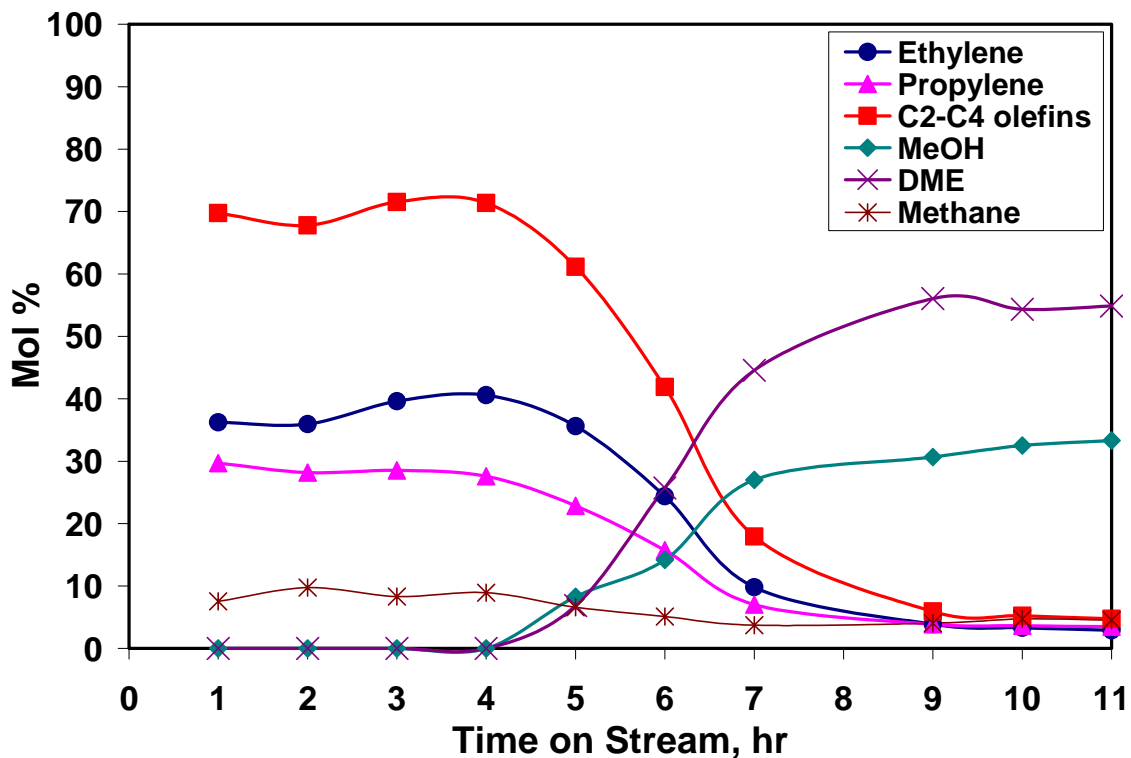


Figure 4.10. Distribution of Ethylene, Propylene, C<sub>2</sub> – C<sub>4</sub> Olefins, MeOH, and DME SAPO-44 (P-6), 400 °C, After 5 min. Grinding.

DME and MeOH breakthroughs did not commence until the fourth hour, then increased rapidly with each passing hour. Unlike the previous run (no grinding), here DME constitutes a major component in the product stream as both olefins and paraffins amounts abated. DME to MeOH ratio is nearly two. Methane presence was well below 10% for the first four hours and decreased thereafter.

**Figure 4.11** depicts the selectivity profile with catalyst particles ground for 10 minutes. During the first three hours  $C_2$  to  $C_4$  selectivity was a little above 70% (**Table 4.1**). Again the  $C_2$  to  $C_3$  ratio was slightly above unity for a long time until hour 9 when the ratio became exactly one. MeOH and DME breakthrough started right after the third hour accompanying a decline of  $C_2$  to  $C_4$  output and rapidly decreasing until hour nine. Methane selectivity remained relatively low throughout the course of the reaction, with minor fluctuation between hours 3 to 9. As in the previous run (5 min grinding), DME became the major component in the product stream along with MeOH as the catalyst undergoes deactivation. From the third hour MeOH began rising gently and continued increasing steadily until hour eight when it jumped from 20% to 25% and remained there until the end of the reaction.



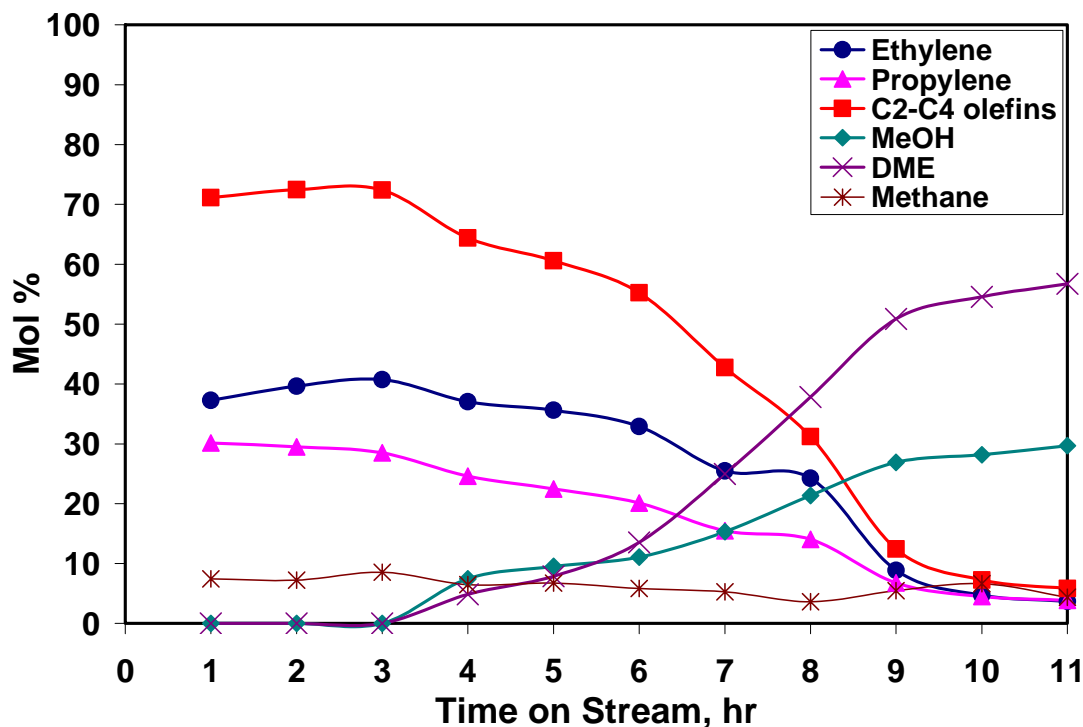


Figure 4.11. Distribution of Ethylene, Propylene, C<sub>2</sub> – C<sub>4</sub> Olefins, MeOH, and DME SAPO-44 (P-6), 400 °C, After 10 min. Grinding.

Table 4.1. Product Distribution over SAPO-44 (P-6), After 10 min. Grinding.

TOS(hr)	COMPONENT											
	1 <sup>st</sup>	2 <sup>nd</sup>	3 <sup>rd</sup>	4 <sup>th</sup>	5 <sup>th</sup>	6 <sup>th</sup>	7 <sup>th</sup>	8 <sup>th</sup>	9 <sup>th</sup>	10 <sup>th</sup>	11 <sup>th</sup>	
C <sub>1</sub> <sup>-</sup>	7.44	7.23	8.56	6.47	6.72	5.84	5.28	2.85	4.01	4.78	3.07	
C <sub>2</sub> <sup>-</sup>	1.98	1.98	1.81	1.79	1.73	1.59	1.29	0.80	0.74	0.79	0.62	
C <sub>2</sub> <sup>=</sup>	37.26	39.63	40.72	37.04	35.62	32.91	25.49	19.07	6.49	3.40	2.59	
C <sub>3</sub> <sup>-</sup>	8.90	8.16	7.49	6.34	5.91	4.98	4.26	2.61	3.01	2.99	2.85	
C <sub>3</sub> <sup>=</sup>	30.15	29.51	28.51	24.63	22.46	20.11	15.49	11.05	4.94	3.22	2.72	
C <sub>4</sub> <sup>-</sup>	6.49	5.79	5.71	4.66	4.05	3.50	2.62	1.78	0.90	0.65	0.55	
C <sub>4</sub> <sup>=</sup>	2.65	2.53	2.49	2.07	1.88	1.62	1.26	0.79	0.70	0.62	0.52	
C <sub>5</sub> <sup>-</sup>	1.10	0.81	0.70	0.67	0.62	0.60	0.49	0.30	0.33	0.00	0.00	
C <sub>5</sub> <sup>=</sup>	2.25	2.26	2.30	2.05	1.82	1.87	1.50	0.90	0.82	0.81	0.66	
C <sub>6</sub> <sup>-</sup>	0.69	1.18	1.17	1.12	1.02	0.95	0.82	0.24	0.29	0.00	0.00	
C <sub>6</sub> <sup>=</sup>	0.00	0.00	0.00	0.00	0.00	0.59	0.50	0.00	0.00	0.00	0.00	
DME	1.10	0.93	0.54	0.86	0.82	0.83	0.70	0.44	0.00	0.00	0.00	
DME	0.00	0.00	0.00	4.87	7.86	13.52	24.96	37.81	50.87	54.57	56.73	
MeOH	0.00	0.00	0.00	7.45	9.51	11.07	15.33	21.37	26.91	28.17	29.70	

**Figure 4.12** was by far the best outcome for the product profile for SAPO-44. This experiment used particles ground for 15 minutes with the catalyst particle size being the smallest (Appendix B, **Figure B-5**). In the second hour when C<sub>2</sub> to C<sub>4</sub> selectivity reached its highest peak at 82% (**Table 4.2**) and olefin production remained relatively high well above 70%. From the first hour to the eighth hour, C<sub>2</sub> to C<sub>3</sub> ratio slowly increases with each passing hour. All other products remained relatively low, below 5%, for the first six hours. DME and MeOH breakthroughs started early (3<sup>rd</sup> and 4<sup>th</sup> hour, respectively) – and remained steady at a 5% level until the 6<sup>th</sup> hour and C<sub>2</sub> to C<sub>4</sub> outputs did not deviate much. At the 6<sup>th</sup> hour olefin production began to decline accompanying increases in MeOH and DME production. Here, DME accounts for much of the product and reaches its highest amount at the 11<sup>th</sup> hour. At the same time, the DME to MeOH ratio increased rapidly with time from one at the sixth to more than two and a quarter at the end point of the reaction.

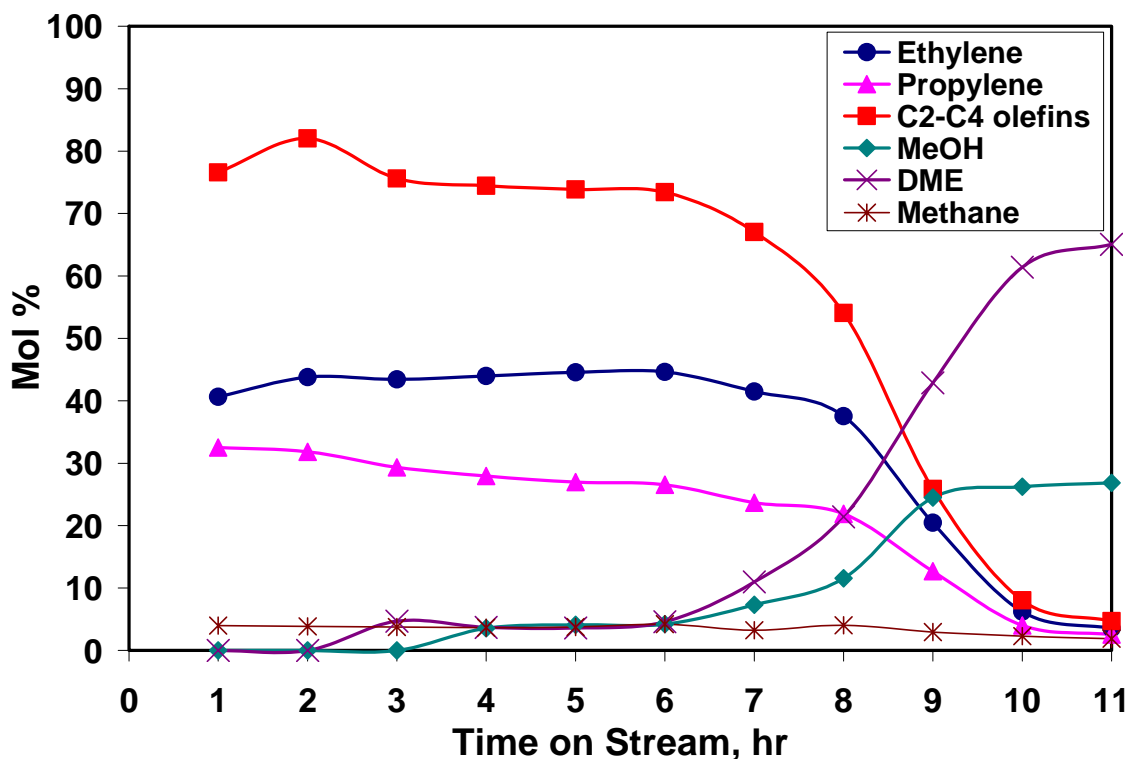


Figure 4.12. Distribution of Ethylene, Propylene, C<sub>2</sub> – C<sub>4</sub> Olefins, MeOH, and DME SAPO-44 (P-6), 400 °C, After 15 min. Grinding.

Table 4.2. Product Distribution over SAPO-44 (P-6), After 15 min. Grinding.

TOS(hr)	COMPONENT											
		1 <sup>st</sup>	2 <sup>nd</sup>	3 <sup>rd</sup>	4 <sup>th</sup>	5 <sup>th</sup>	6 <sup>th</sup>	7 <sup>th</sup>	8 <sup>th</sup>	9 <sup>th</sup>	10 <sup>th</sup>	11 <sup>th</sup>
	C <sub>1</sub> <sup>-</sup>	4.00	3.85	3.75	3.67	3.75	4.20	3.23	3.59	2.23	1.69	1.38
	C <sub>2</sub> <sup>-</sup>	1.48	1.72	1.67	1.67	1.60	1.74	1.56	1.17	0.65	0.42	0.34
	C <sub>2</sub> <sup>=</sup>	40.64	43.77	43.43	43.99	44.57	44.62	41.49	33.20	15.46	4.59	2.57
	C <sub>3</sub> <sup>-</sup>	7.34	6.30	5.55	4.82	4.44	4.36	3.47	2.90	1.84	1.27	1.13
	C <sub>3</sub> <sup>=</sup>	32.50	31.82	29.33	27.94	26.97	26.57	23.69	19.37	9.59	2.96	1.88
	C <sub>4</sub> <sup>-</sup>	6.92	2.95	5.86	5.36	4.98	4.78	3.92	2.98	1.42	0.52	0.33
	C <sub>4</sub> <sup>=</sup>	2.44	2.38	2.19	2.01	1.86	1.75	1.48	1.13	0.63	0.34	0.26
		1.01	4.07	0.65	0.52	0.48	0.47	0.39	0.37	0.21	0.13	0.00
	C <sub>5</sub> <sup>-</sup>	2.07	1.88	0.26	0.69	1.10	0.49	0.23	0.51	0.00	0.00	0.00
	C <sub>5</sub> <sup>=</sup>	0.49	0.64	2.11	2.09	2.05	1.96	1.72	1.42	0.65	0.43	0.22
	C <sub>6</sub> <sup>-</sup>	0.81	0.34	0.00	0.00	0.00	0.00	0.30	0.00	0.00	0.00	0.00
	C <sub>6</sub> <sup>=</sup>	0.28	0.27	0.52	0.00	0.49	0.23	0.24	0.41	0.00	0.00	0.00
	DME	0.00	0.00	4.68	3.68	3.58	4.61	10.98	21.40	42.86	61.41	65.05
	MeOH	0.00	0.00	0.00	3.55	4.12	4.22	7.32	11.55	24.48	26.24	26.84

Adekkannattu, (2003) in his final report conducted a similar reaction over SAPO-44. His findings when compared to what is reported here (**Figure 4.9**, no grinding), showed some differences. In his report, the catalyst remained active for the first four hours with high olefin C<sub>2</sub> to C<sub>4</sub> production, above 80%, with the highest point reached at 87%. Unlike the case here where catalyst showed deactivation after the 2<sup>nd</sup> hour, in Adekkannattu's case the catalyst remained active for nearly twice that time. In addition selectivity remained considerably higher during that time.

**Figure 4.13** provides an overall assessment of grinding effects on catalyst activity and product yield. It is obvious from the graphical representation that the catalyst maintained a longer activity with longer grinding time coupled with more olefins C<sub>2</sub> to C<sub>4</sub> selectivity. With no grinding, the catalyst deactivated rather quickly.

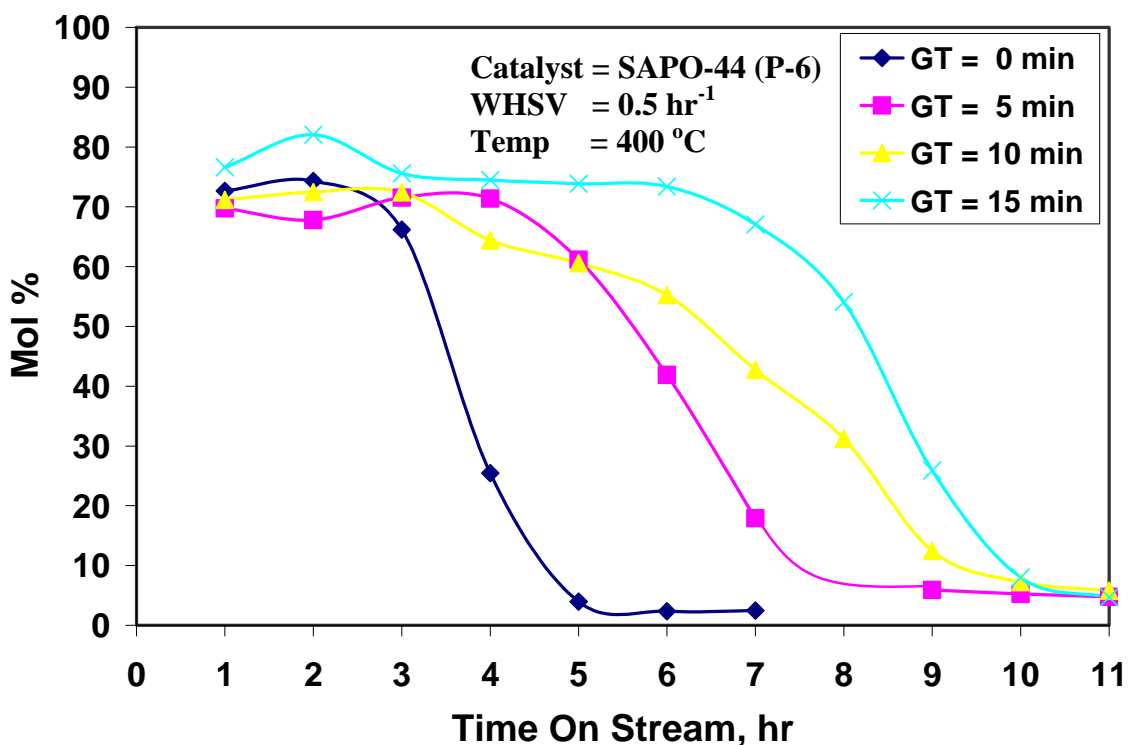


Figure 4.13. Effect of Grinding Time on Product Distribution. (GT = Grinding Time).

### Catalytic Reactions (SAPO-34), (P-5)

Figure 4.14 provides the profile for product selectivity over SAPO-34 (no grinding). Catalyst remained active for almost four hours. For the first two hours olefins C<sub>2</sub> -- C<sub>4</sub> selectivity reached their peak at nearly 75% while C<sub>2</sub> to C<sub>3</sub> ratio remained a little above unity. DME and MeOH breakthroughs didn't become noticeable until after the second hour and accompanied a rather sharp decline in C<sub>2</sub> to C<sub>4</sub> outputs, which decreased to nearly zero by the fourth hour. DME selectivity was relatively low from a high of 17% at the 3<sup>rd</sup> hour while decreasing to 15% and remained at that level through the end of the reaction. The DME profile ran counter to that was reported by Adekkanattu from his experiment where DME was the main product constituent once deactivation commenced (Adekkanattu, 2003). By the 4<sup>th</sup> hour MeOH selectivity was at its highest at 88%.

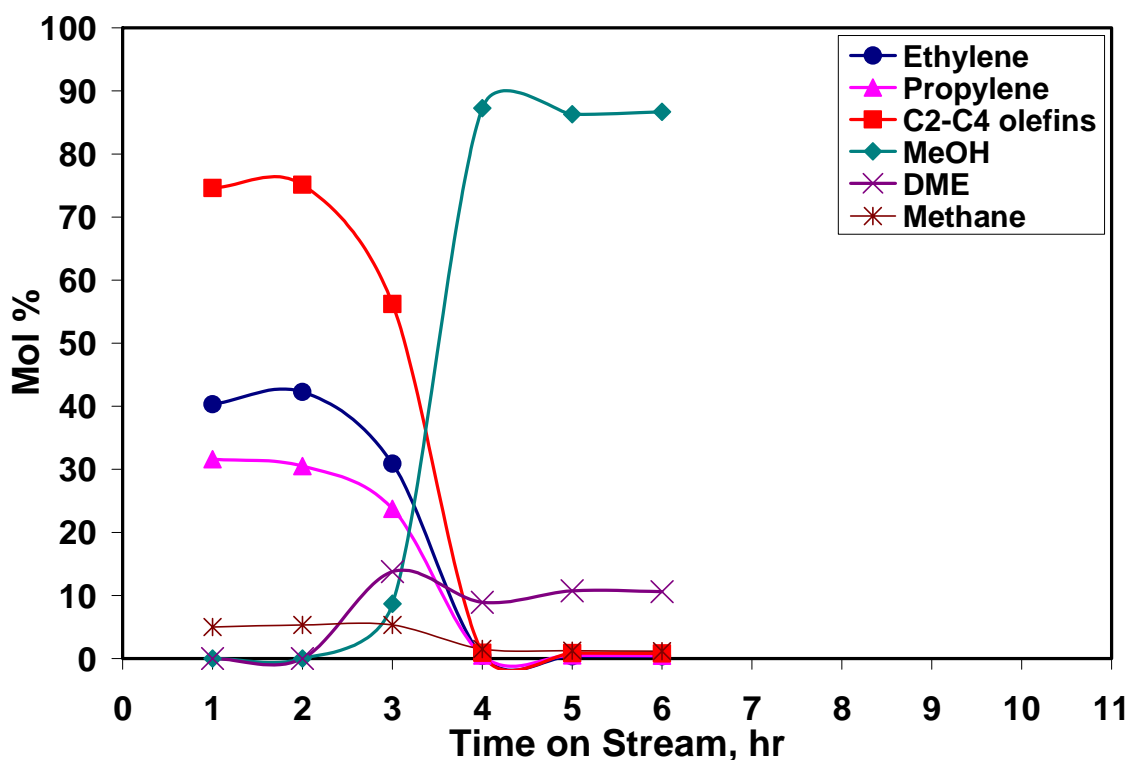
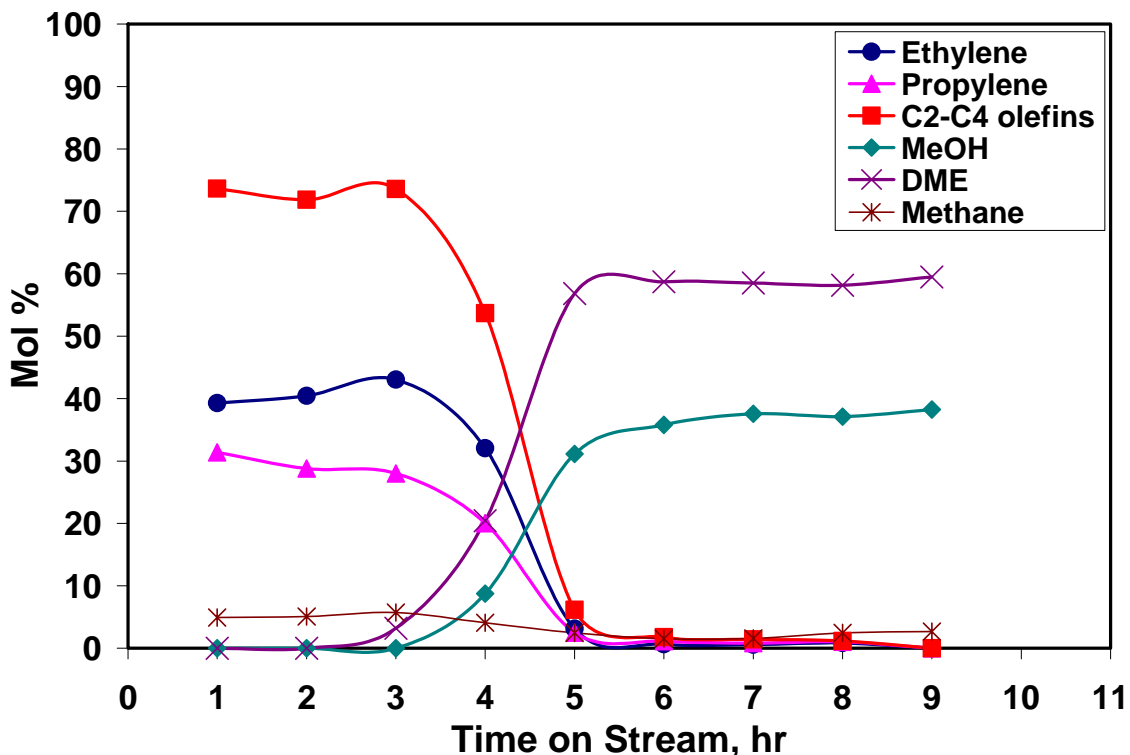


Figure 4.14. Distribution of Ethylene, Propylene, C<sub>2</sub> – C<sub>4</sub> Olefins, MeOH, and DME SAPO-34(P-5), 400°C, No Grinding.

Particles ground for 5 minutes showed improvements both in terms of activity and product distribution (**Figure 4.15**). Both DME and MeOH breakthroughs commenced at the 2<sup>nd</sup> and 3<sup>rd</sup> hours, respectively. The catalyst remained active a little less than six hours. As in the previous cases C<sub>2</sub> to C<sub>3</sub> ratio remained at above unity with the highest value attained at the 3<sup>rd</sup> hour. As expected both DME and MeOH constitute the main product constituents through the remainder of the reaction with DME to MeOH ratio above 1.5. Methane selectivity was small, ranging from around 5%, to about 0 by the 6<sup>th</sup> hour.



**Figure 4.15.** Distribution of Ethylene, Propylene, C<sub>2</sub> – C<sub>4</sub> Olefins, MeOH, and DME SAPO-34 (P-5), 400 °C, After 5 min. Grinding.

**Figure 4.16** shows SAPO-34 activity over catalyst ground for 10 min. Very early both DME and MeOH broke away and rapidly increased to their highest levels. C<sub>2</sub> to C<sub>4</sub> selectivity remained high for the first couple of hours, then began to decline fairly

steadily and rapidly decreased from the 5<sup>th</sup> hour to the 7<sup>th</sup> hour. Although coke formation occurred early and rapidly increased with time, the catalyst did however remain active for seven hours. C<sub>2</sub> to C<sub>3</sub> ratio remained above unity until the 7<sup>th</sup> hour. As in almost all of the other reactions over ground particles, DME remained as the main constituent in the product stream, where DME to MeOH ratio remains around 2.0.

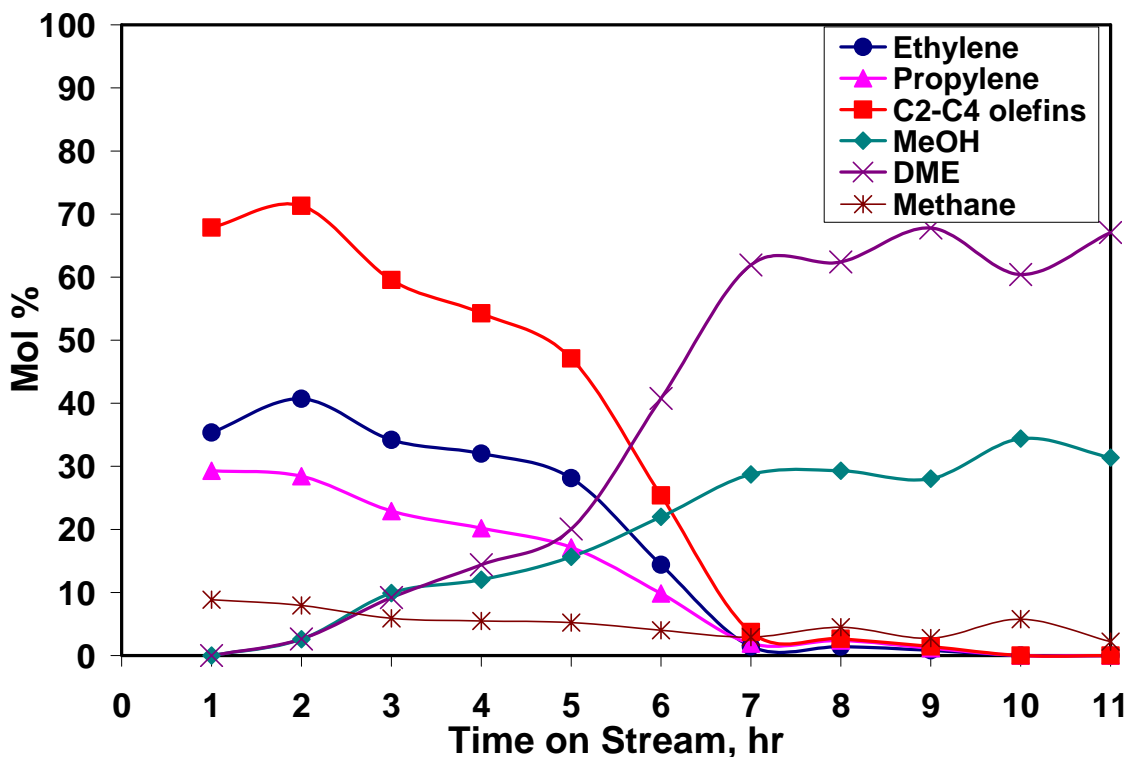


Figure 4.16. Distribution of Ethylene, Propylene, C<sub>2</sub> – C<sub>4</sub> Olefins, MeOH, and DME SAPO-34(P-5), 400°C, After 10 min. Grinding.

Figure 4.17 shows the product selectivity profile after 15 min. catalyst grinding time. Coke formation occurred fairly early, but the catalyst remained active for nearly ten hours. Deactivation began soon after the first hour. Both DME and MeOH started along the same path and crisscrossed one another up to the seventh hour where they each

settled on their individual path. DME selectivity was rather significant, slightly above 60% and nearly double the amount of MeOH present.

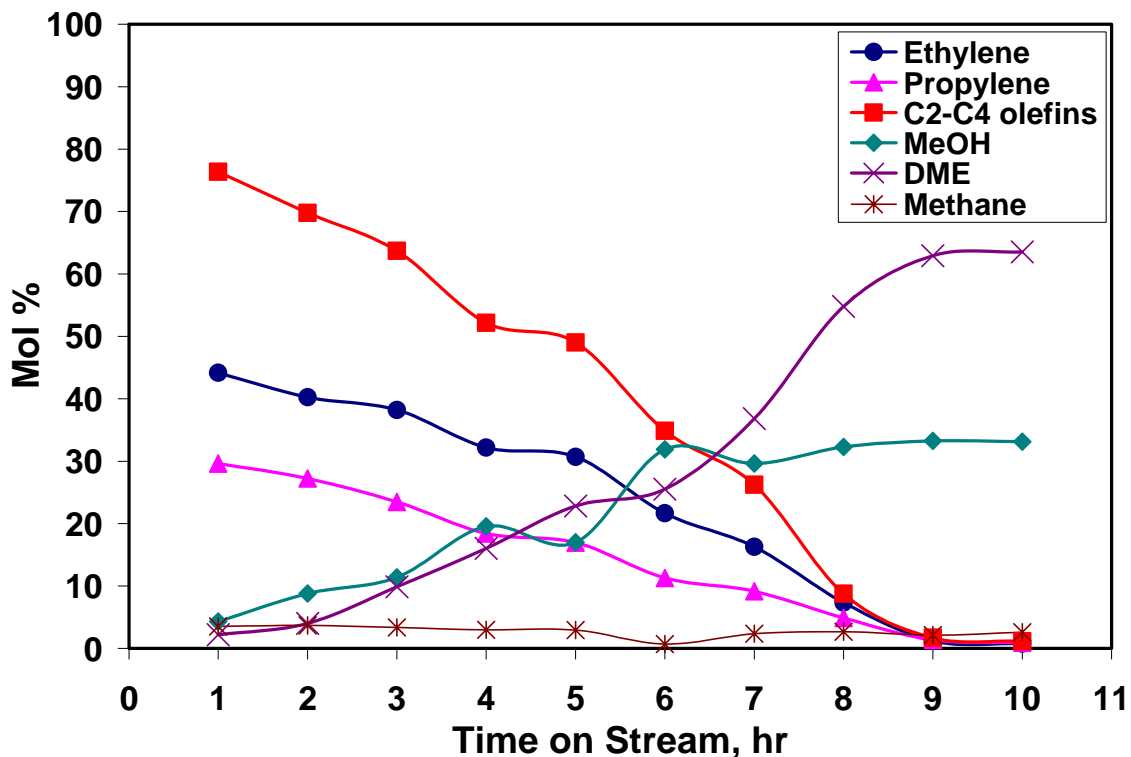


Figure 4.17. Distribution of Ethylene, Propylene, C<sub>2</sub> – C<sub>4</sub> Olefins, MeOH, and DME SAPO-34(P-5), 400 °C, After 15 min. Grinding.

Figure 4.18 shows the general particle size effect on C<sub>2</sub> -- C<sub>4</sub> selectivity. Just as in the case of SAPO-44, each increase in grinding time accompanies an increase in C<sub>2</sub> -- C<sub>4</sub> selectivity coupled with a further increase in catalyst lifetime. However, unlike SAPO-44, SAPO-34 showed a great tendency for deactivation even after the 1<sup>st</sup> hour. SAPO-44 showed a great resistance to deactivation up after the 3<sup>rd</sup> hour. But in both cases effects of grinding on olefin distribution was significant.



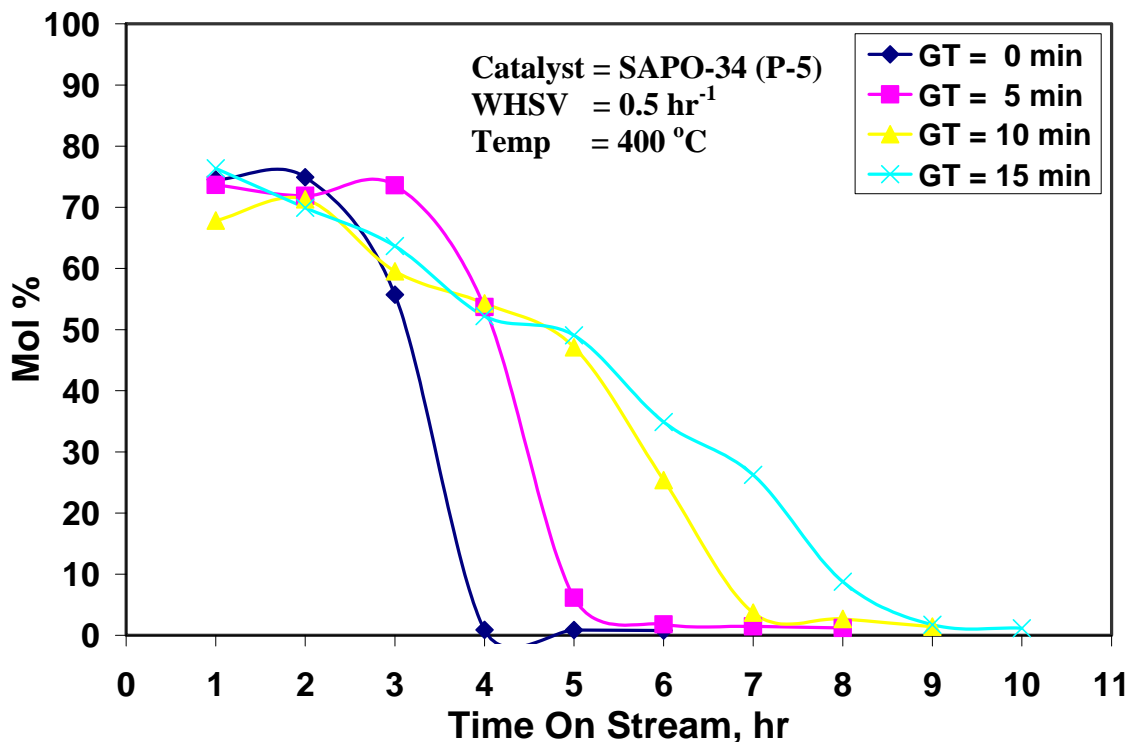


Figure 4.18. Effect of Grinding Time on Product Distribution. (GT = Grinding Time)

#### SAPO-47, (P-31)

As reported earlier SEM analysis for SAPO-47 showed a wide particle size distribution with an elongated cubic morphology (Appendix B, **Figures B-6 – B-8**), therefore, particles were separated in two fractions by water settling: a finer fraction and a coarser fraction. Catalyst testing over the coarse fraction showed very little activity. Even when the coarse particles were ground, no significant olefin production occurred and the entire product was DME and MeOH (**Figures 4.19** and **4.20**). As reported in the literature, a spent catalyst can be regenerated by thermal treatment. Here however, the sample was recalcined for over 15 hours at 560 °C, and even then very little activity occurred when tested.

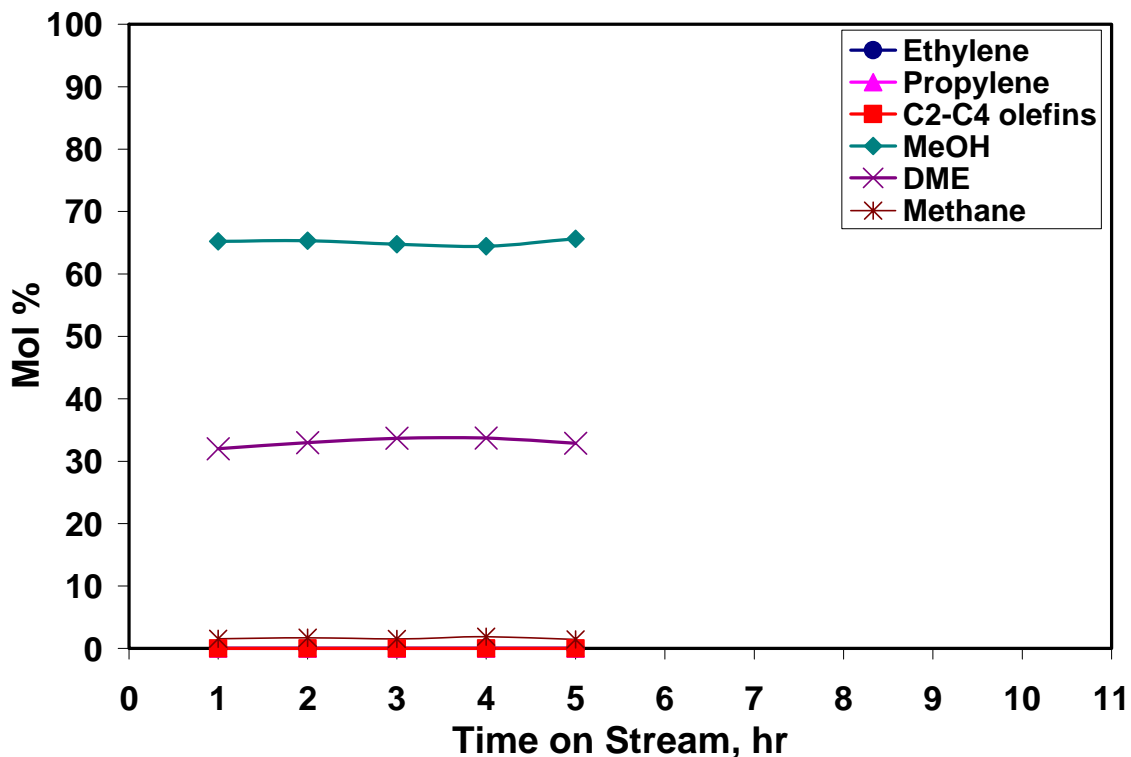


Figure 4.19. Distribution of Ethylene, Propylene, C<sub>2</sub> – C<sub>4</sub> Olefins, MeOH, and DME over spent SAPO-47 (P-31), 400 °C, Coarser Particles, After 15 min. Grinding.

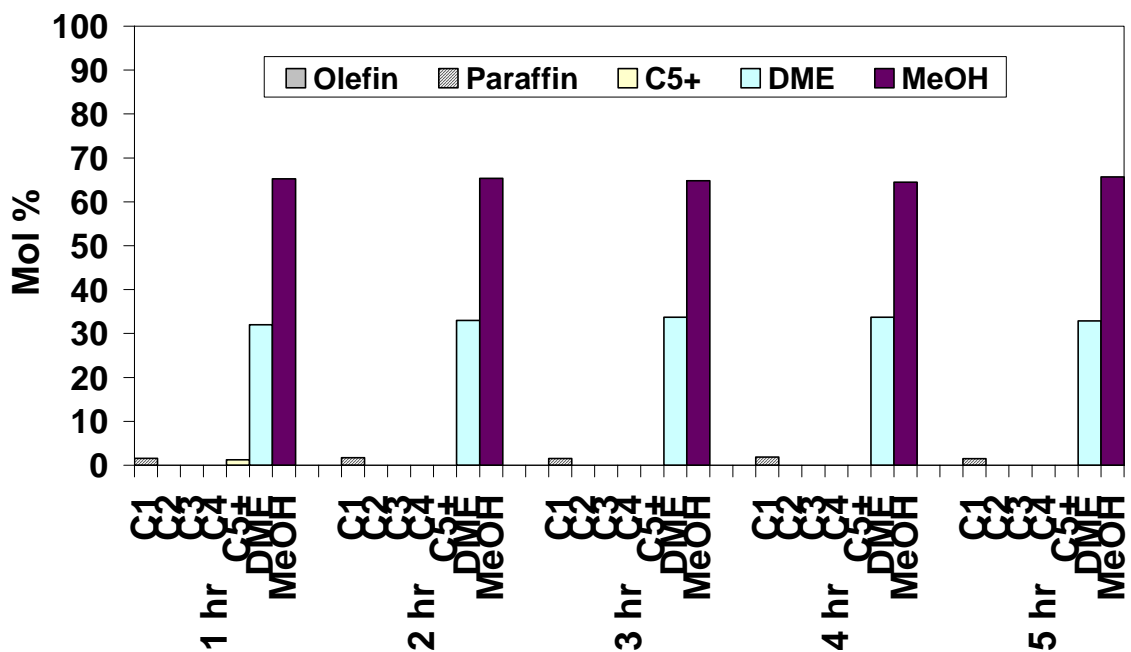
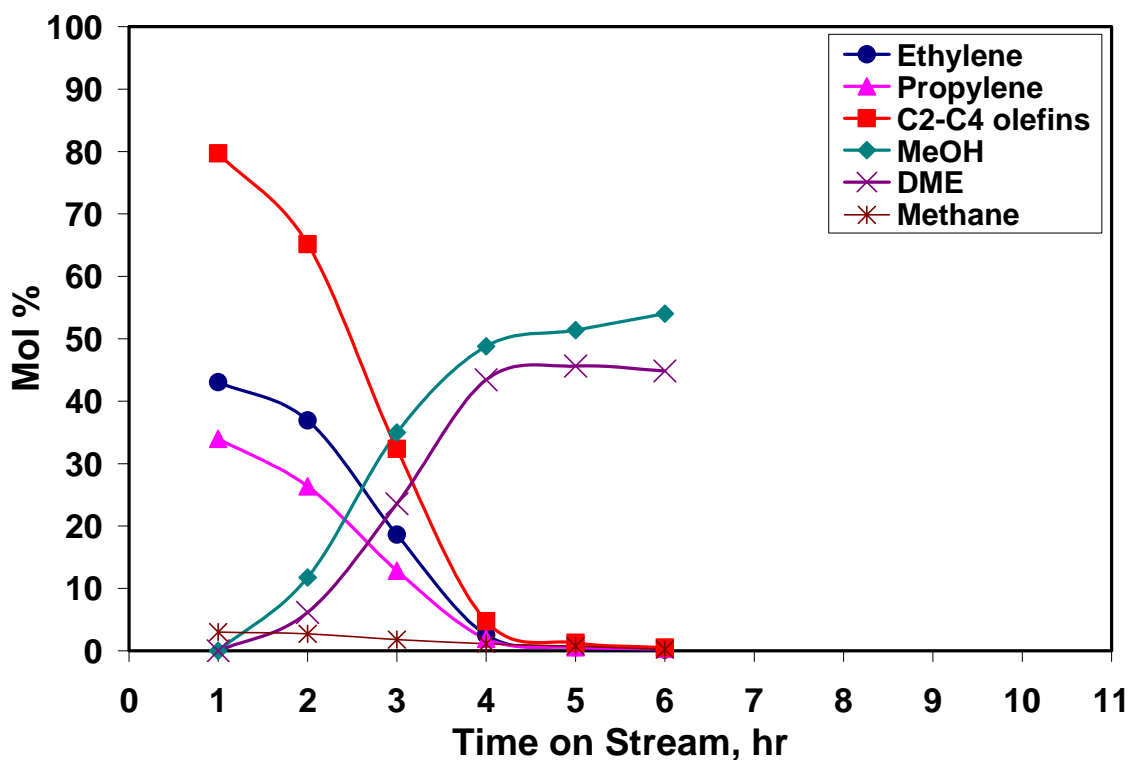


Figure 4.20. Distribution of Ethylene, Propylene, C<sub>2</sub> – C<sub>4</sub> Olefins, MeOH, and DME over spent SAPO-47 (P-31), 400°C, Coarser Particles, After 15 min. Grinding.

**Figure 4.21** shows product selectivity profile over the finer size particle fractions. Although the catalyst remained active for a little more than 4 hours, deactivation occurred very early on. Methanol conversion decreased rather rapidly as reaction proceeded. C<sub>2</sub> to C<sub>4</sub> selectivity achieved its highest point at the first hour, and then declined precipitously. C<sub>2</sub> to C<sub>3</sub> ratio was fairly constant at little above unity. DME and MeOH were the main product components after the third hour and remained as such until the end of the reaction. A similar reaction of SAPO-47 was reported by Adekkanattu (2003), however, direct comparison could not be made here due to different reaction conditions (i.e. particle size effects).



**Figure 4.21.** Distribution of Ethylene, Propylene, C<sub>2</sub> – C<sub>4</sub> Olefins, MeOH, and DME SAPO-47(P-31), 400 °C, Finer Particles, No Grinding.

**Figures 4.22** depict profiles of product selectivity over finer size particles ground for 15 minutes. Compared with **Figure 4.21** improvements in catalyst activity and

lifetime are obvious. Similarly, olefin distributions remained fairly significant over the course of the reaction coupled with increased MeOH conversion (**Figure 4.23**). The DME to MeOH ratio is about 2.0.

We see the same tendency for rapid coke formation for SAPO-47 just like that found for SAPO-34 even when particles were ground. In Adekkanattu's finding MeOH conversion was fairly high at 100% for the first four hours and then began to decrease rather quickly thereafter.

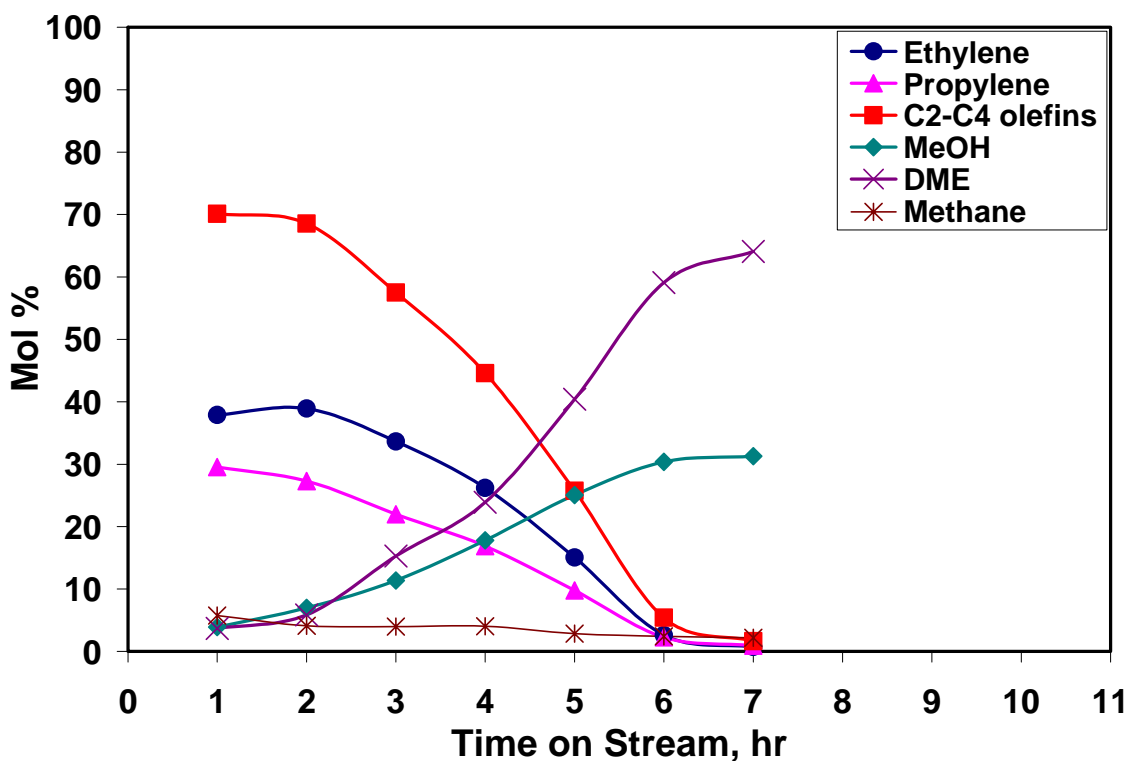


Figure 4.22. Distribution of Ethylene, Propylene, C<sub>2</sub> – C<sub>4</sub> Olefins, MeOH, and DME SAPO-47(P-31), 400 °C, Finer Particles, After 15 min Grinding.

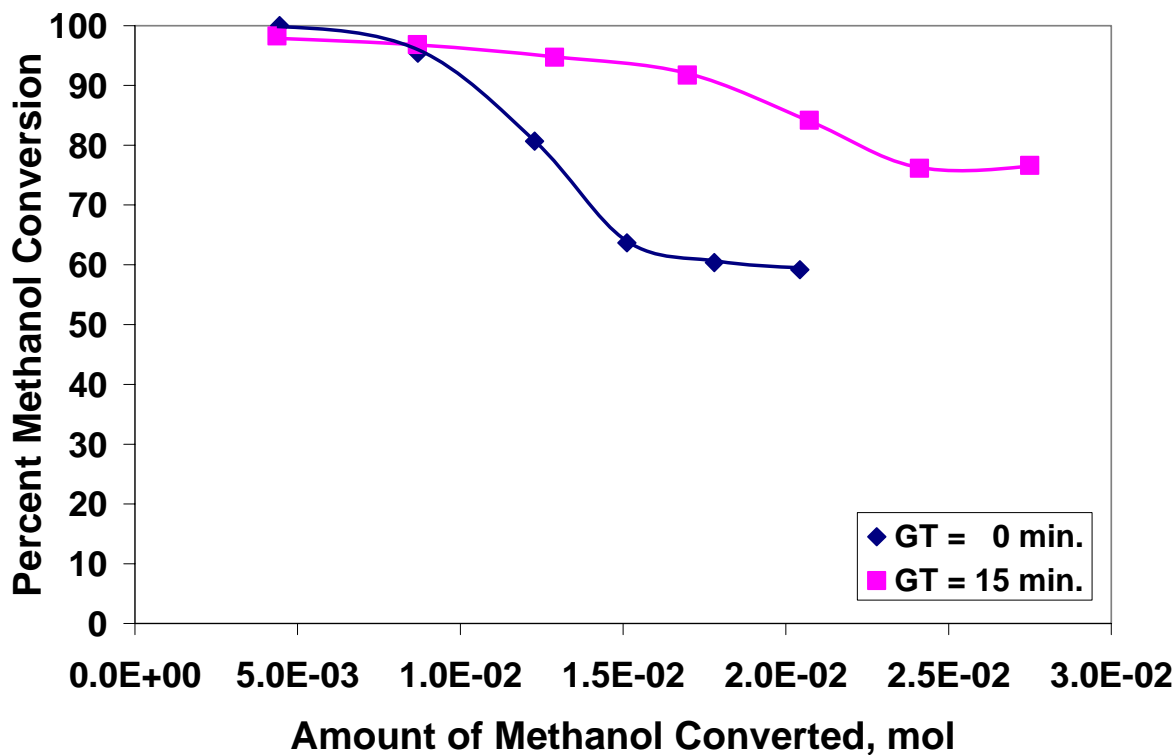


Figure 4.23. Methanol Conversion Profile over SAPO-47 (P-31), 400°C, Finer Particles, Before and After Grinding.

### SAPO-56

SAPO-56 being a novel catalyst with structure analogous to the AFX type remained as one catalyst about which the least information was available. Here, we look at SAPO-56 with three silicon contents embedded within its framework: (0.3 Si), (0.6 Si), and (0.9 Si)

#### SAPO-56 (P-18), (0.6 Si)

Figures 4.24 and 4.25 depict profiles for product selectivity and distribution over SAPO-56 with (0.6 Si) content. During the first couple of hours C<sub>2</sub> to C<sub>4</sub> selectivity was its highest being above 70%. During that period both DME and MeOH remained

essentially flat for the first 3 hours, then started their ascent and reached their maximum at the 8<sup>th</sup> hour where selectivities leveled off at 69% and 28%, respectively. What is significant in this profile is the DME to MeOH ratio at around 2.5 indicating a sizable portion of MeOH is being converted to DME. Results for this experiment did not match Adekkanattu's findings (Adekkanattu, 2003). In his experiment C<sub>2</sub> to C<sub>4</sub> outputs remained fairly stable for the first 9 hours before coke formation occurred. Methane levels were rather high, however. Like the findings here, DME and MeOH in his experiment became increasingly dominant once catalyst deactivation began.

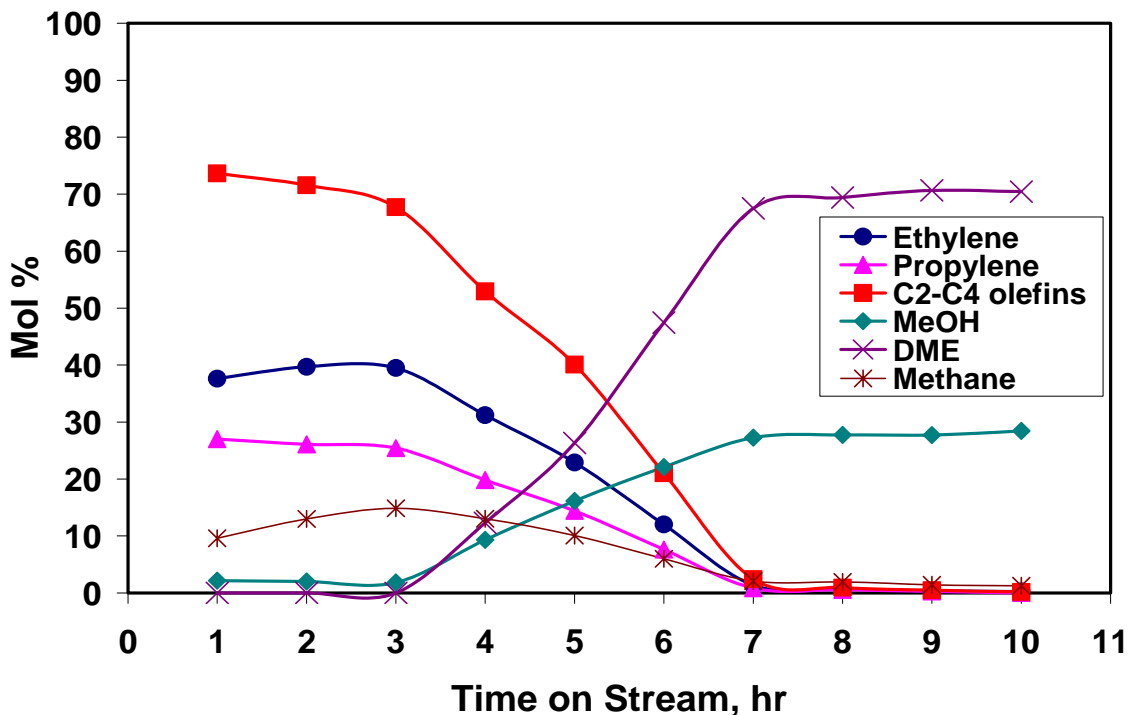


Figure 4.24. Distribution of Ethylene, Propylene, C<sub>2</sub> – C<sub>4</sub> Olefins, MeOH, and DME SAPO-56(P-18), (0.6 Si), 400 °C, No Grinding.

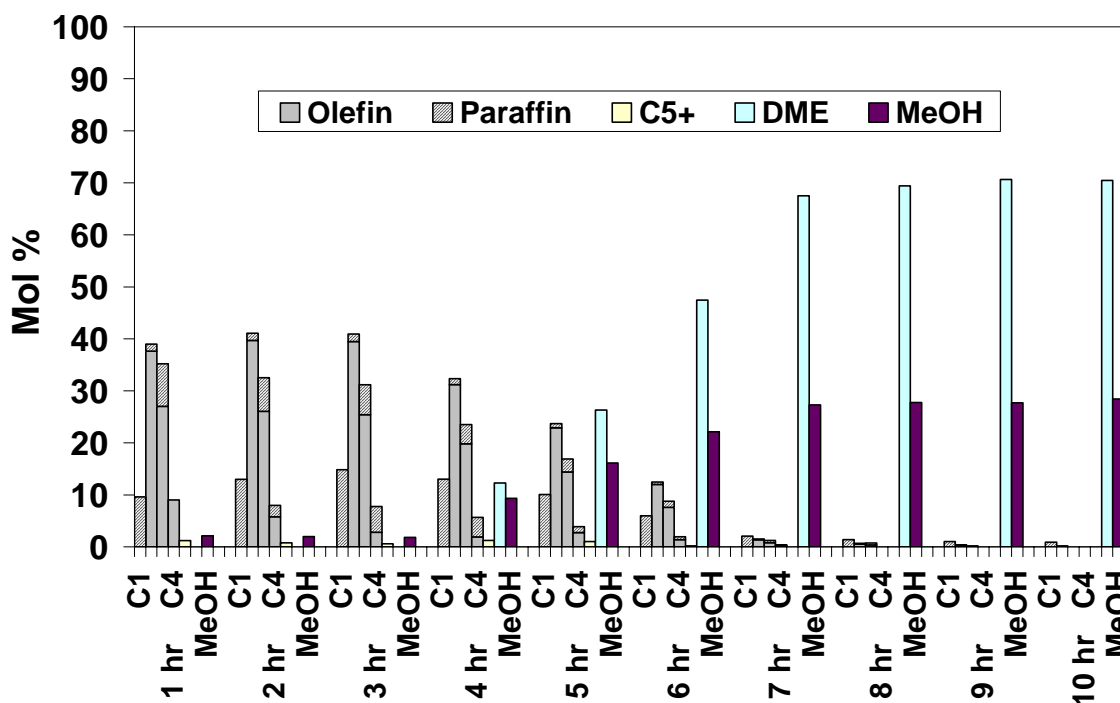


Figure 4.25. Distribution of Ethylene, Propylene, C<sub>2</sub> – C<sub>4</sub> Olefins, MeOH, and DME SAPO-56(P-18), (0.6Si), 400 °C, No Grinding.

Figures 4.26 and 4.27 show profiles for catalytic activity and product distribution over ground particles (15 min.). Coke formation was not significant for the first 5 hours, and olefin selectivity remained extremely high and steady for first 6 hours. Altogether, C<sub>2</sub> to C<sub>4</sub> olefins account for about 65% to 74% of the total product during that period. Methane on the other hand remained below 20% and faded away after the 8<sup>th</sup> hour. Activity did not improve, however. In fact the catalyst maintained the same lifetime (8 hours) both before and after grinding. By the end of the reaction DME selectivity nearly quadrupled MeOH's.

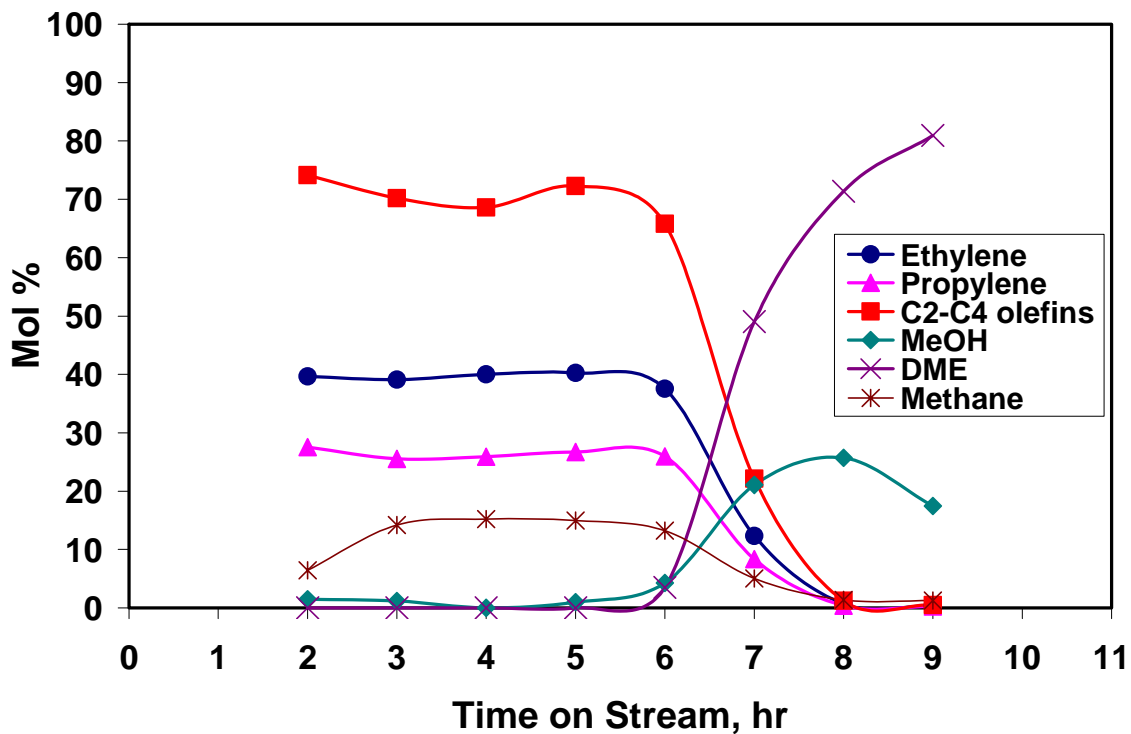


Figure 4.26. Distribution of Ethylene, Propylene, C<sub>2</sub> – C<sub>4</sub> Olefins, MeOH, and DME, SAPO-56 (P-18), (0.6Si), 400 °C, After 15 min Grinding.

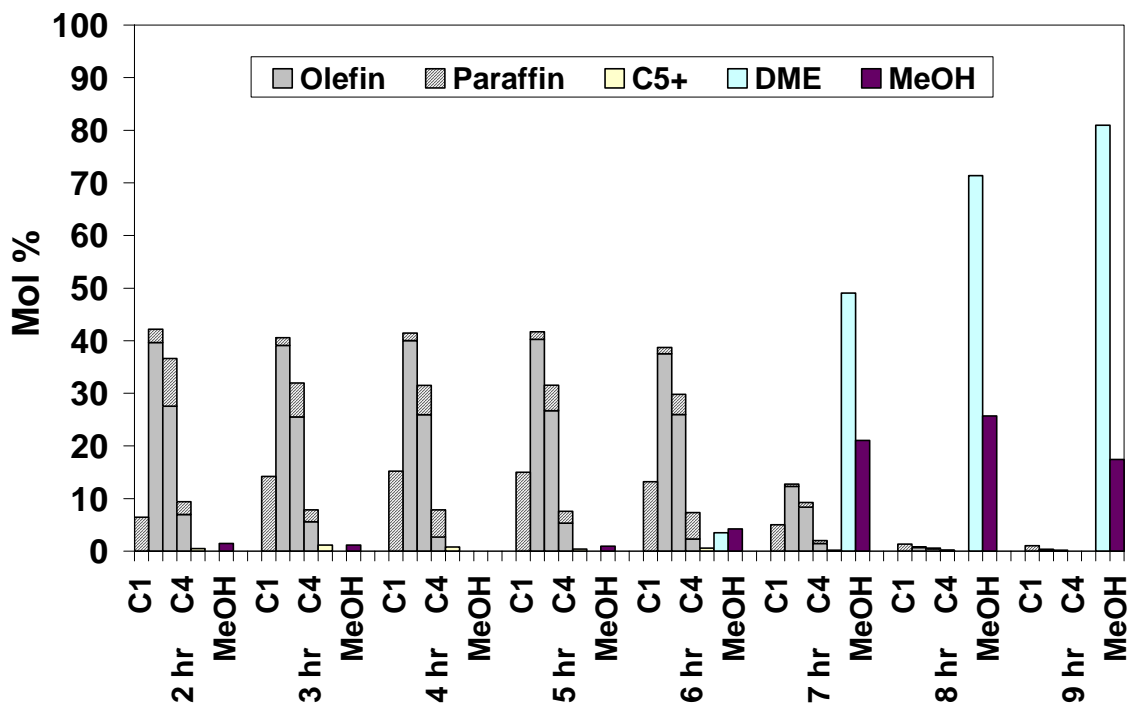


Figure 4.27. Distribution of Ethylene, Propylene, C<sub>2</sub> – C<sub>4</sub> Olefins, MeOH, and DME SAPO-56(P-18), (0.6Si), 400 °C, After 15 min Grinding.



**SAPO-56 (P-28), (0.3 Si)**

**Figure 4.28** depicts the profile of product selectivity over SAPO-56 with 0.3 Si silicon content. Product selectivity appears fairly stable during the first four hours. Although MeOH conversion was below 100%, coke formation remained fairly low during that period. Both ethylene and propylene production remained at moderate levels with C<sub>2</sub> to C<sub>3</sub> ratio a little above unity. Total olefin production reached its maximum at 61% after 3 hours on stream (**Table 4.3**). After the 4<sup>th</sup> hour, C<sub>2</sub> to C<sub>4</sub> olefins outputs declined rapidly to below 5% selectivity, while DME and MeOH selectivities increased significantly to levels above 62% and 64%, respectively.

Despite the catalyst's strong performance during the active period, this result did not match Adekkanattu's findings (Adekkanattu, 2003). In fact, his result showed catalyst activity remaining for almost 10 hours.

**Table 4.3. Product Distribution over SAPO-56 (P-28), No Grinding.**

TOS(hr)	COMPONENT						
		1 <sup>st</sup>	2 <sup>nd</sup>	3 <sup>rd</sup>	4 <sup>th</sup>	5 <sup>th</sup>	6 <sup>th</sup>
	C <sub>1</sub> -	10.03	12.55	13.77	13.02	3.19	2.99
	C <sub>2</sub> -	1.51	1.69	1.72	1.53	0.46	0.57
	C <sub>2</sub> =	31.58	32.82	33.61	30.57	3.10	0.70
	C <sub>3</sub> -	10.25	8.55	8.21	6.79	1.35	0.79
	C <sub>3</sub> =	25.96	24.86	24.78	22.43	2.43	0.84
	C <sub>4</sub> -	5.87	5.34	5.21	4.56	0.48	0.24
	C <sub>4</sub> =	2.22	1.99	1.92	1.68	0.36	0.00
		1.44	1.09	1.03	0.91	0.16	0.00
	C <sub>5</sub> -	2.41	2.21	2.41	2.17	0.44	0.00
	C <sub>5</sub> =	1.24	0.78	0.85	0.84	0.00	0.00
	C <sub>6</sub> -	1.01	1.47	1.55	1.59	0.00	0.00
	C <sub>6</sub> =	0.34	0.00	0.00	0.00	0.00	0.00
	DME	0.00	0.81	0.00	6.09	62.48	66.71
	MeOH	6.14	5.83	4.95	7.82	25.54	27.17

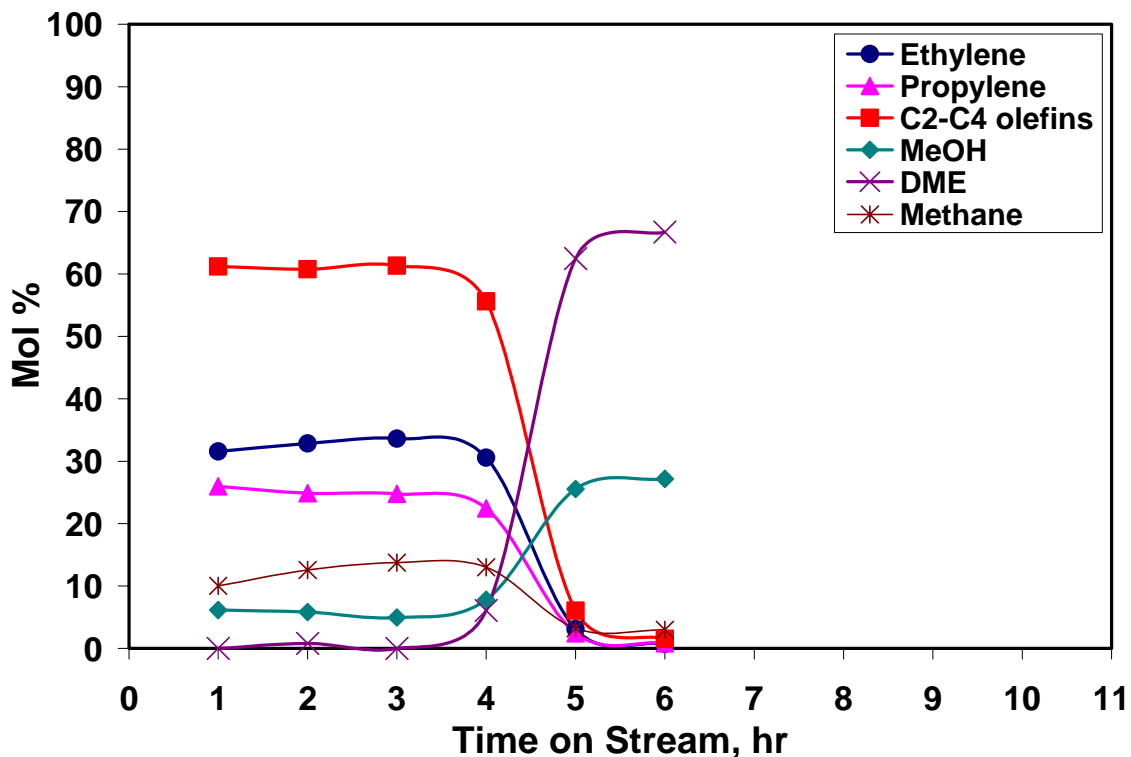


Figure 4.28. Distribution of Ethylene, Propylene, C<sub>2</sub> – C<sub>4</sub> Olefins, MeOH, and DME SAPO-56(P-28), (0.3Si), 400 °C, No Grinding.

When the same catalyst was ground for 15 minutes – as shown in **Figure 4.29** and **Table 4.4** – catalyst yield abated somewhat to levels below those obtained before grinding. C<sub>2</sub> to C<sub>4</sub> outputs declined sharply, accompanied by increases in DME and MeOH outputs. Only methane remained fairly stable during the first 5 hours, and then decreased after that. The catalyst did, however, last for an extra hour (6 hours total). As in all the previous catalyst runs, DME constituted the main component in the product stream from the 5<sup>th</sup> hour onward.

Table 4.4 Product Distribution over SAPO-56 (P-28), After 15 min. Grinding

TOS(hr)	COMPONENT	1 <sup>st</sup>	2 <sup>nd</sup>	3 <sup>rd</sup>	4 <sup>th</sup>	5 <sup>th</sup>	6 <sup>th</sup>	7 <sup>th</sup>
		C <sub>1</sub> <sup>-</sup>	10.91	11.77	9.14	8.97	4.96	2.32
	C <sub>2</sub> <sup>-</sup>	1.40	1.39	0.97	0.95	0.56	0.50	0.00
	C <sub>2</sub> <sup>=</sup>	30.81	28.06	19.42	17.73	8.04	0.74	0.61
	C <sub>3</sub> <sup>-</sup>	8.68	7.10	6.01	3.94	2.12	0.82	0.00
	C <sub>3</sub> <sup>=</sup>	25.31	21.65	15.72	13.59	6.49	0.89	0.89
	C <sub>4</sub> <sup>-</sup>	5.59	4.57	3.43	2.67	1.22	0.00	0.00
	C <sub>4</sub> <sup>=</sup>	1.99	1.66	1.59	1.04	0.56	0.00	0.00
		1.27	0.96	0.88	0.53	0.26	0.00	0.00
	C <sub>5</sub> <sup>-</sup>	2.22	1.88	1.98	1.38	0.71	0.00	0.00
	C <sub>5</sub> <sup>=</sup>	0.82	0.70	1.11	0.54	0.19	0.00	0.00
	C <sub>6</sub> <sup>-</sup>	1.00	1.41	1.66	0.98	0.71	0.00	0.00
	C <sub>6</sub> <sup>=</sup>	0.31	0.00	0.52	0.00	0.00	0.00	0.00
	DME	3.17	9.28	19.29	27.62	48.16	66.63	67.85
	MeOH	6.53	9.59	18.28	20.05	26.02	28.10	28.23

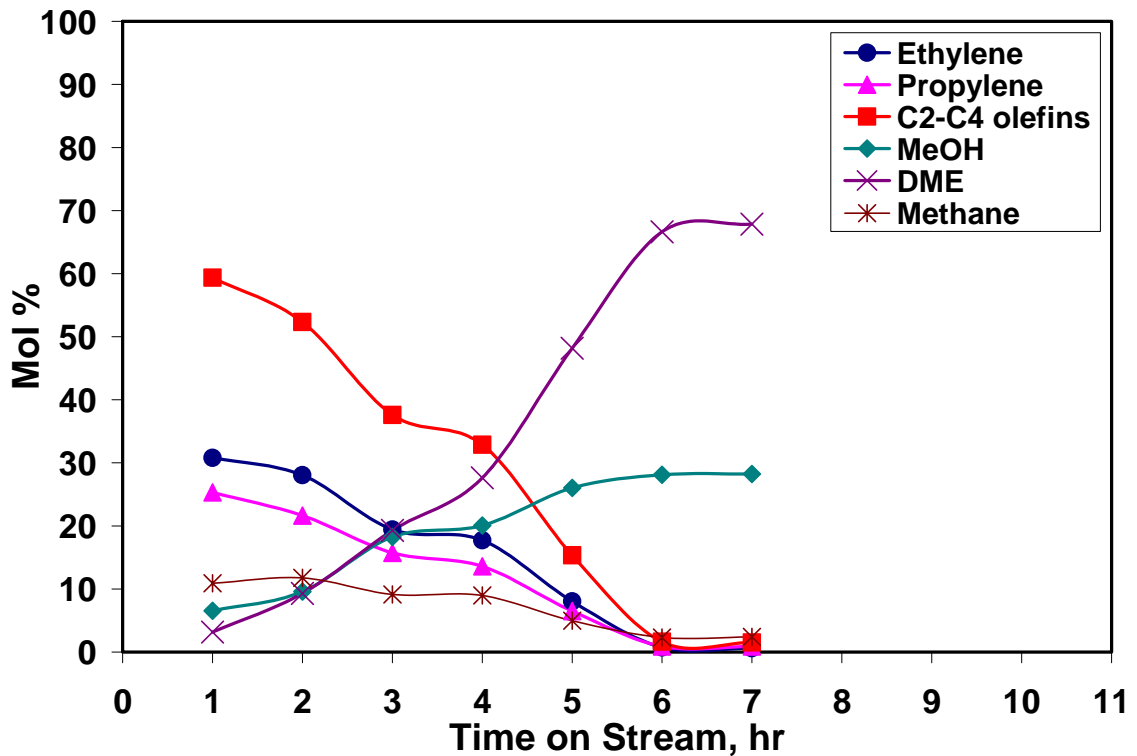


Figure 4.29. Distribution of Ethylene, Propylene, C<sub>2</sub> – C<sub>4</sub> Olefins, MeOH, and DME SAPO-56(P-28), (0.3Si), 400°C, After 15 min. Grinding.

### SAPO-56 (P-29), (0.9 Si)

**Figure 4.30** shows the product selectivity profile for SAPO-56 with (0.9 Si) silicon content. This catalyst, with the highest silicon content present in its framework, turned out to be the poorest performing catalyst among the SAPO-56 types tested. Reaction remained ongoing for about 4 hours total, but by the third hour, all catalyst activity ceased. By the second hour C<sub>2</sub> to C<sub>4</sub> outputs equaled MeOH output. In the first hour C<sub>2</sub> to C<sub>4</sub> selectivity appeared below 60% and decreased precipitously afterwards to essentially zero by the third hour. Both methane and DME formations remained fairly low. MeOH selectivity was significant near the end of the reaction at about 83% (**Table 4.5**).

**Table 4.5. Product Distribution over SAPO-56 (P-29), No Grinding**

TOS(hr)	COMPONENT	1 <sup>st</sup>	2 <sup>nd</sup>	3 <sup>rd</sup>	4 <sup>th</sup>
		C <sub>1</sub> <sup>-</sup>	10.68	7.51	1.83
	C <sub>2</sub> <sup>-</sup>	2.23	1.48	0.70	0.52
	C <sub>2</sub> <sup>=</sup>	28.15	17.64	0.56	0.41
	C <sub>3</sub> <sup>-</sup>	16.38	9.39	1.22	0.74
	C <sub>3</sub> <sup>=</sup>	21.71	12.98	0.87	0.00
	C <sub>4</sub> <sup>-</sup>	4.54	3.03	0.18	0.00
	C <sub>4</sub> <sup>=</sup>	2.02	1.08	0.00	0.00
		2.13	1.10	0.00	0.00
	C <sub>5</sub> <sup>-</sup>	2.29	1.90	0.00	0.00
	C <sub>5</sub> <sup>=</sup>	1.01	0.64	0.00	0.00
	C <sub>6</sub> <sup>-</sup>	1.06	0.74	0.00	0.00
	C <sub>6</sub> <sup>=</sup>	0.00	0.27	0.00	0.00
	DME	0.00	8.78	12.25	9.15
	MeOH	7.79	33.46	82.39	87.60

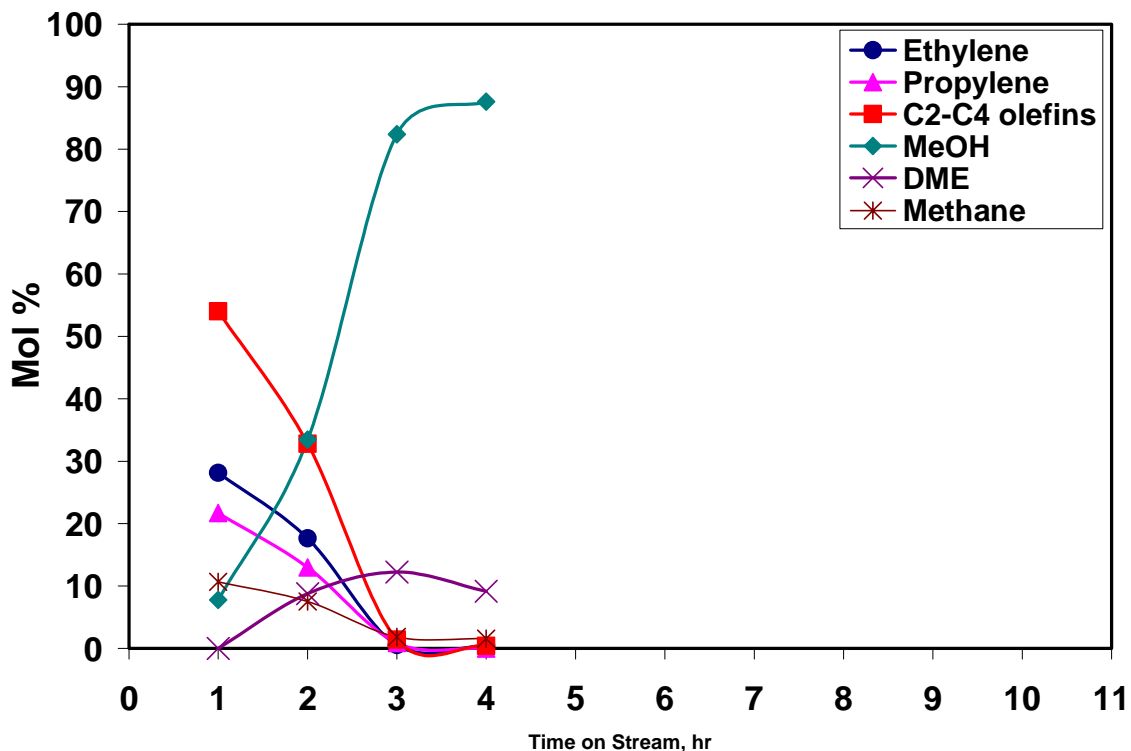


Figure 4.30. Distribution of Ethylene, Propylene, C<sub>2</sub> – C<sub>4</sub> Olefins, MeOH, and DME SAPO-56(P-29), (0.9Si), 400 °C, No Grinding.

When same catalyst was ground for 15 minutes (**Figure 4.31**), both activity and selectivity increased with MeOH remaining at moderately low levels. There was a sharp increase in C<sub>2</sub> to C<sub>4</sub> selectivity with ethylene to propylene ratio maintained at above 1.0. Methane formation was fairly stable for the first 3 hours at roughly 11% before declining to nearly 0 (**Table 4.6**). DME became dominant after the 4<sup>th</sup> hour. From the 2<sup>nd</sup> hour MeOH selectivity increased at a constant slope to a maximum 28% in product selectivity.

Although SAPO-56 (0.6 Si) was more active and lasted longer for time on stream, but results for SAPO-56 (0.9 Si) indicate greater improvement after grinding when compared with those of SAPO-56 (0.3 Si) and (0.6 Si). One reason for the behavior of SAPO-56 (0.9 Si) may be that the particles are larger (thicker) than the other SAPO-56 as

revealed from the SEM micrographs (See **Figures B-10 to B12**). Thus, they may be less active originally but show more improvement after grinding as found here.

**Table 4.6. Product Distribution over SAPO-56 (P-29), After 15 min Grinding**

TOS(hr)	COMPONENT	1 <sup>st</sup>	2 <sup>nd</sup>	3 <sup>rd</sup>	4 <sup>1/4</sup> th	6 <sup>1/2</sup> th
	C <sub>1</sub> <sup>-</sup>	10.91	11.77	9.14	8.97	4.96
	C <sub>2</sub> <sup>-</sup>	1.40	1.39	0.97	0.95	0.56
	C <sub>2</sub> <sup>=</sup>	30.81	28.06	19.42	17.73	8.04
	C <sub>3</sub> <sup>-</sup>	8.68	7.10	6.01	3.94	2.12
	C <sub>3</sub> <sup>=</sup>	25.31	21.65	15.72	13.59	6.49
	C <sub>4</sub> <sup>-</sup>	5.59	4.57	3.43	2.67	1.22
	C <sub>4</sub> <sup>=</sup>	1.99	1.66	1.59	1.04	0.56
		1.27	0.96	0.88	0.53	0.26
	C <sub>5</sub> <sup>-</sup>	2.22	1.88	1.98	1.38	0.71
	C <sub>5</sub> <sup>=</sup>	0.82	0.70	1.11	0.54	0.19
	C <sub>6</sub> <sup>-</sup>	1.00	1.41	1.66	0.98	0.71
	C <sub>6</sub> <sup>=</sup>	0.31	0.00	0.52	0.00	0.00
	DME	3.17	9.28	19.29	27.62	48.16
	MeOH	6.53	9.59	18.28	20.05	26.02

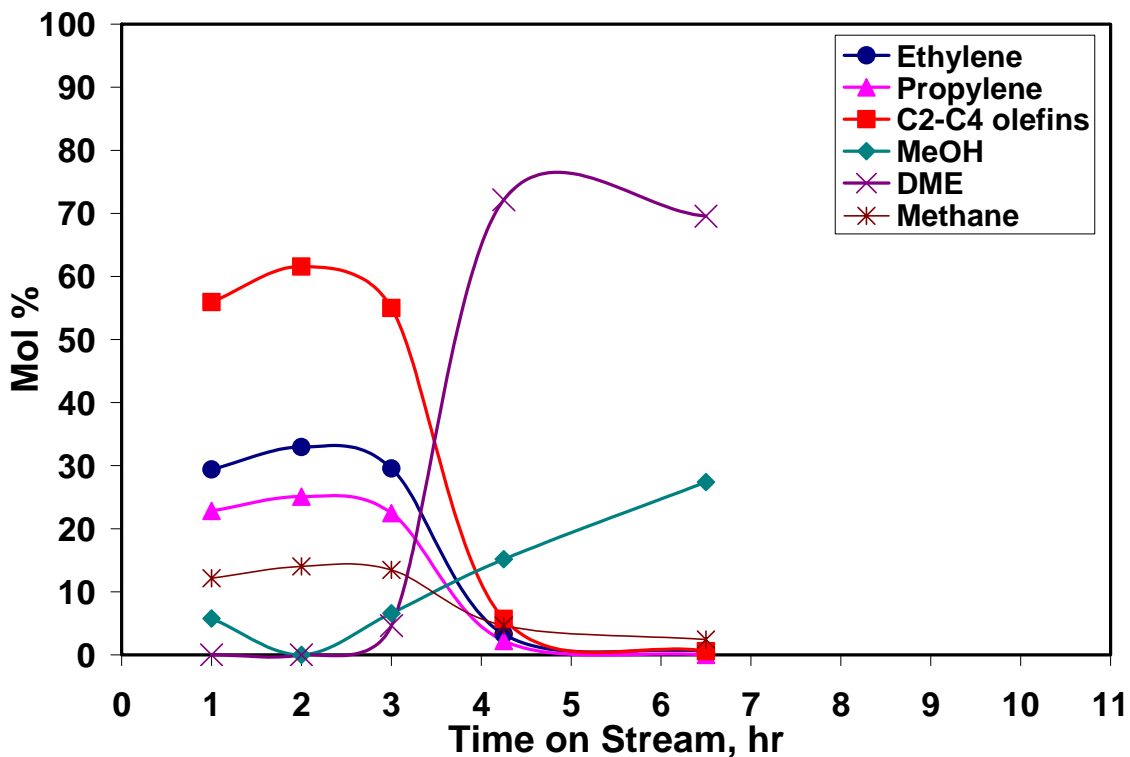


**Figure 4.31. Distribution of Ethylene, Propylene, C<sub>2</sub> – C<sub>4</sub> Olefins, MeOH, and DME SAPO-56(P-29), (0.9Si), 400°C, After 15 min. Grinding.**

## Effect of Silicon Content

While introduction of silicon atoms into the framework of aluminophosphate molecular sieves enable them to exhibit Brønsted acidity, thereby facilitating their use as acid catalysts, the effect of the silicon content on SAPO-56 is being examined here. **Figures 4.32** and **4.33** depict profiles of the olefins selectivity over these catalysts before and after grinding, respectively. When silicon content is increased from 0.3 to 0.6, an increase in olefins selectivity was observed. However, increasing the silicon content further to 0.9 showed a reverse in olefins selectivity. This finding indicates that too much silicon content inside the framework posed a detrimental effect on the catalyst's overall effectiveness. Again after grinding, a slight improvement was apparent for catalysts with 0.6 and 0.9 silicon content.

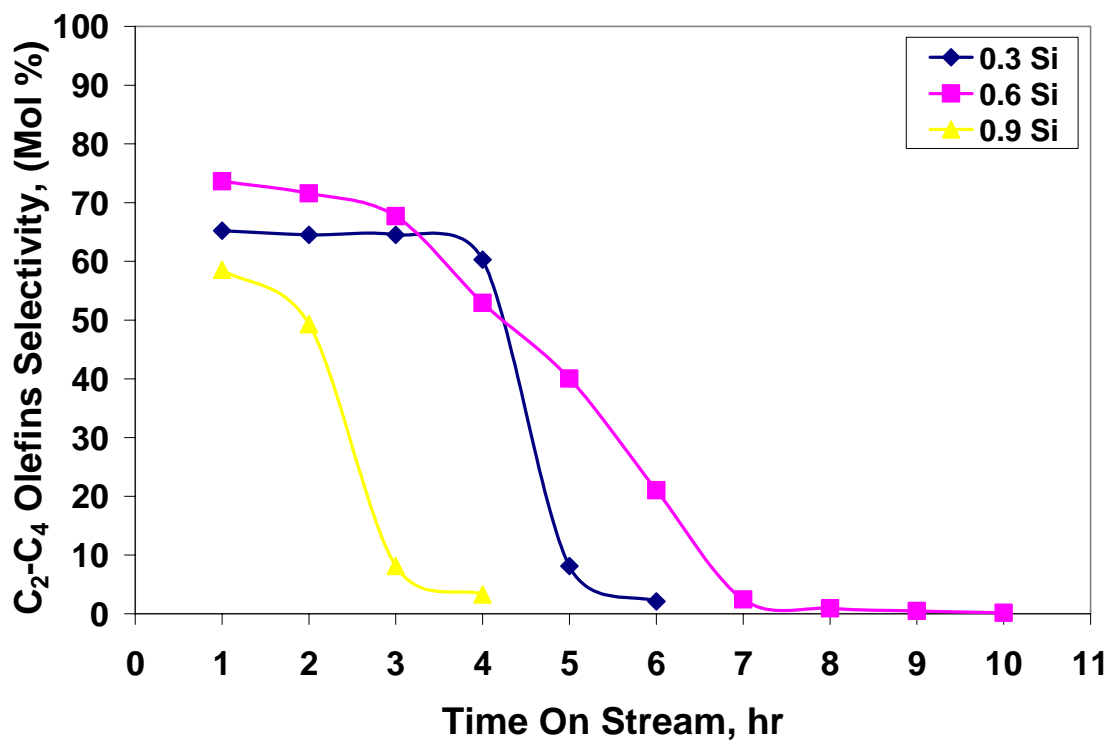


Figure 4.32. Effect of Silicon Content on Olefins Selectivity over SAPO-56, No Grinding.

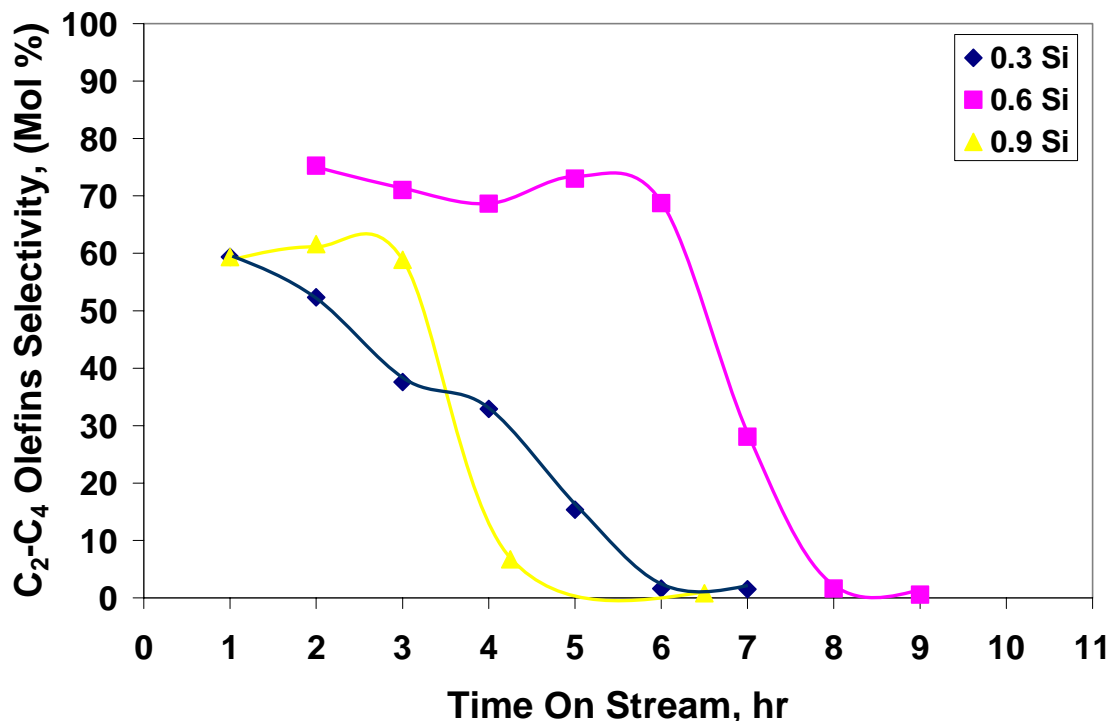


Figure 4.33. Effect of Silicon Content on Olefins Selectivity over SAPO-56, After 15 min. Grinding

#### SAPO-56 (P-18), (0.6 Si) Spent Catalyst

It is well known and noted in the literature that spent catalysts can be regenerated when thermally treated. Here, however, we tried a different approach by grinding the spent catalyst. Bear in mind this catalyst is the same one tested in **Figure 4.24** and was ground for approximately 15 min. before testing in the new experiment (**Figure 4.34**).

In this new experiment, little activity was observed. Nearly all components with the exception of DME and MeOH remained near 0. From this figure it looks as though DME and MeOH selectivities mirrored one another over the course of the reaction. Since not much activity was apparent for the initial 4 hours, the experiment was eventually terminated. It thus appears that particle size reduction alone, i.e. grinding, is not effective



in restoration of catalyst activity, indicating that the deactivation occurs throughout the particles, not just around the outer edges.

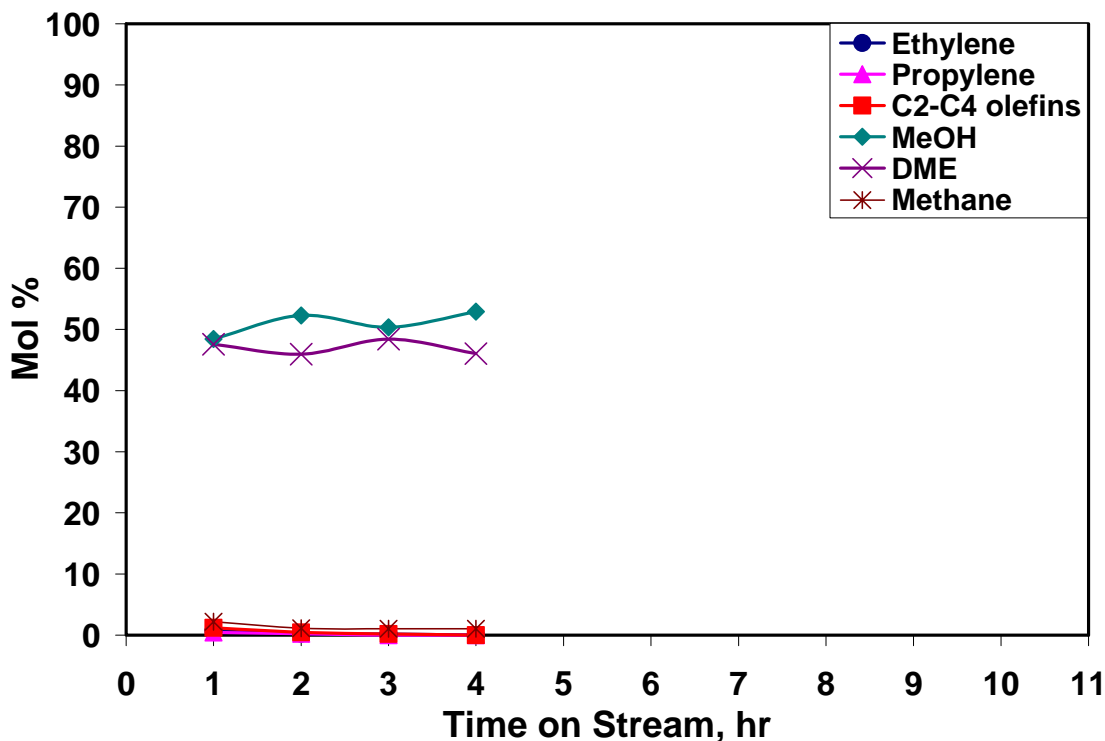


Figure 4.34. Distribution of Ethylene, Propylene, C<sub>2</sub> – C<sub>4</sub> Olefins, MeOH, and DME SAPO-56, (P-18), (0.6Si), 400°C, Spent Catalyst Ground for 15 min.

### SAPO Incorporated with Ruthenium

In this section findings based on SAPOs incorporated with ruthenium are reported and discussed. Samples treated with Ru include: SAPO-34, SAPO-44, and SAPO-56 (0.6 Si). The incorporation process was performed in Dr. Richard Ernst's lab in the University of Utah Chemistry Department.

#### Ru-SAPO-34 (Ru-P-5)

The product distribution over Ru incorporated SAPO-34 was not improved as is shown in **Figure 4.35**. Compared with **Figure 4.14** for unmodified SAPO-34, the Ru

catalyst performed poorly. While SAPO-34 remained active for nearly 4 hours with C<sub>2</sub> to C<sub>4</sub> selectivity relatively high during the first 3 hours, Ru impregnated SAPO-34 only lasted for 3 hours. Both ethylene and propylene levels were very low compared to unmodified SAPO-34. MeOH conversion was also very low. After the second hour, the product consisted mainly of MeOH indicating very poor activity. MeOH to DME ratio was high, between 3.5 to 4.

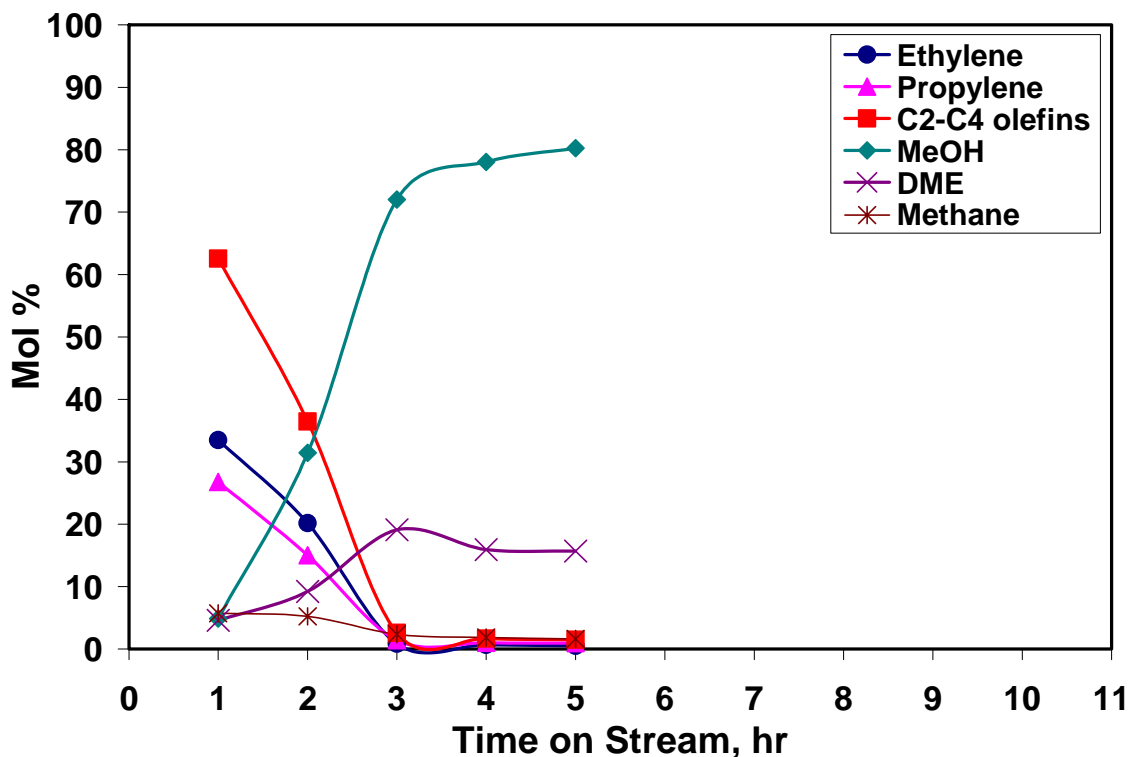


Figure 4.35. Distribution of Ethylene, Propylene, C<sub>2</sub> – C<sub>4</sub> Olefins, MeOH, and DME over Ru impregnated SAPO-34 (Ru-P-5), 400 °C.

#### Ru-SAPO-44 (Ru-P-6)

SAPO-44 modified with ruthenium (Figure 4.36) likewise did not show much improvement compared with the corresponding unmodified sample, with both catalysts remaining active for quite a while with the modified sample lasting about 2 hours longer. C<sub>2</sub> to C<sub>4</sub> selectivity profiles in both experiments were almost the same, however, with

slightly lower amounts present with the Ru modified catalyst. In both experiments methane selectivity occurred around the same level, 10% and lower. Additionally, both DME and MeOH exhibited almost identical profiles in these two experiments with MeOH amounts being almost 8 times DME.

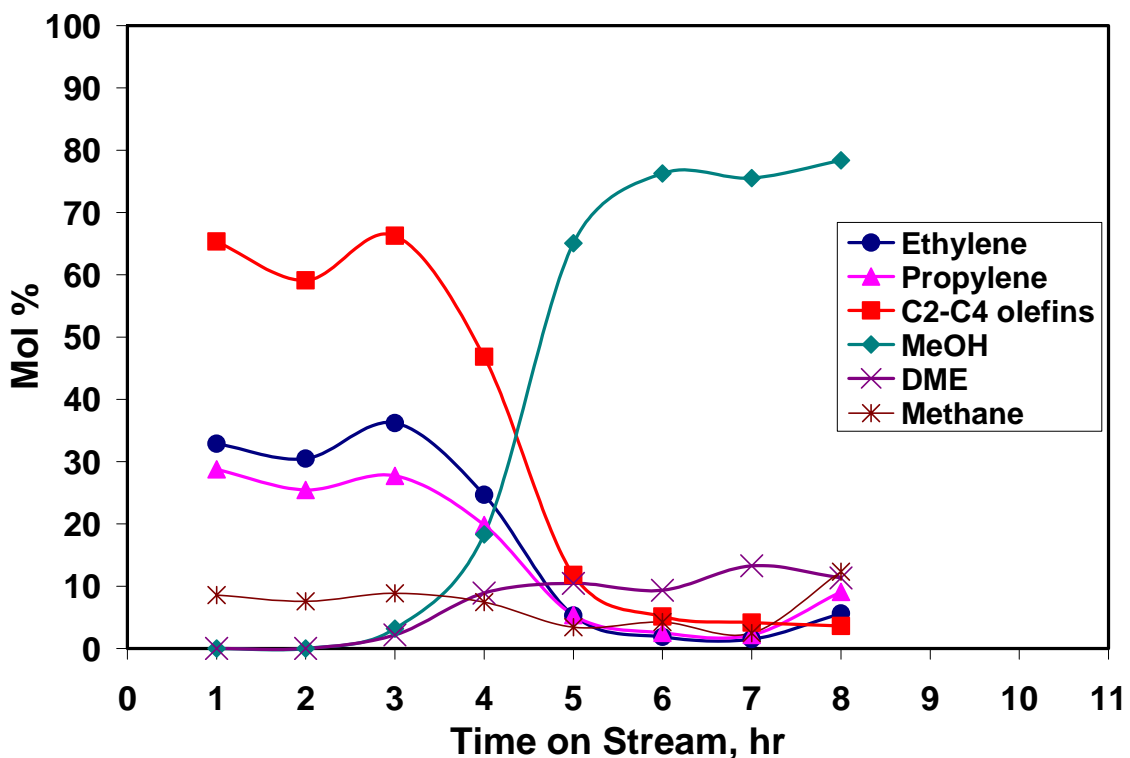


Figure 4.36. Distribution of Ethylene, Propylene, C<sub>2</sub> – C<sub>4</sub> Olefins, MeOH, and DME Ru impregnated SAPO-44 (Ru-P-6), 400 °C.

#### Ru-SAPO-56 (Ru-P-18)

Like SAPO-34, and SAPO-44, SAPO-56 (0.6 Si) did not show much improvement when modified with ruthenium (Figure 4.37). Unlike the unmodified sample where a gradual C<sub>2</sub> – C<sub>4</sub> olefin decline was noticed early on, RuSAPO-56 remained fairly stable early on for the first 4 hours before starting its descent. Catalyst activity profiles for both samples were just about the same with the modified sample

lasting a bit longer at relatively low olefins selectivity levels. Methane amounts in both these cases reach their peaks at around 16 mol %. Furthermore, DME amounts were present in significant amount above MeOH levels from the 6<sup>th</sup> hour forward (**Table 4.7**).

In summary, three SAPO catalysts were incorporated with ruthenium and tested for activity. When results from these tests were compared with corresponding tests of unmodified samples, no significant improvements were observed. In fact for Ru-SAPO-44 and Ru-SAPO-56, selectivity profiles and catalyst yield were nearly identical except that catalyst activity lasted about an hour longer for the Ru treated samples. Ru-SAPO-34, however, performed poorly and deactivated much faster as compared to the unmodified version. Huang et al. (2005) in studying temperature effects over SBA-15 modified with Ru and Pt for the dehydrogenation of cyclohexane found catalytic activity to be superior for Pt supported catalyst. Improvement in catalysis performance for Ru modified SBA-15 was minimal. It may very well be that metals other than Ru would give improved SAPO performance.

**Table 4.7. Product Distribution over Ru-SAPO-56 (Ru-P-18)**

TOS(hr)	COMPONENT									
		1 <sup>st</sup>	2 <sup>nd</sup>	3 <sup>rd</sup>	4 <sup>th</sup>	5 <sup>th</sup>	6 <sup>th</sup>	7 <sup>th</sup>	8 <sup>th</sup>	9 <sup>th</sup>
	C <sub>1</sub> <sup>-</sup>	10.62	15.33	15.20	15.49	13.23	11.67	6.25	4.19	4.50
	C <sub>2</sub> <sup>-</sup>	1.66	2.13	2.02	1.91	1.59	1.38	0.78	0.69	0.84
	C <sub>2</sub> =	26.75	33.95	31.41	31.63	27.12	22.69	5.74	1.88	1.41
	C <sub>3</sub> <sup>-</sup>	11.46	9.96	10.55	9.86	7.72	5.84	3.28	2.37	2.12
	C <sub>3</sub> =	23.79	27.19	25.79	25.49	21.44	18.52	4.90	2.63	2.20
	C <sub>4</sub> <sup>-</sup>	5.23	5.55	5.57	5.54	4.47	3.67	1.00	0.53	0.20
	C <sub>4</sub> =	2.37	1.88	2.48	2.39	1.91	1.59	0.72	0.55	0.00
		1.48	1.11	1.09	1.01	0.90	0.76	0.34	0.00	0.00
	C <sub>5</sub> <sup>-</sup>	2.68	1.84	2.90	2.91	2.56	2.16	0.93	0.50	0.00
	C <sub>5</sub> =	0.74	0.39	0.79	1.44	1.23	1.06	0.27	0.00	0.00
	C <sub>6</sub> <sup>-</sup>	1.74	0.37	1.57	1.75	2.12	1.41	0.00	0.00	0.00
	C <sub>6</sub> =	0.59	0.30	0.63	0.58	0.00	1.27	0.00	0.00	0.00
	DME	0.00	0.00	0.00	0.00	5.83	14.65	49.68	58.86	60.91
	MeOH	10.89	0.00	0.00	0.00	9.89	13.34	26.11	27.79	27.80

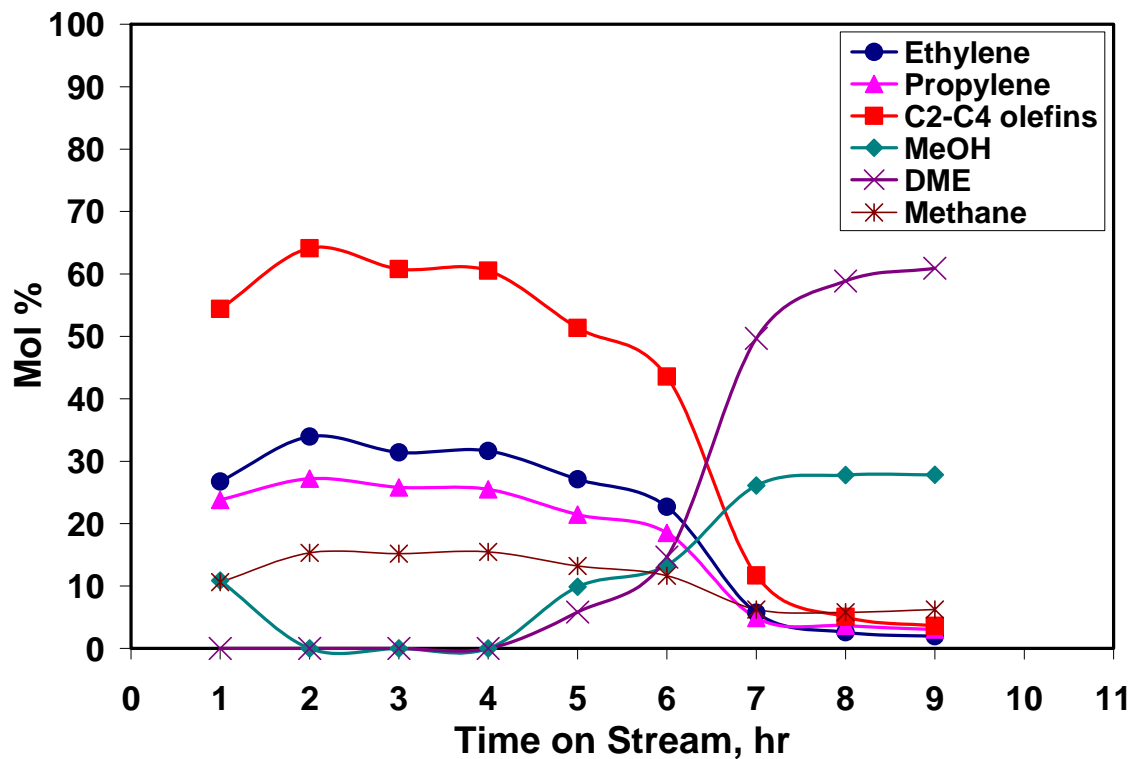


Figure 4.37. Distribution of Ethylene, Propylene, C<sub>2</sub> – C<sub>4</sub> Olefins, MeOH, and DME Ru impregnated SAPO-56 (Ru-P-18), 400 °C.

## V. CONCLUSION

Although SAPO catalysts have been in existence for over 25 years, many efforts have been under way in studying them to make them more efficient. Incorporation of various metals into their framework is one method often employed to achieve that. Process conditions have been investigated very thoroughly by various groups in order to systematically understand the optimum conditions in regard to product distribution, olefins selectivity, catalysis yield and catalytic activity. This thesis was based on experiments carried out over several microporous SAPO catalysts and various process conditions including temperature, particle size, and catalyst modification effects were studied and analyzed.

Results from comparing the scaled-down and standard operating conditions revealed almost identical product selectivity profiles with negligible differences in catalyst lifetime and MeOH conversion. This finding confirmed our original hypothesis that maintaining WHSV at the same level ( $0.5 \text{ hr}^{-1}$ ) when reducing all operating conditions by the same factor would not greatly change the reaction outputs. Results from the temperature study led us to believe that when catalyst particles were ground, the ability for catalysts to resist rapid deactivation might be improved. Some, but not all, catalysts were improved by the particle size reduction. Of the three SAPOs tested, SAPO-44 turned out to be better in terms catalytic performance and catalyst yield after grinding treatments. However, SAPO-56 maintained the same activity level before and

after grinding treatment. SAPO-56 (0.9 Si) gave a slight improvement. Due to the effective particle size of SAPO-56 (0.3 and 0.6 Si), diffusional effects could have played less of an effect while for SAPO-56 (0.9 Si) the effect was more apparent as revealed from the catalysis performance. SAPO-34, did not perform well in any of the categories studied compared to the other samples. Further, results from this study indicated the optimum operating temperature condition yielding the greatest C<sub>2</sub> to C<sub>4</sub> ratio was between 400 °C to 450 °C. This finding is in agreement with reports by Dubois et al. (2003) and Wu et al. (2004).

Various SAPOs incorporated with ruthenium based on a gas phase deposition method were tested for catalytic activity. Data for these samples did not show much improvement for any of the categories analyzed: yield, product distribution or lifetime. These catalysts were incorporated with only 1% Ru loading, and it is possible an increase of 5% to 10% loading could quantitatively and qualitatively lead to major performance improvements. In any event both SAPO-44 and SAPO-56 maintained nearly the same levels before and after Ru modification with slight improvements. SAPO-34 performed poorly, even to the point of losing activity as a result of the Ru treatment. Impregnation with other metals such as Pd and Pt remains a possible avenue for improvement. We also looked at the possibility of whether a spent catalyst would show any improvement in activity after grinding. Results from an experiment with SAPO-56 (0.6 Si) did not show any evidence of regeneration or restored activity following grinding. DME and MeOH were the only products present in abundant amounts in the product stream.

## VI. REFERENCES

- Adekanattu, P.A.; Internal Report “Catalytic Performance of Small Pore SilicoAluminoPhosphate (SAPO) and Nickel Modified SilicoAluminoPhosphate (NiSAPO) Molecular Sieves”, 2003; Consortium for Fossil Fuel Science, U.S. Department of Energy; Contract Nos DE-FC26-99FT40540 and DE-FC26-02FT41594, Auburn University, AL., see also Prakash, et al. (2003).
- Aguayo, A.T., del Campo, A. E., Gayubo, A.G., Tarrio, A., Bilbao, J., *Journal of chemical Technology and Biotechnology* 74 (1999) 315 – 321.
- Aguayo, A.T.; Gayubo, A.G.; Atutxa, A.; Olazar, M.; Bilbao, J.; *Journal of chemical Technology and Biotechnology* 74 (1999) 1082 – 1088.
- Attfield, Martin P., *Science Progress* 85 (2002) 319 – 345.
- Beyne, A.O.E., Froment, G.F., *Chem. Engng. Sci.* 45 (1990) 2089-2096.
- Beyne, A.O.E., Froment, G.F., *Chem. Engng. Sci.* 48 (1993) 503-511.
- Bos, A.N.R., Tromp, P.J.J., Aske, H.N., *Ind Engng Chem. Res.* 34 (1995) 3808.
- Buffham, B.A., *Chem. Eng. Sci.* 55 (2000) 5803.
- Cai, G., Liu, Z., Shi, R., He, C., Yang, L., Sun, C.; Chang, Y., *Applied Catalyst A: General* 125 (1995) 29 – 38.
- Campello, J.M., Lafont, J.M. *J. Catal.* 156 (1995) 11.
- Chang, C.D., Bibby, D.M., Howe, R.F., Yurchak, S, *Methane Conversion*, Elsevier, Amsterdam, 1988.
- Chen, J., Wright, P. A., Natarajan, S., Thomas, J. M., *Studies in Surface Science and Catalysis* 84 (1994) 1731 – 1737.
- Chen, D., Rebo, H. P., Moljord, K., Holmen, A., *Ind. Eng. Chem. Res* 36, (1997) 3473 – 3479.



- Dahl, I. M., and Kolboe, S.; *Catal. Lett.* 20 (1993) 329.
- Dahl, I. M., and Kolboe, S.; *J. Catal.* 149 (1994) 458.
- Dahl, I.M., Mostad, H., Akporiaye, D., Wendelbo, R, *Microporous and Mesoporous Materials* 29 (1999) 185 – 190.
- Database of Zeolite of Zeolite Structures: International Zeolite Association (2000), 'http://topaz.ethz.ch/IZA-SC/Introduction.htm'.
- Derouane, E. G., Nagy, J. B., Fernandez, C., Gabelica, E., Laurent, E. and Maljean, P., *Appl. Catal.* 40 (1988) 40.
- Djieugoue, M.-A, Prakash, A.M., Kevan, L., *J. Phys. Chem., B* 104 (2000) 10726.
- Dubois, Delphine R., M.S. Thesis, “Methanol To Olefins Conversion Over Modified SilicoAluminoPhosphate Molecular Sieves”, (2002) Auburn University, AL.
- Dubois, Delphine R, Obrzut, Daniel L., Liu, Jing, Thundimadathil, Jyothi, Adekkanattu, Prakash M., Guin, James A., Punnoose, Alex, Seehra, Mohindar S., *Fuel Processing Technology* 83 (2003) 203 – 218.
- Dumitriu, E., Azzouz, A., Hulea, V., Lutic, D., Kessler, H., *Microporous Materials* 10 (1977) 1 – 12.
- Eberly, Jr., P. E, Kimberlin, Jr., C. N., Miller, W. H., Drushell, H. V., *Ind. Eng. Chem., Process Des. Dev.* 5 (1966) 193-198.
- Eberly, Jr , P. E., *J. Phys. Chem.* 71 (1967) 1717-1722.
- Eisenbach, D., and Gallei, E., *J. Catal.* 56 (1974) 377-389.
- Flanigen, E. M., Lok, B. M., Patton, R. L., Wilson, S. T., New Developments in Zeolites Science and Technology – Proceedings of the 7<sup>th</sup> International Zeolite Conference Tokyo, August 17-22, 1986 -- *Studies in Surface Science and Catalysis* 28.
- Flanigen, E. M., Bekkum, H. van, Jacobs, P. A., and Jansen, J. C. (Editors): *Studies in Surface Science and Catalysis* 137 (2001) pg. 14.
- Fougret, C. M. and Holderich, W. F., *Applied Catalyst A: General* 207 (2001) 295 - 301.
- Froment, G.F.;Dehertog, W.J.H.; Marchi, A.J., *Catalysis* 9 (1992) 1.
- Gayubo, A.G., Aguayo, A.T., del Campo, A.E.S., Atutxa, A., Tarrío, A.M., Bilbao, J., *Ind. Eng. Chem. Res.* 39 (2000) 292 – 300.

- Guisnet, M., *Journal of Molecular Catalysis A: Chemical* 182 – 183 (2002) 367 – 382.
- Hocevar, S., Batista, J., Kaucic, V., *Journal of Catalysis* 139 (1993) 351 – 361.
- Huang, Xiwen; Internal Report, “Platinum Supported on Mesoporous SBA for Cyclohexane Dehydrogenation”, (2005); Consortium for Fossil Fuel Science, U.S. Department of Energy; Contract Nos DE-FC26-02NT41594, Auburn University, AL.
- Inui, T., Kang, M., *Applied Catalysis A: General* 164 (1997) 211 – 223.
- Jhung, S. H., Chang, J., Hwang, J.S., Park, S.; *Microporous and Mesoporous Materials* 64 (2003) 33 – 39.
- Kang, M.; Inui, T., *J. Mol. Catal.* 144 (1999) 329.
- Kano, J., Saito, F., *Powder Technology* 98 (1998) 166 – 170.
- Kasanovic, C., Bronic, J., Subotic, B., Smit, I., Stubicar, M., Tonejc, A., Yamamoto, T., *Zeolites: The international journal of molecular sieves*, vol. 13, 4 (1993) 261-268.
- Liang, J.; Li, H.; Zhao, S.; Guo, W.; Wang, R.; Ying, M., *Appl. Catal.* 64 (1990) 31.
- Lohmander, S., *Nordic Pulp & Paper Res. J.*, 15 (2000b) 300.
- Marchi, A.J., Froment, G.F. *Appl. Catal* 71 (1991) 139.
- McCusker, L. B., Baerlocher, C., *Studies in Surface Science and Catalysis* 137 (2001).
- Miller, S.J.; US Pat. 5 135 638, 1992.
- Miller, S.J., *Microporous Mater.* 2 (1994) 439.
- Prakash, A., Huang, X., Dubois, D., Obrzut, D., Jyothi, T., Liu, J., Guin, J., “Development of Microporous Shape-Selective Catalysts for Ethylene, Propylene, and other Value-Added Products via C-1 Chemistry”, in C1 Chemistry for the Production of Ultra-Clean liquid Transportation Fuels and Hydrogen, Annual Report for October 1, 2002 – September 30, 2003, Consortium for Fossil Fuel Science, U.S. Department of Energy Contract No. DE-FC26-02NT41594, (2003), 72-89.
- Rollmann, L.D., *J. Catal.* 47 (1977) 113-121.
- Rollman, L.D. Walsh, D.E., *J. Catal.* 56 (1979) 139-140.
- Sahirni, M., Tsotsis, T., *J. Catal.*, 96 (1985) 552-562.
- Shamlou, P.A., Jones, A.G., Djamarami, K., *Chem. Eng. Sci.*, 45 (1990) 809.

- Song, W., Fu, H., Haw, J.F., *J. Am. Chem. Soc.* 123 (2001) 4749 – 4754.
- Soundararajan, S., Dalai, A.K., Berruti, F., *Fuel* 80 (2001) 1187 – 1197.
- Stocker, M., *Microporous and Mesoporous Materials* 29 (1999) 3 – 48.
- Taylor, R.J., Petty, H., *Appl. Catal. A* 119 (1994) 121.
- Weisz, P.B., *Pure Appl. Chem.* 52 (1980) 2091.
- Wilson, D.R., Stahl, L., Ernst, R. D., *Organometallic Synthesis*, 3 (1986) 136.
- Wilson, S.T., Broach, R.W., Blackwell, C.S., Bateman, C.A., McGuire, N.K., Kirchner, R.M., *Microporous and Mesoporous Materials* 28 (1999) 125 – 137.
- Wilson, S., Barger, P., *Microporous and Mesoporous Materials* 29 (1999) 117 – 126.
- Wu, X., Abraha, M.G., Anthony, R.G.; *Applied Catalysis A: General* 260(1) (2004) 63-69.
- Zhao, Y.X., Wojciechowski, B.W., *J. Catal.* (1996) 163 – 365.

## **VII. APPENDICES**

**Appendix A: Table of Zeolites and Grinder**

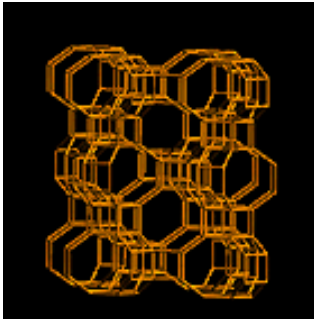
**Appendix B: SEM Micrographs**

**Appendix C: List of Calculations**

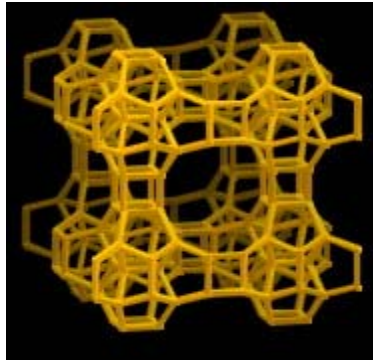
## **APPENDIX A**

### **Zeolites and Grinder**

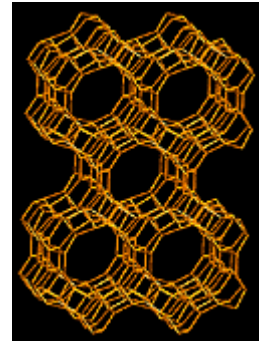
## Table of Zeolite Structures



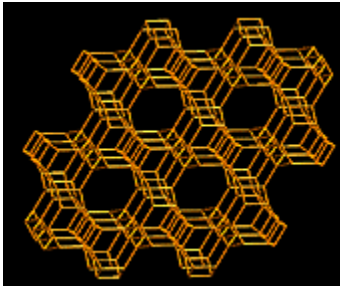
AFX



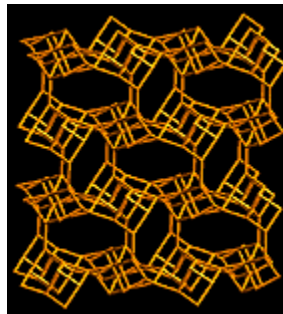
BEC



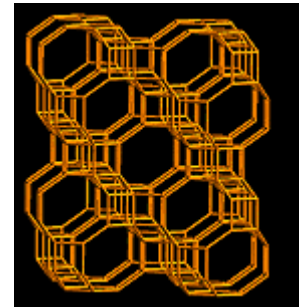
BOG



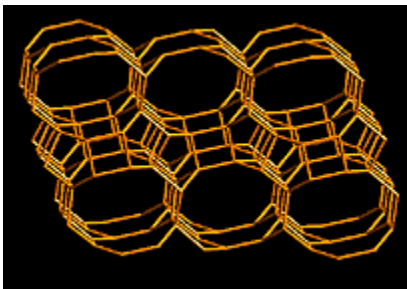
CAN



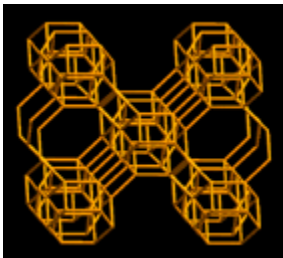
CGF



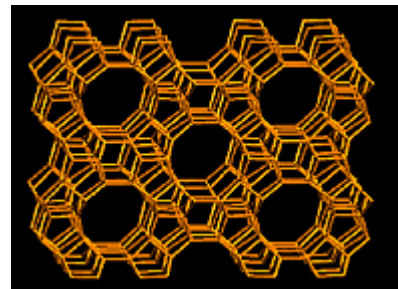
CHA



DAC



AEI



MEL

**Table A-1. Zeolite Structures**  
( Database of Zeolite of Zeolite Structures: International Zeolite Association (2000) )  
Source: '<http://topaz.ethz.ch/IZA-SC/Introduction.htm>'

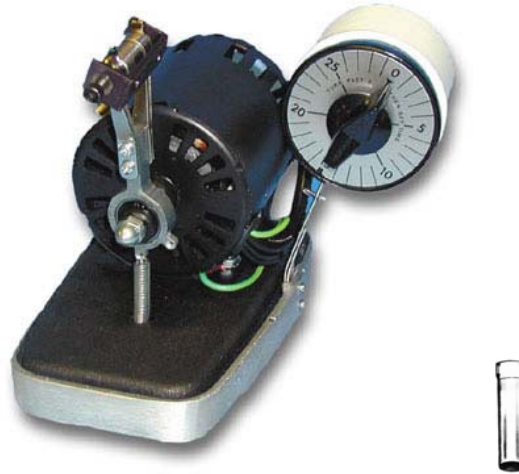


**Figure A-2. Wig-L-Bug from Dentsply/Rinn.**  
On the left hand side is the actual grinder, and on the right side is the agate vial which holds the sample.

## **APPENDIX B**

### **SEM Micrographs**



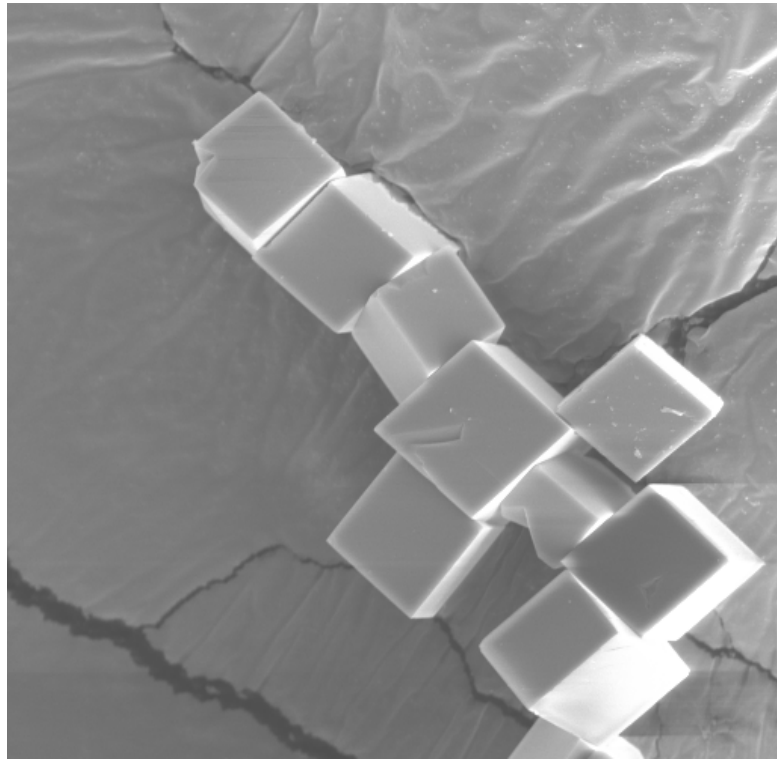


Figure B-1. SAPO-34 (P-5), X1000, 10kV, 14mm

13.4  $\mu\text{m}$

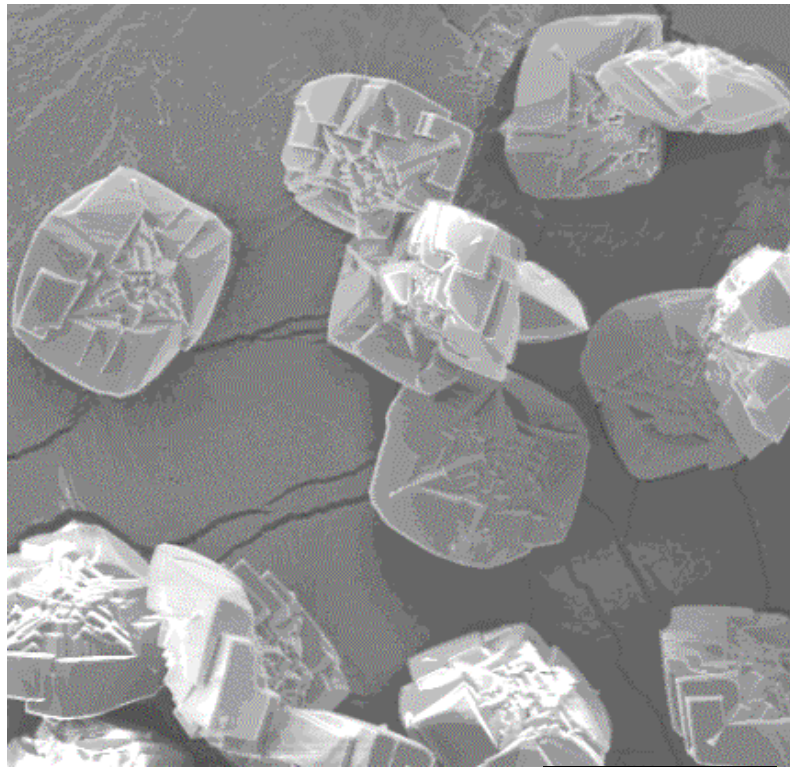


Figure B-2. SAPO-44 (P-6), X500, 10kV, 14mm

50  $\mu\text{m}$

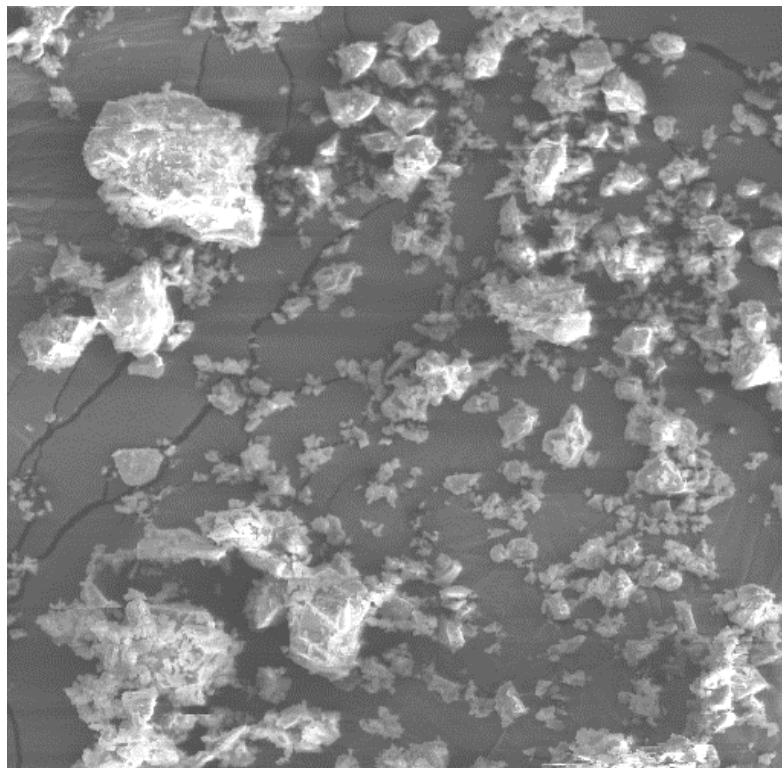


Figure B-3. SAPO-44 (P-6), After 5 min Grinding, X500, 10kv, 12mm

10.5  $\mu\text{m}$

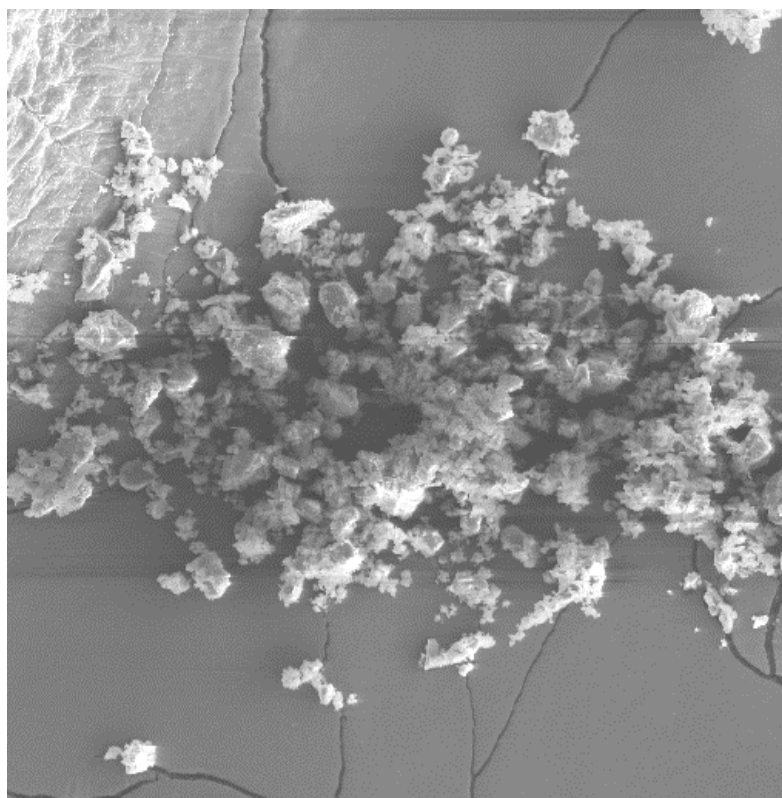


Figure B-4. SAPO-44 (P-6), After 10 min Grinding, X500, 10kv, 12mm

9.1  $\mu\text{m}$

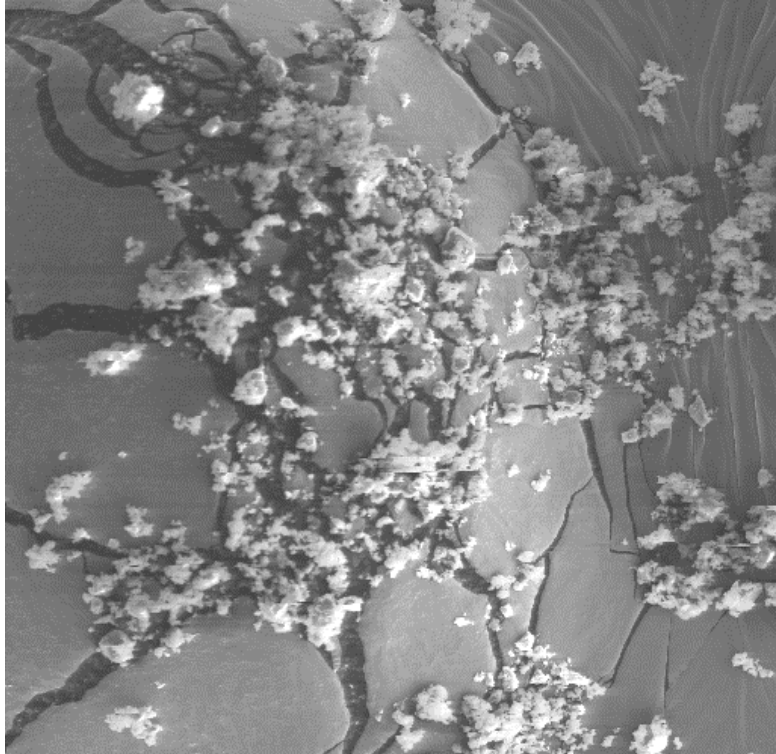


Figure B-5. SAPO-44 (P-6), After 15min Grinding, X500, 10kV, 12mm

6.3  $\mu\text{m}$

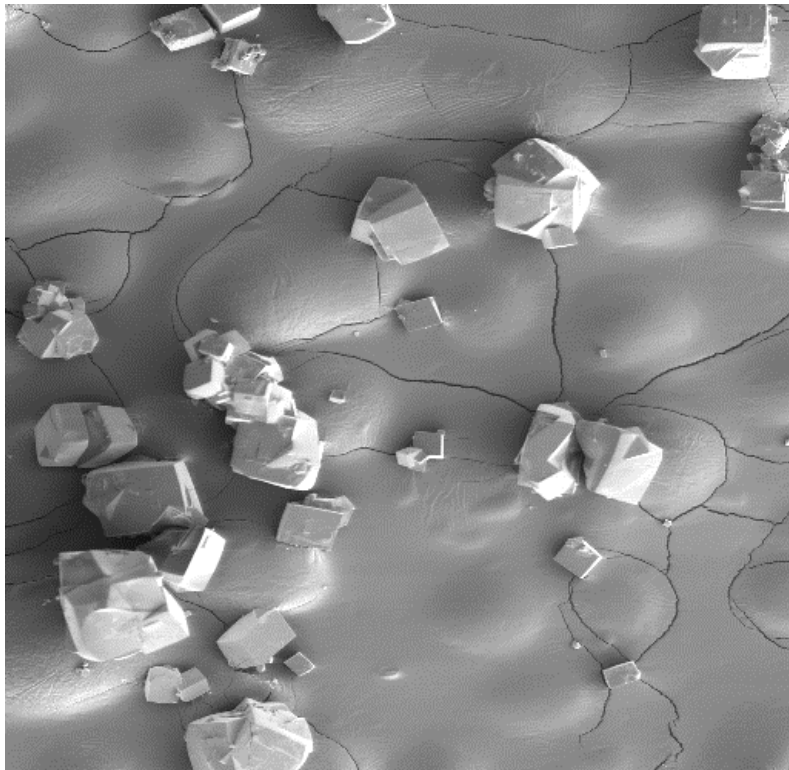


Figure B-6. SAPO-47 (P-31), X50, 10kv, 13mm

112  $\mu\text{m}$

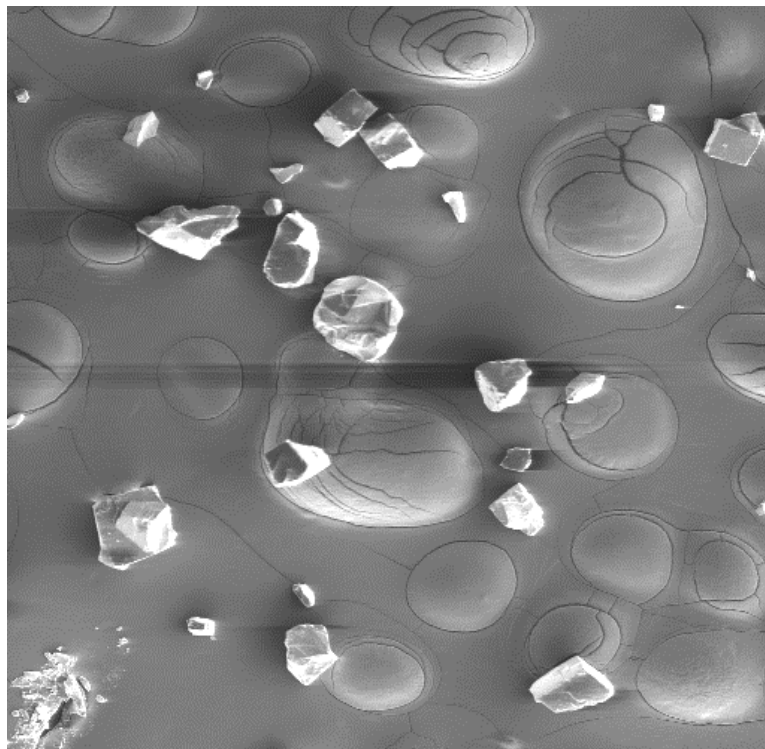


Figure B-7. SAPO-47 (P-31), X50, 10kV, 14mm

141  $\mu\text{m}$

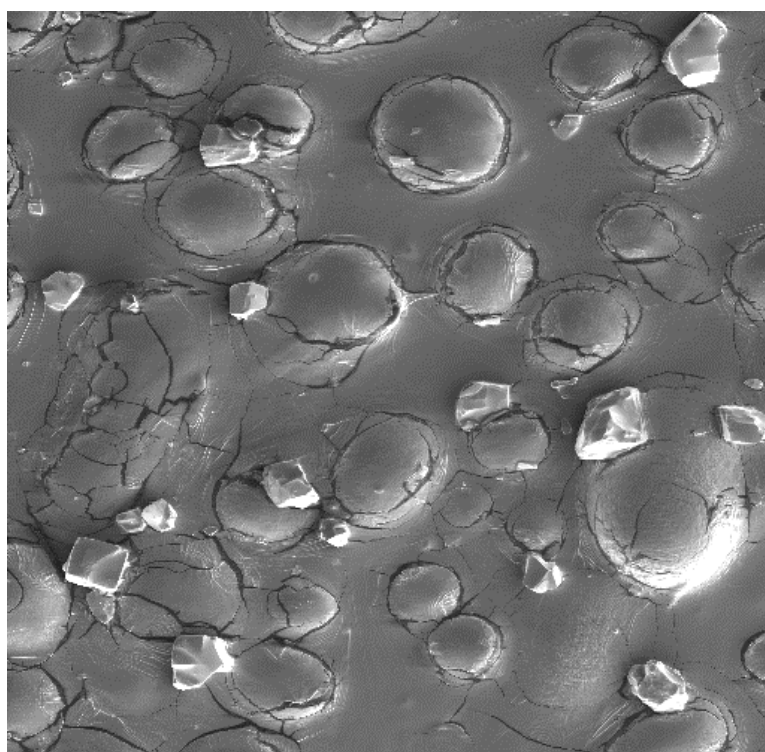


Figure B-8. SAPO-47 (P-31), X50, 10kV, 14mm, (Sonicated in Acetone)

141  $\mu\text{m}$

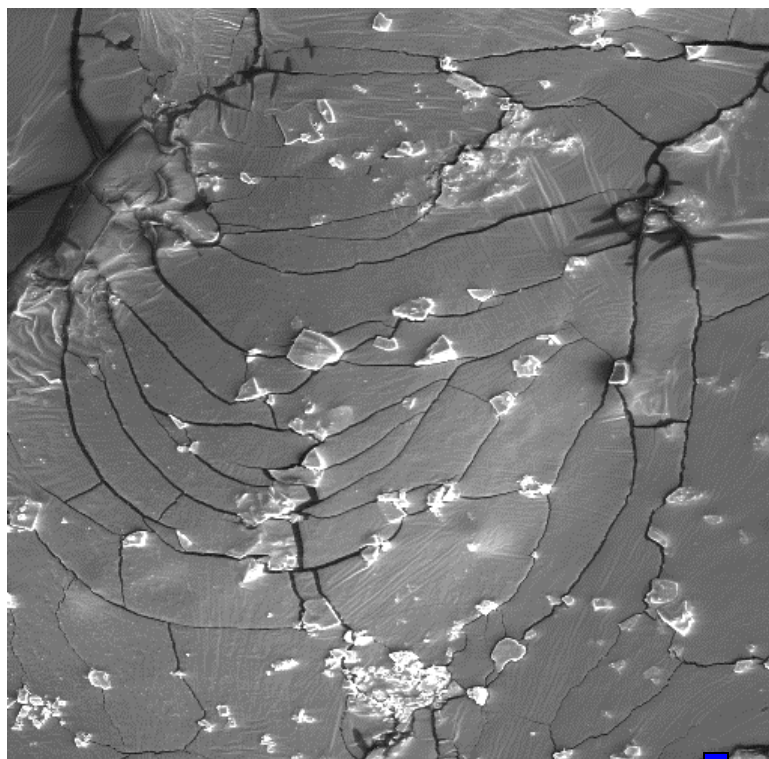


Figure B-9. SAPO-47 (P-31), X200, 10kV, 13mm, (Sonicated in Acetone)

14.1  $\mu\text{m}$

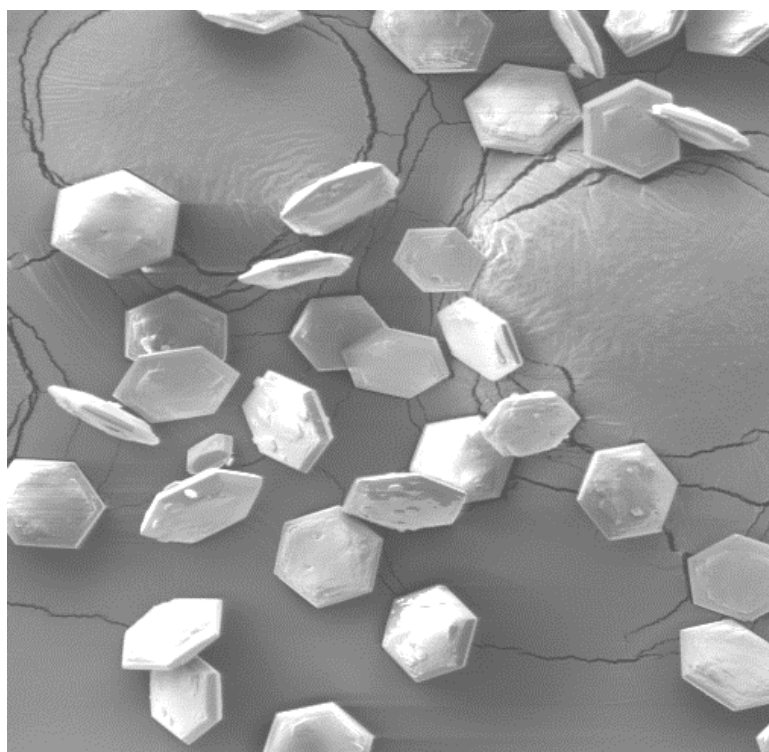


Figure B-10. SAPO-56 (P-28), (0.3 Si)

70  $\mu\text{m}$

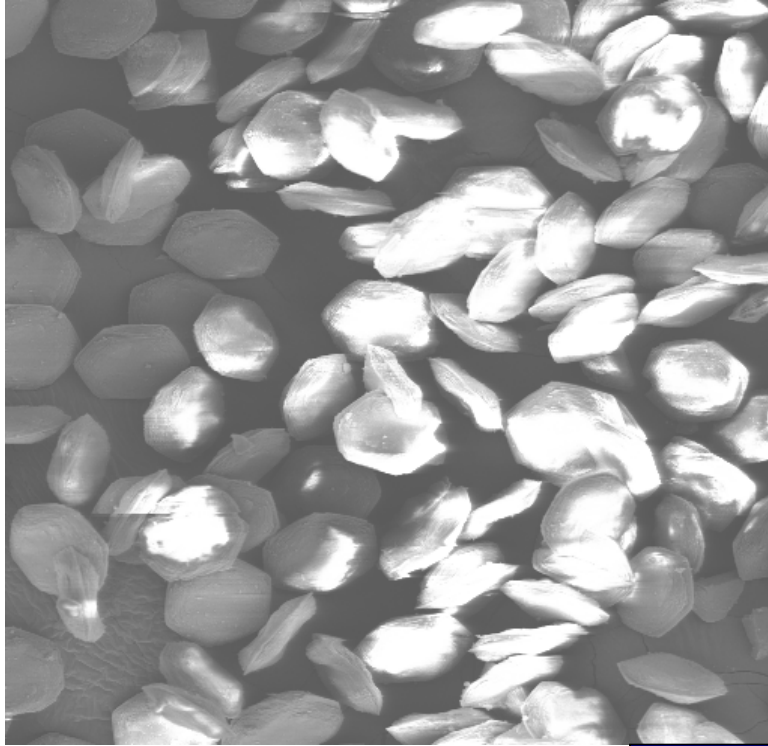


Figure B-11. SAPO-56 (P-28), (0.6 Si), X200, 10kV, 12mm

60 μm

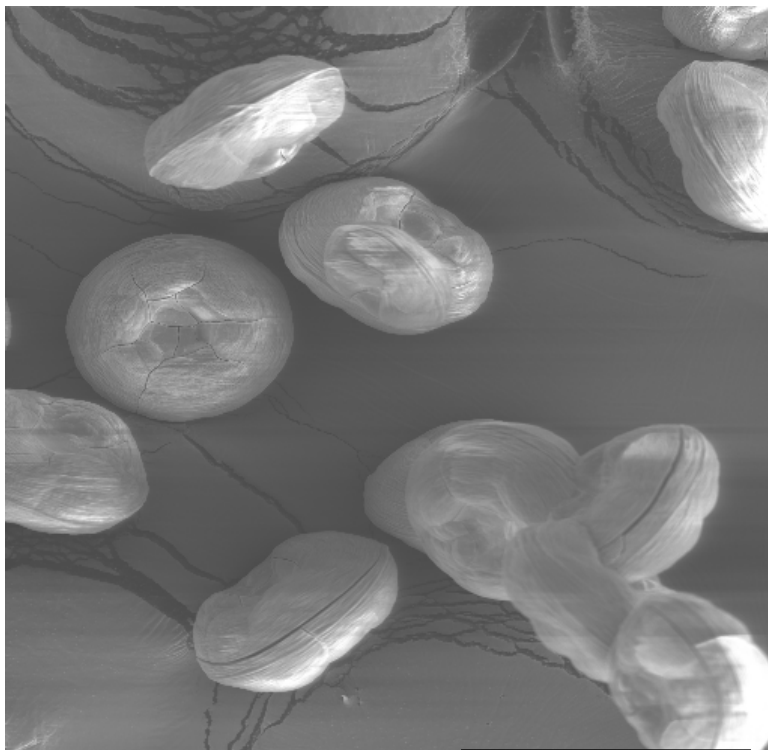


Figure B-12. SAPO-56 (P-29), (0.9 Si), X200, 10kV, 14mm

135.8 μm

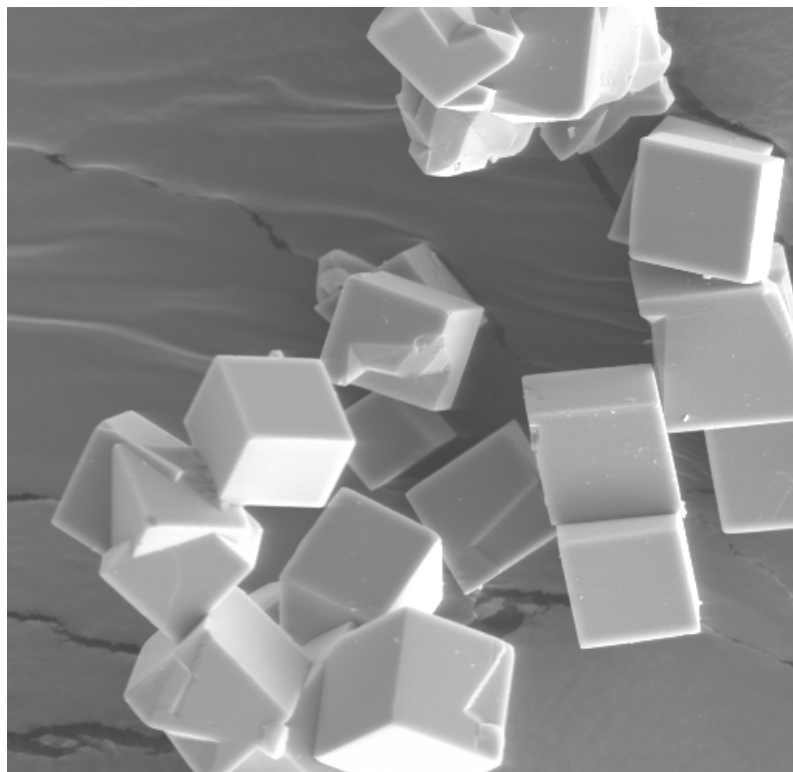


Figure B-13. Ru-SAPO-34 (Ru-P-5), X1000, 10kV, 14mm

13.4  $\mu\text{m}$

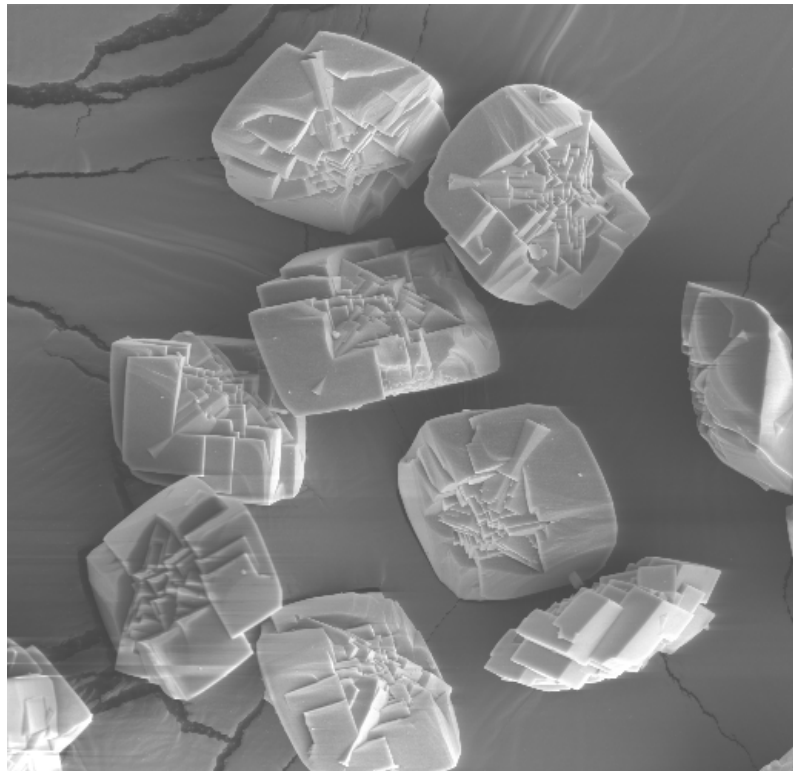


Figure B-14. Ru-SAPO-44 (Ru-P-6), X500, 10kV, 14mm

49.4  $\mu\text{m}$

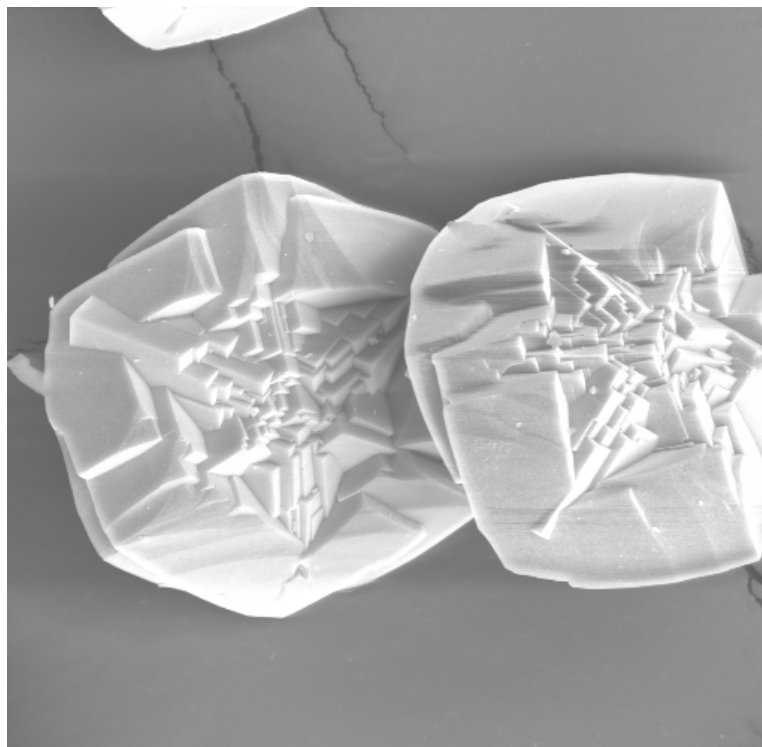


Figure B-15. Ru-SAPO-44 (Ru-P-6), X1000, 10kV, 14mm ████████████████████  
30  $\mu\text{m}$

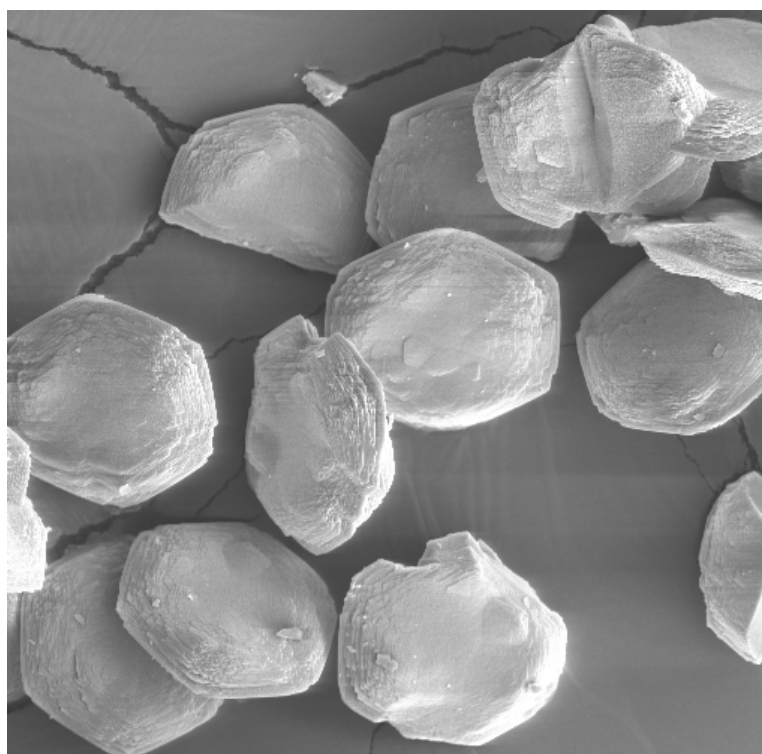


Figure B-16. Ru-SAPO-56 (Ru-P-18), X500, 10kV, 14mm ████████████████████  
52.5  $\mu\text{m}$



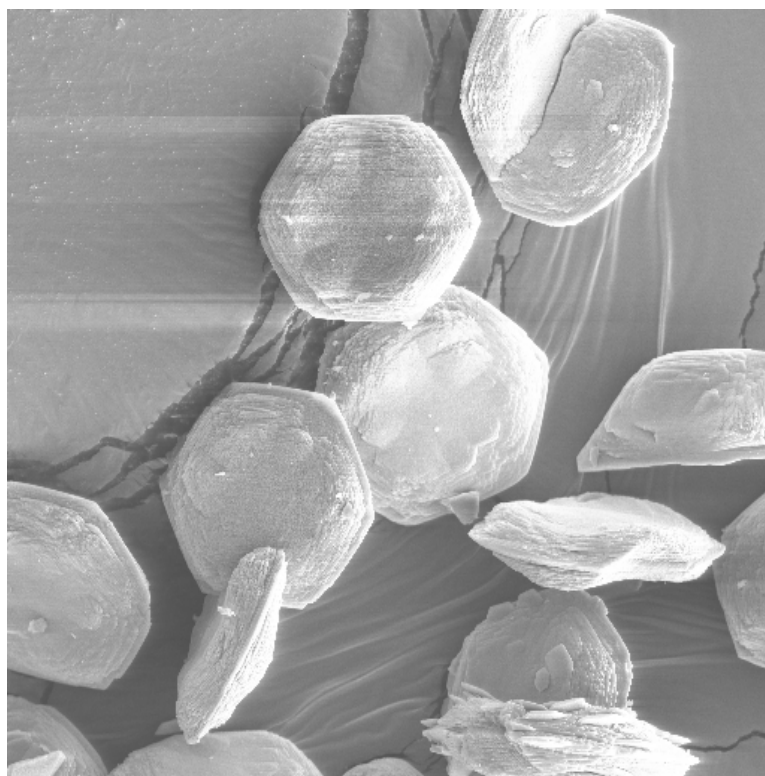


Figure B-17. Ru-SAPO-56 , X500, 10kV, 14mm

52.5  $\mu\text{m}$

## **APPENDIX C**

### **CALCULATION PROCEDURE**

This section provides detailed information on calculation procedure. Please refer to Standard Analysis in Experimental Section for further clarification:

Column labeled with 'Retention Time' contains information obtained directly from standard calibrations.

Column labeled with 'Standard ppm' refers to concentration of standard components. Separate calculations were made in order to arrive at ppm values for DME and MeOH.

Column labeled with 'Standard Area for 100µl' refers to standard values obtained during GC analysis.

Column labeled 'Sample peak area 100µl' contains values reported from actual experiments.

Column labeled 'ppm of sample product' contains concentration values for individual product components and is based on the following equation:

$$\text{ppm product} = \frac{(\text{Standard ppm} \times \text{Peak Area})}{\text{Standard Area for 100}\mu\text{l}} \quad \text{C-1}$$

Column labeled '% of compound' refers to percent of individual component present in product mixture and is calculated as follow:

$$\% \text{ of compound } i = \frac{(\text{ppm of compound } i \times 100)}{\sum \text{ All components}} \quad \text{C-2}$$

Column labeled with 'mol/min of compound' refers to the mole per minute of ith component and is calculated as follow:

$$\text{mol/min of compound } i = \frac{(\text{ppm of compound } i \times \text{outlet molar flowrate})}{1000000}$$

C-3

Column labeled with 'mol C/min' refers to the number of moles of carbons per component and is calculated as follow:

$$\text{mol C / min} = (\text{mol/C of compound } i) \times (\text{\# of Carbons present}) \quad \text{C-4}$$

The followings are calculated as follows (Please refer to figure):

$$\text{MeOH In (mol/min)} = \frac{(\text{MeOH flowrate} \times \text{MeOH density})}{\text{M.W. of MeOH}} \quad \text{C-5}$$

$$\text{Carbon in (mol/min)} = \text{Methanol in (mol)} \quad \text{C-6}$$

$$\text{Carbon out (mol/min)} = (\text{Total mol C / min}) \quad \text{C-7}$$

$$\text{Carbon balance} = (\text{Carbon out} - \text{Carbon in}) \text{ mol/min} \quad \text{C-8}$$

$$\% \text{ Loss or Gain} = \frac{[(\text{Carbon out} - \text{Carbon in}) \times 100]}{\text{Carbon in}} \quad \text{C-9}$$

Selectivity is the mole percent of a species produced by the reaction. The selectivity of products is calculated as follow:

$$\text{Methane Selectivity} = \frac{(\text{mol of Methane} \times 100)}{[(\text{Total products} - \text{MeOH}) \text{mol}]} \quad \text{C-10}$$

$$\text{Propylene Selectivity} = \frac{(\text{mol of Propylene} \times 100)}{\text{Total mol of products}} \quad \text{C-11}$$

The methanol conversion calculates how much of the methanol is being converted. The calculation goes as follow:

$$\text{MeOH Conversion} = \frac{[(\text{MeOH in} - \text{MeOH products}) \text{mol} \times 100]}{\text{MeOH in (mol)}} \quad \text{C-12}$$